Order Number 9033242

Thermodynamics and particle formation during vacuum pump-down

Zhao, Jun, Ph.D.

University of Minnesota, 1990

U·M·I
300 N. Zeeb Rd.
Ann Arbor, MI 48106

THERMODYNAMICS AND PARTICLE FORMATION DURING VACUUM PUMP-DOWN

A THESIS

SUBMITTED TO THE FACULTY OF THE GRADUATE SCHOOL OF

THE UNIVERSITY OF MINNESOTA

BY

JUN ZHAO

IN PARTIAL FULFILLMENT OF THE REQUIRMENTS

FOR THE DEGREE OF

DOCTOR OF PHILOSOPHY

FEBRUARY, 1990

ACKNOWLEDGEMENTS

I would like to express my sincerest gratitude to my advisers, Dr. Benjamin. Y. H. Liu and Dr. Thomas. H. Kuehn, for their guidance, encouragement, patience, and help during the course of this work and my stay at Minnesota. Their insight into the physical phenomena involved, and their approach to scientific research have always impressed me. They have made me feel fortunate in many ways with two items of special mention. First, Dr. Liu helped me get started at the Particle Technology Laboratory. Secondly, they found this very interesting problem for my Ph.D. dissertation research.

I wish to thank all professors and friends who provided direct or indirect assistance to this work. Specially, Drs. P. H. McMurry, D. Y. H. Pui, and K. Rubow for their helpful discussions and advice; Dr. W. W. Szymanski, who is the key developer of the vacuum particle sampler -- a tool for this research; and Bernard Olson and Jim Rooney, who read part of this thesis and made grammatical corrections. I also like to thank my future colleague, Pat Kinney, for his friendship and great help.

Thanks to all my friends in the Particle Technology Laboratory, because they made my stay here such a cherished experience.

I am deeply indebted to my wife, Ying Yu, who spent many hours in preparing the manuscript. I don't know how I could have accomplished this work without her patience, companionship, and support. I also like to thank my parents, for their love, believe, and inspiration.

This work is supported by the Particle Contamination Control Research Consortium at the University of Minnesota.

ABSTRACT

It is very important to understand the phenomena of particle formation, transport, and deposition in vacuum systems in order to improve semiconductor manufacturing processes. Nearly half of more than 100 operations in the current very large scale integrated circuit (VLSI) technology are performed in vacuum environments. Particles generated in vacuum equipment or vacuum processing have become a major contamination source which causes degradation in product performance and loss in product yield in semiconductor manufacturing.

Vacuum pump-down has been identified as a step that can generate a large number of particles. This thesis has investigated, theoretically and by experiment, the process of pump-down from two aspects: thermodynamics and particle formation. The important contributions of this work are as follows:

(1) This research provides a complete and systematic measurement of the transient gas temperature during pump-down. A substantial drop in the gas temperature is observed. In a chamber of 47.3 liters, when the effective pumping speed is 705 lpm and the initial temperature is 25°C, the maximum temperature drop is about 70 °C for 50%RH room air, 95°C for dry nitrogen, 105°C for high purity argon. It is found that the following factors have a significant effect on the gas temperature: effective pumping speed, chamber geometry, gas medium, initial pressure, water vapor, and measurement location.

(2) A mathematical model of the vacuum pump-down process, based on fundamentals of thermodynamics and heat and mass transfer processes in the continuum regime, has been developed to predict pressure and temperature of the gas, and saturation ratio of the condensable species. The predictions of the model agree well with measured data.

(3) A dimensionless Z number has been introduced to describe the adiabaticity of pump-down, where $Z = \frac{\tau \omega}{\xi}$, τ is the pumping time constant, ξ is the ratio of chamber volume to surface area, and ω is the heat penetrating rate of the gas. When $Z = 0$, the pump-down is adiabatic, and when $Z = \infty$, it is isothermal. Based on the Z number, a similarity solution of the gas thermodynamic state during pump-down is found.

(4) A theory has been developed to predict the critical condition of pump-down that initiates water vapor condensation and nucleation processes during pump-down. It is found that the critical condition depends on both the dimensionless Z number and the initial relative humidity. Based on this theory, a design criterion for clean vacuum pump-down is found.

(5) Particle formation during pump-down has been quantitatively measured. It is found that the particles formed are mainly water droplets containing impurities. These particles are formed by water vapor homogeneous nucleation, or nucleation on ions, or both. The impurities scavenged by droplets may chemically react to form residue particles. The most likely reaction is that involving liquid phase oxidation of pollution species such as SO_2 and neutralization by NH_3 to form $(NH_4)_2SO_4$.

TABLE OF CONTENTS

CHAPTER 4 SIMILARITY AND CHARACTERISTICS OF PUMP-DOWN PROCESSES

CHAPTER 5 CRITICAL PUMP-DOWN CONDITIONS FOR WATER VAPOR CONDENSATION AND NUCLEATION

LIST OF TABLES

LIST OF FIGURES

NOMENCLATURE

A_s	surface area
A_{or}	area of orifice
A, B	vapor constants for vapor saturation pressure
$d\vec{A}$	differential surface area
Bi	Biot number
c^*	collision frequency between vapor molecules and critical nuclei
c_d	dimensionless drag coefficient
c_p	specific heat at constant pressure
c_{pj}	specific heat of thermocouple junction
c_pT	enthalpy of ideal gas
c_v	specific heat at constant volume
c_vT	internal energy of ideal gas
C	combined conductance of piping line
C'_d	orifice discharge coefficient for choked flow
C''_d	orifice discharge coefficient for unchoked flow
C_c	Cunningham slip correction factor
C_{or}	conductance of orifice
CS	control surface
CV	control volume
d	diameter of nucleus or particle
d_d	diameter of droplet
d_j	diameter of TC junction
d_r	diameter of residue particle
d_o	initial diameter of nucleus

d^*	Kelvin diameter
D	diameter of vacuum chamber
D_{ch}	characteristic dimension of chamber
D_d	diffusion coefficient of particle
D_n	nominal dimension of vacuum component
D_v	diffusion coefficient of vapor
e	electromotive force (emf)
E_c	cooling effect
E_h	heating effect
$\vec{f}$	external body force
F_a	adhesive force
F_c	fraction of vapor molecule converted to liquid
F_d	drag force on particle
F_i	conversion factor of impurity
g	gravitational constant
gz	gravitational potential energy of unit mass
ΔG	free energy associated with condensation
ΔG_d	free energy change in the formation of droplet
Gr	Grashof number
h	heat transfer coefficient
h_L	laminar heat transfer coefficient
h_s	heat source rate
h_T	turbulent heat transfer coefficient
H	height of vacuum chamber
I	particle generation rate
J	nucleation rate

k	thermal conductivity
k_e	eddy diffusion coefficient
k_g	thermal conductivity of gas medium
k_o	thermal conductivity at initial temperature T_o
k_w	thermal conductivity of wall
Kn	Knudsen number
L_d	wall deposition loss
L_e	particle evaporation loss
L_v	latent heat of vaporization
L_s	heat of fusion
LT	life time of water droplet
m_s	mass source rate
M	molecular weight
Ma	Mach number
M_v	molecular weight of vapor molecule
n	particle concentration
n_1	concentration of vapor molecules
n_d	concentration of droplet
n_d^*	concentration of critical nuclei
n_{max}	maximum particle concentration
n_o	initial particle concentration
n_s	particle surface concentration
n_t	total number of droplet in a unit volume
n_w	water vapor molecule concentration
N	number of particles in chamber
N_{cnc}	cumulative CNC count

N_o	number of particle after venting
Nu	Nusselt number
p	gas pressure
p^*	dimensionless pressure
$\tilde{p}$	dimensionless pressure at minimum gas temperature
$\hat{p}$	dimensionless pressure at maximum vapor saturation
p'	indicated pressure of convectron vacuum gage
p_1	onset pressure for particle generation
p_2	onset pressure for near steady particle concentration
p_3	stop pressure for particle generation
p_d	vapor pressure at droplet surface
p_{max}	gas pressure at maximum particle concentration
p_o	initial gas pressure
p_s	saturation pressure of vapor
p_{sg}	saturation pressure of vapor in gas medium
p_{so}	initial saturation pressure of vapor
p_v	vapor pressure
p_{vj}	vapor pressure at the surface of TC junction
p_{vo}	initial vapor pressure
Pr	Prandtl number
q	ion charge
$\dot{Q}$	rate of heat transfer
Q_{or}	choked flow volumetric flow rate
r	ratio of gas pressure at pump inlet to that inside the chamber
r^*	critical pressure ratio
R	universal gas constant

Re	Reynolds number
Re_d	particle Reynolds number
Re_o	Renolds number associated with p_o
RH	relative humidity
RH_c	critical relative humidity
S	vapor saturation ratio
$\dot{S}$	rate of energy generation
S'	potential vapor saturation ratio (PVSR)
S_c	critical saturation for nucleation or condensation
S_e	effective pumping speed
S_{max}	maximum saturation ratio
S_p	intrinsic pumping speed of vacuum pump
S_v	venting speed
t	time
t^*	dimensionless time
t_2	terminal time of pump-down
t_{23}	pausing time between pump-down and venting
t_3	venting time
t_F	total sampling time
t_p	sampling period
T	absolute gas temperature
$\tilde{T}$	dimensionless minimum temperature
$\hat{T}$	dimensionless temperature associated with S_{max}
T^*	dimensionless temperature
T_d	vapor temperature at droplet surface
T_J	temperature of TC junction

T_o initial gas temperature

T_v vapor temperature

T_w wall temperature

u magnitude of velocity vector

$\vec{u}$ velocity vector

$u^2/2$ kinetic energy of unit mass

v_1, molecule volume

V volume of vacuum chamber

dV differential volume

V_c critical chamber volume for turbulent natural convection

V_p measured voltage for pressure

Vs particle setting velocity

V_T measured voltage for temperature

$\dot{W}$ rate of external work

Z dimensionless number

Z_c critical Z number

Ze Zeldovich nonequilibrium factor

Greek

α thermal diffusivity

α_o initial thermal diffusivity

δ boundary layer thickness

δ_1 atom diameter

δ_w water molecule diameter

ε liquid dielectric constant

ε_g dielectric constant of gas

η	boundary layer coefficient
γ	ratio of specific heat c_p to c_v
κ	Boltzmann constant
λ	gas mean free path
μ	dynamic viscosity
μ_o	dynamic viscosity at initial temperature T_o
μ_L	chemical potential of a molecule in liquid phase
μ_V	chemical potential of a molecule in vapor phase
ρ	gas density
ρ^*	dimensionless gas density
ρ'	liquid density
ρ_j,	junction density
ρ_o	initial gas density
ρ_p	particle density
ρ_v	vapor density
ρ_v/ρ	mass fraction of the vapor
σ	surface tension
σ'	Stefan-Boltzmann constant
τ	pumping time constant
τ_j	time constant of TC response
τ_w	wall shear stress
ω	heat penetrating rate
Ω	parameter list for condition of pump-down
Ω_c	critical W that indicates vapor condensation or nucleation
ξ	ratio of volume to surface area
Ψ	type of condensation process and associated parameter

CHAPTER 1

INTRODUCTION

1.1 MOTIVATION

This work is motivated by the need for contamination control in semiconductor manufacturing, which is one of the most critical issues for success in fabricating very large scale integrated circuits (VLSI). The integrated circuit is made from semiconductor substrate, mostly silicon, or GaAs wafer. As the scale of integration increases, the feature size of the circuits (the distance between circuit lines) shrinks. For a 1 M dynamic random access memory (DRAM) chip, the feature size is on the order of 0.9 μm. Particulate contamination is a major reason for the degradation in product performance and loss in product yield, because particles one tenth of the feature size have potential to cause circuit defect. The quantitative measurements indicated that 50% of defects in 64K, 70% in 256K, and 80% in 1M DRAMs were due to contamination (O'Hanlon, 1989).

Particles generated in vacuum systems, from equipment or processing, are a major contamination source (O'Hanlon, 1989; Smith, 1989). Because of advances in filtration and cleanroom technology, the contamination caused by cleanroom and personal has been significantly reduced. The contamination caused by particles generated from process and equipment has become more important, even dominant. Moreover, nearly half of the more than 100 operations in the current VLSI technology are performed in vacuum environments (Smith, 1989). Table 1-1 lists some vacuum processes and their pressure ranges. Therefore, it is very important to understand the phenomena of particle formation, transport and deposition in vacuum systems in order to improve semiconductor manufacturing processes.

Table 1-1 Vacuum classifications and processes[a]

Degree of Vacuum	Pressure Range, Torr	Process Performed
Low	$760 \geq p \geq 20$	• Epitaphial growth of semiconductor film
Medium	$20 \geq p \geq 10^{-3}$	• Sputtering • Plasma etching • Plasma deposition • Low pressure chemical vapor deposition
High	$10^{-3} \geq p \geq 10^{-7}$	• Thin film preparation • Electron microscopy • Mass spectroscope • Crystal growth • X-ray and electron beam lithograph • Production of cathode ray and other vacuum tubes
Ultrahigh	$10^{-7} \geq p \geq 10^{-10}$	• Ion implanter
Extreme Ultrahigh	$10^{-13} \geq p$	• Surface and material study

a. Abstracted from O'Hanlon (1980, Chap. 1)

A vacuum process involves many steps, as shown in Fig.1-1, which includes loading wafers into chambers, pump-down of gas in the chamber, processing, venting gas to the chamber, and unloading the wafers. Particles may be generated in any one of these steps. Borden and Baron (1987) have monitored the processing in an ion implanter by using a light scattering particle counter. They found that (i) during the pump-down period, a very high particle generation rate exceeding 1000 particles/min can be seen, many particles larger than 10 μm were observed; (ii) during the processing period, there were 300 to 700 particles/min, their size were less than 1 μm; (iii) during the venting period, almost no particles were observed.

In this thesis, the physical phenomena that occurs during the vacuum pump-down are investigated. The investigation is divided into two major aspects: thermodynamics and particle formation. Both will be studied theoretically and experimentally.

Although this study was initiated by needs of semiconductor manufacturing, the results can be applied to other vacuum related processes. Table 1-1 summarizes the classification of vacuum levels and various processes performed within vacuum systems.

1.2 PUMP-DOWN AS A THERMODYNAMIC PROCESS

Any vacuum process that utilizes a pumping device to evacuate gas molecules from a vacuum chamber is called a vacuum pump-down. This may cover a pressure range from 760 Torr (1 atm) to about 10^{-13} Torr, which is the best man-made vacuum on earth. According to the kinetic theory of gases, an ideal gas contains about 10^{19} molecules/cc at the standard temperature and pressure (STP), i.e., at 760 Torr (1 atm) and 0°C. When the number of molecules is reduced, the gas is rarefied. The gas contains only about 10^{4} molecules/cc at 10^{-13} Torr. Vacuum actually refers to the rarefied state of gas.

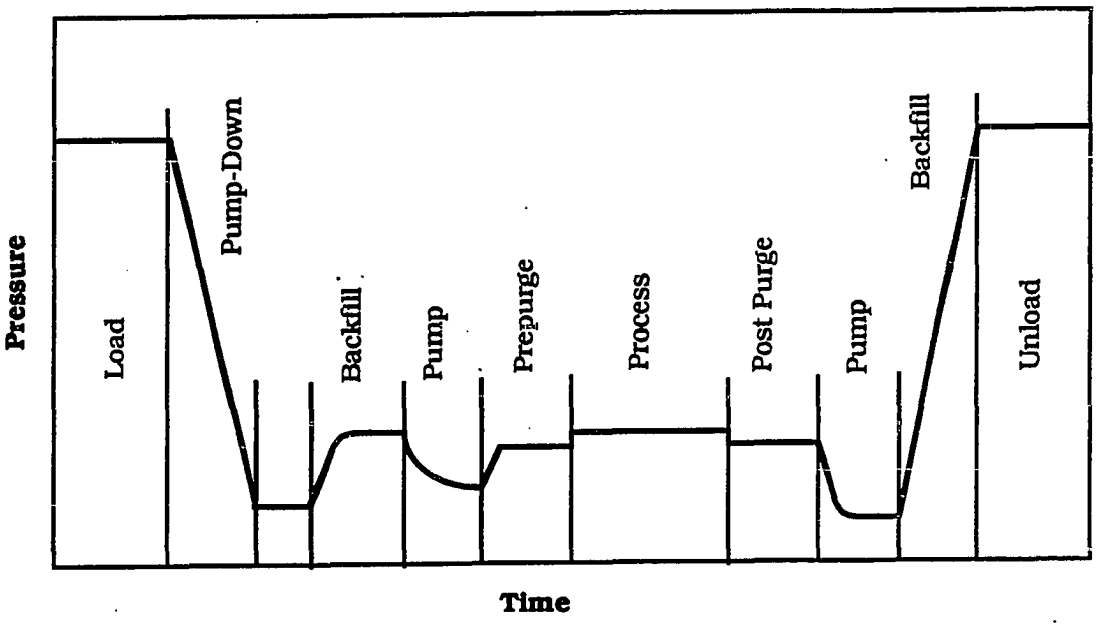

Figure 1-1 Schematic diagram showing typical vacuum process cycle

From the standpoint of thermodynamics, a pump-down is a nonequilibrium process which involves a continuous change in gas thermodynamic state, defined by the pressure, temperature, and composition of gas. The changes in gas state depend on the transport phenomena including gas flow, and heat and mass transfer that occur during pump-down.

Fig.1-2 shows a typical pump-down curve in evacuating a metal-gasketed vacuum system from one atmosphere pressure to ultrahigh vacuum. This curve is taken from O'Hanlon (1980, p130), and modified to include the roughing period (from 760 to 0.1 Torr) and baking action. At high pressure, the gas inside the vacuum chamber is first pumped out. When leaks and oil backstreaming are negligible, pressure decays nearly exponentially: $p \propto e^{-t/\tau}$, where t represents time and τ represents the pumping time constant (the ratio of chamber volume to pumping speed).

As the pressure is reduced below 10^{-5} Torr, outgassing from surfaces becomes important. Outgassing is the result of surface vapor evaporation, surface gas desorption (by thermal energy or electron and ion bombardment), and gas diffusion and permeation within solid material of walls. According to O'Hanlon, molecules on the surface, mostly water vapor up to 100 monolayers, are first desorbed, and in this period, $p \propto t^{-1}$. The gas such as hydrocarbon that is initially absorbed in the solid will diffuse to the surface, then degas, and in this period, $p \propto t^{-1/2}$ (the diffusion controls pressure decreasing rate). Finally, the pressure reaches its lowest limit when permeation becomes dominant. Permeation refers to the process by which gases are first absorbed from outside, then diffuse through the wall, and finally are desorbed. Actually, if ultrahigh vacuum is required, baking is absolutely necessary. Baking refers to the step in which the chamber wall temperature is elevated (maybe up to 400°C). Without this step, reaching 10^{-10} Torr may take years or may not be possible.

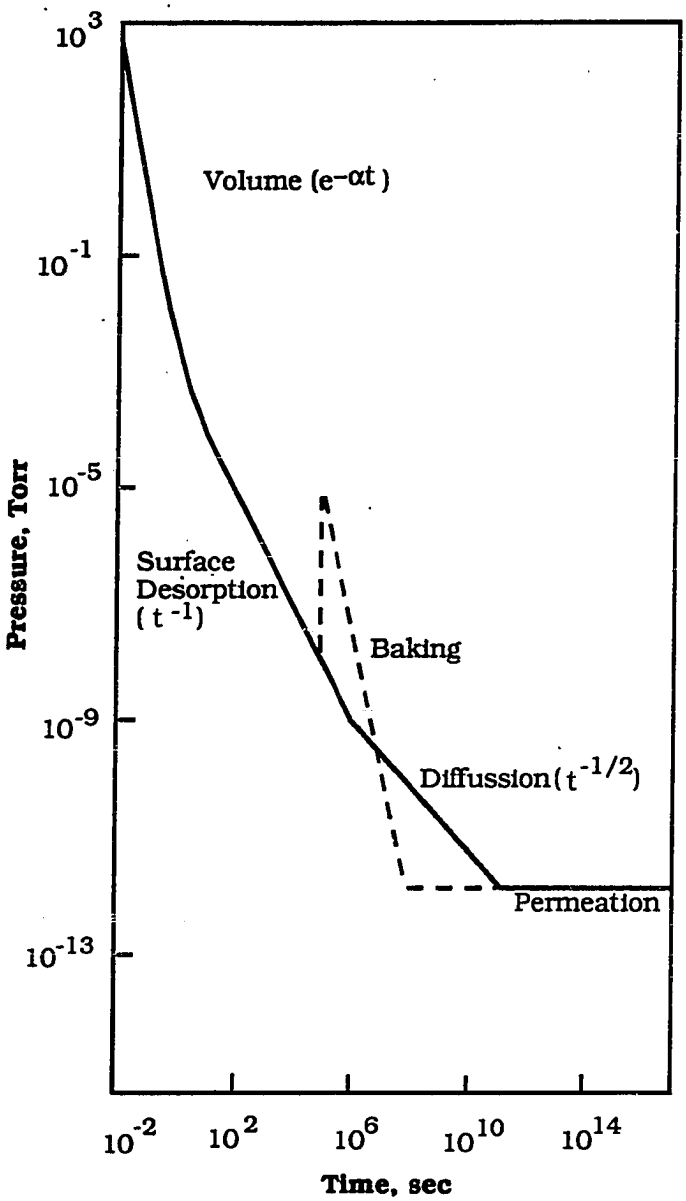

Figure 1-2 Schematic diagram of a pump-down curve from 1 atm to ultrahigh vacuum

Clearly, at very high or ultra high vacuum condition during pump-down ($p < 10^{-5}$ Torr), the surface phenomena and gas diffusion in the solid are the predominant physical processes, controlling the composition of residue gases inside the vacuum chamber. Pump-down in this range will not be studied in this thesis. Analyses of pump-down process including baking for this pressure range are available (for example, Kazazawa, 1989).

This work is limited to the study of the physical phenomena which occurs at high pressure during pump-down, and within the gas volume. The studies include gas flow through the valve and pump, heat transfer between the gas and chamber walls, and particle formation and transport in the vacuum system.

Because of the nature of vacuum work, the characteristics of pressure during pump-down have been thoroughly investigated both theoretically and experimentally (for example, O'Hanlon,1980, Chap. 10; Dushman, 1962, Chap. 2; Lewin,1965, Chap 4). However, it has been assumed in all these studies that temperature is time-independent, i.e., the pump-down is an isothermal process. As shown by the measurements in the present study, the temperature actually varies significantly in both time and space when pressure is reduced from 760 Torr to a lower value (about 0.1 Torr in this work). Below 0.1 Torr, temperature indeed remains constant (equal to wall temperature). There is no known theory, or systematic measurements of study this transient temperature variation, and of the accompanying phenomena such as thermally induced natural convection, change in vapor saturation, and variations in gas pressure and pumping speed because of temperature variation. The goals of the thermodynamic study in this work include:

1) Conduct systematic measurements to demonstrate the features of the gas transient temperature variation. Investigate all the parameters that may affect the gas temperature including pumping

speed, chamber geometry, gas medium, initial pressure, water vapor, and measurement location. This is the main goal of Chapter 2.

2) Develop a mathematical model for the process of vacuum pump-down to predict the temperature and pressure of the gas, and the saturation ratio of the condensable species. Carry out an order-of-magnitude study to find the predominant physical phenomena that may occur during pump-down (Chapter 3).

3) Find the characteristics of gas flow and heat transfer processes that occur in pump-down, the similarity solution to the gas thermodynamic state, and the dimensionless group that governs the pump-down processes (Chapter 4).

1.3 PARTICLE FORMATION DURING VACUUM PUMP DOWN

The earliest and the most complete "pump-down" experiments on the particle formation were performed in the end of last century by C.T. Wilson in his famous clouds chamber. In his experiments, Wilson demonstrated the nature of aerosol formation caused by condensation and nucleation during gas expansion, which is the similar situation to pump-down. Wilson's cloud chamber work has been described by many authors (for example, Friedlander, 1977; Wegner; 1969). Since Wilson's experiments reveal the nature of particle formation in pump-down, it is worthwhile to first review some details of these experiments.

Wilson filled the chamber with air which was saturated with water vapor, and then quickly expanded the air by actuating the motion of a piston. By assuming that the expansion was adiabatic, he then calculated the vapor saturation ratio from the expansion ratio. He found that during the expansion, the condensation of water vapor first

occurs on particles originally in the air when the saturation ratio just exceeded 1.

Wilson then removed these particles by repeatedly expanding the air in the chamber to allow particles in air to settle. After the air was free of particles, he found that the cloud droplets did not form until the saturation ratio reached about 4. Wilson postulated that under these condition the water vapor condenses on air ions which were created by cosmic rays and the decay products of radioactive gases that emanated from soil. He later supported this postulate by observing that the scale of condensation was enhanced when the chamber air was exposed to x-ray that produced a large amount of air ions.

Wilson removed these air ions by applying an electrical field, and then found that the appearance of droplets only occurred after the saturation ratio exceeded 8. Wilson interpreted this phenomena as the result of vapor condensation onto molecule clusters, a process known as homogeneous nucleation.

Since Wilson's experiments, many studies, both experimental and theoretical, have been performed. The Pollack counter is an instrument which uses the principle of a cloud chamber to measure particles in the atmosphere. The theories of homogeneous nucleation and nucleation on ions are available to predict the critical saturation ratio and nucleation rate. However, these studies have largely remained in the field of scientific research. Relating water vapor nucleation or condensation to particle formation during pump-down has only occured recently (see Borden and Baron, 1987; Zhao et al, 1987; and Wu et al, 1989).

Although the nature of particle formation is the same, the thermodynamic processes which occur during pump-down may differ from those that occurs in a cloud chamber. Studies on the cloud

chamber assume that the expansion process to be adiabatic. This is a good assumption because the expansion time is very short, which does not allow heat transfer from the chamber wall to the inner gas to occur. However, this is not true in most pump-down processes. As shown by this thesis, heat transfer process has a significant effect on particle formation during pump-down.

Direct observations of particles in vacuum chambers during pump-down have also been made. The early studies have been summarized by O'Hanlon (1987), and the main observation supporting particle formation during pump-down are: (i) water mist is observed in a glass bell jar during pump-down, (ii) decorative metallizers eliminate dull appearance of aluminum film by throttling the roughing pump, (iii) Ames et al. (1962) applied soft pumping to reduce particulate contamination in metal and insulation films for superconductive devices, and (iv) restricted pumping speed had been adapted in industrial practice. For example, one-half of vacuum deposition equipments manufactured by IBM had a flow restricting device. O'Hanlon also pointed out that little quantitative data was available to determine the flow restriction needed to reduce particulate generation and contamination.

Hoh (1984) first counted particles deposited on substrate caused by pumping and venting. The particles ware counted by a high oblique light instrument (SP20T), which was capable of resolving 2 μm latex spheres. He placed a substrate in a high vacuum silicon monoxide evaporator with a chamber volume of 75 liter, then performed fast pumping and venting, or slow pumping and venting. He found that the fast pumping and venting caused an enormous number of particles to deposit on the substrate, while the slow pumping and venting reduced the particle counts very effectively, from an uncountable number to 50 per 57 mm diameter substrate. Since the pumping and venting were combined, it was not known whether the particles were produced by pumping or by venting.

Bowling and Larrabee (1986) counted particles deposited in an Epi-Reactor during pump-down. Using a surface scanner, they counted the number of particles, size from 0.5 to 2μm, being a range of 820 to 2169 on a 100 mm wafer. Meeba et al. (1987) also measured particles deposited on a wafer as a function of pumping time constant.

Borden and Baron (1987) used a laser particle film monitor (PM-100), and first detected particle presence during pump-down in real time. Later, real-time measurements with the PM-100 during pump-down were also conducted by other authors (Chen et al, 1989; Wu et al, 1989).

The theoretical and experimental studies of particle formation during pump-down in the Particle Technology Laboratory, University of Minnesota, were started in 1987. Various aspect of these studies have been reported in the Review Meetings of Particulate Contamination Control Consortium, University of Minnesota. The experimental works include: the instrument developments and measurements on the number, volatility, and size of particles (Szymanski et. al, 1987, 1988), the measurements of temperature and pressure during pump-down (Zhao et al, 1988), the measurements of particle charge and the effect of step wise pump-down (Ahn et al., 1988), the investigation of nucleation and condensation in pump-down (Liu et al., 1989). The theoretical works include: thermodynamic and particle formation (Kuehn, et al., 1987), the estimation of particle deposition (Szymanski et al. 1988).

Although particle formation during pump-down has been extensively investigated, many critical issues remain unsolved. There are:

1) The hypotheses of mechanism of particle formation have not been critically tested. The following mechanisms have been proposed to

explain the particle formation during pump-down: (i) turbulent induced (for example, O'Hanlon, 1987; Chen et al, 1989; O'Hanlon, 1989), (ii) heterogeneous condensation on fine particles (Borden and Baron, 1987; Wu et al, 1989), and (iii) water vapor homogeneous nucleation or nucleation on ions (this work).

2) The investigation is still on a level of experimental observation, not quantitative and systematic. Therefore a quantitative criterion to avoid particle formation is not available.

The objectives of the particle formation study in this thesis are:

1) Develop a quantitative theory of particle formation, including condensation, nucleation, and a criterion to avoid particle formation. On the basis of the theory developed, obtain practical guidelines for clean pump-down design (this is the task of Chapter 5).

2) Perform quantitative experiments to verify the theory. Test the various hypotheses of the mechanism of particle formation based on the experimental observation. Show the characteristics of particle formation (Chapter 6).

1.4 APPROACHES IN THE STUDY OF PUMP-DOWN

The transport phenomena during pump-down have two unique features: time dependent and covering of all flow regimes, namely, continuum, transition, and free molecule regime. Although the governing laws of transport phenomena are always the same: conservation of momentum, energy, and mass, the approaches to apply them are different in different regimes.

The classification of flow regimes depends on the Knudsen

number, Kn = λ/d_n, where λ is gas mean free path and d_n is the nominal dimension of the object in the study. If Kn << 1, corresponding to high pressure and large objects, the phenomena is said to be in the continuum regime, which the inner molecule collisions predominate and all the transfer processes are "diffusion like". The approach used here is to represent the processes by a set of continuum equations (continuum mechanics). It is assumed that the driving forces for the transport phenomena are proportional to gradients of velocity, temperature, or concentration. The proportional constants are viscosity, conductivity, or diffusivity. Since the viscous effect is dominant, this regime is also called the viscous flow regime.

When Kn >> 1, corresponding to gas at low pressure or small objects, the process is said to be in the free molecule regime, in which collisions between molecules and the walls dominates, and the motions of molecules are "light like". This type of study is usually called collisionless molecular dynamics (Bird, 1976). Gas is treated as many billiard balls. Statistical thermodynamics is used to study the characteristics of transport phenomena here.

In the intermediate range, Kn is on the order of unity, where the mean free path and the object dimension are comparable. The phenomena here are said to be in the transition regime, in which both inner collision and collision with walls are important. Knudsen made many contributions to this regime. He modeled the phenomena in space as two regions: near the surface and far from the surface. The gas far from the surface still can be regarded as a continuum, while near the surface, the gas molecules interact with the surface individually. Therefore, the discontinuity exists in gas velocity or temperature or concentration near the surface: this is the so called "slip" phenomena. The physical processes that occur in this regime is usually complicated, and the understanding of it is largely based on the experimental knowledge. Advance in supercomputers has made numerical computation an important tool for studies in this regime.

The regimes of the phenomena studied in this work can be determined. The phenomena of interest are in the range of 760 to 0.1 Torr, and the minimum air mean free path $\lambda = 0.066$ μm (at 760 Torr and 20°C) and the maximum $\lambda = 0.05$ cm (at $p = 10^{-1}$ Torr). It can be easily checked that (i) heat transfer between the inner gas and the chamber wall is always in the continuum regime because $Kn \ll 1$ (note that the chamber diameter or height is much greater than 0.05 cm); (ii) gas flow though a tube, or orifice, is always in the continuum regime (the orifice or the pipe diameter is much larger than 0.05 cm); (iii) particle related phenomena, such as transport, condensation, or nucleation, may fall into all three regimes because the particle size covers a wide range of 20 nm to 10 μm.

CHAPTER 2

MEASUREMENT OF TRANSIENT GAS TEMPERATURE AND PRESSURE

ABSTRACT

The transient temperature of gas during vacuum pump-down is systematically measured with a modern data acquisition system. A substantial drop in gas temperature is observed. In a 47.3 liter chamber, when the effective pumping speed is 705 lpm and the initial temperature is 25°C, the maximum temperature drop is 70 °C for 50%RH room air, 95°C for dry nitrogen, and 105°C for high purity argon. It is found that the following factors have a significant effect on gas temperature history: effective pumping speed, chamber geometry, gas medium, initial pressure, water vapor concentration, and measurement location.

2.1 INTRODUCTION

The gas pressure during pump-down is a transient variable, but the gas temperature is commonly assumed to remain constant (Dushman, 1962, Chap. 2; Lewin, 1965, Chap. 4; or O'Hanlon, 1980, Chap. 10). For this reason, measurements of gas temperature during pump-down have not been reported in the literature of vacuum work.

Actually, the gas temperature in a chamber may vary significantly during pump-down, as shown by measurement, in both time and space when the pressure is reduced from 760 Torr to a lower value (about 1 Torr in our experiment). However, as the pressure is further reduced, the temperature indeed remains nearly constant (the same as the temperature of the chamber wall). It is the purpose of this chapter to

consider the transient gas temperature during pump-down from 760 to 0.1 Torr.

Before explaining the experimental details, overall aspects of this measurements will first be examined.

1) In addition to gas temperature, the gas pressure and the wall temperature are also measured. For finding correlations between these parameters, a modern data acquisition system is utilized to measure all variables simultaneously.

2) The pumping time constant, τ, determines the time scale of the transient events during pump-down. By definition, $\tau = V/S_e$, where V is the chamber volume and S_e is the effective pumping speed. A pump-down process reducing gas pressure from 760 to 0.1 Torr takes approximately 9τ. In this work, τ ranged from 0.7 to 25 seconds which covered a wide range of transient events.

3) Experimental factors affecting the measurements were identified as chamber size, gas medium, effective pumping speed, initial pressure, water vapor, and measurement location. The measurements were systematically conducted in order to show all the effects of the listed factors. The pump-down was performed in two cylindrical chambers, namely

Large chamber: V = 47.3 liters (D x H = 45 x 30 cm)
Small chamber: V = 0.26 liters (D x H = 8 x 5.2 cm)

where V is the chamber volume, and D and H are chamber diameter and height respectively. Three types of gases were tested: room air, dry nitrogen, and high purity argon. With a given gas and chamber, pumping rate S_e and initial pressure, p_o, were controlled independently, and two experiments have been conducted: (i) fixing p_o and changing S_e; (ii) fixing S_e and changing p_o. To check the

uniformity of the gas temperature, the gas temperatures are measured at six different locations in the large chamber.

4) Efforts were made to make the measurements accurate. Effects on temperature measurement from thermal inertia, wall radiation, and water vapor condensation were considered. Effect of gas temperature variation on pressure has also been considered.

2.2 EXPERIMENTAL METHOD

Figures 2-1 and 2-2 are schematic diagrams of the apparatus for pump-down in the large chamber and small chamber respectively. The vacuum system for the large chamber experiment is assembled by Applied Materials Inc. for the Particle Technology Laboratory, University of Minnesota. The small chamber setup is developed by Szymanski et al. (1987). I have developed a data acquisition system for pressure and temperature measurements and designed orifices for flow control. I have modified the small chamber setup to allow the temperature measurement.

Most of the measurements were performed in the large chamber. Fig.2-3 shows the measurement locations for gas temperature and wall temperature. The experimental method for the large chamber are described in detail from Section 2.2.1 to Section 2.2.2.

The experimental method for the small chamber is similar to that in the large chamber, and it will be briefly discussed in Section 2.2.3. Since the main purpose here is to show the effect of chamber size on gas temperature, only dry nitrogen is tested. All the gas temperature measurements are made at the center of the chamber. The effective pumping speed is varied, but the initial pressure is held at 760 Torr.

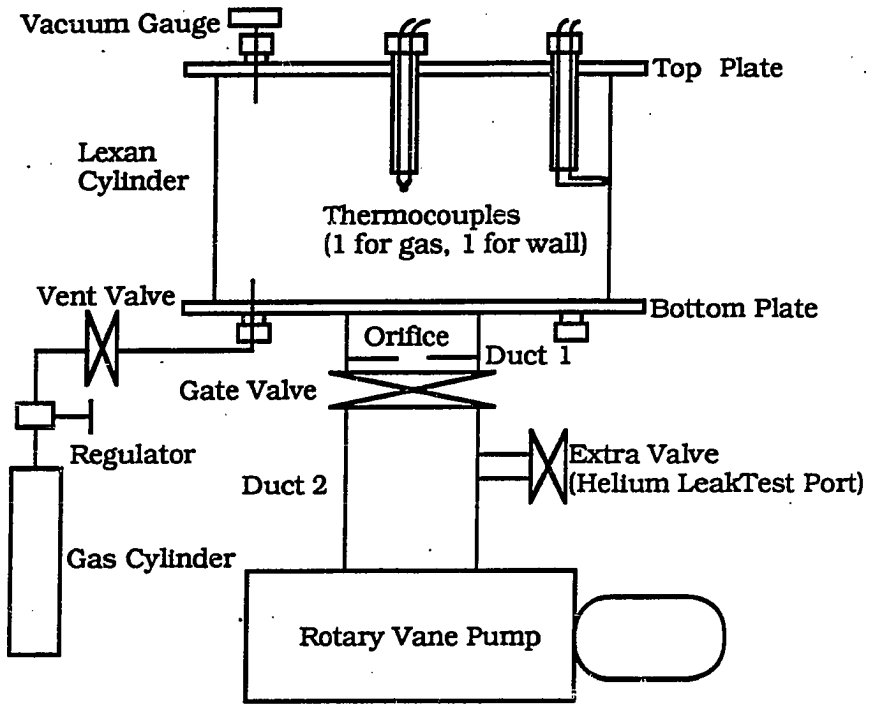

Major Component Specifications

Chamber 47.3 liters
Top Plate: Aluminum, 1.5 cm thick
Bottom Plate: Aluminum, 2.5 cm thick
Cylinder: Lexan, 1 cm thick
Diamter(ID) x Height = 45 x 30 cm

Vacuum Pump Trivac D60A
Maximum Pumping Speed: 705 lpm at 1 atm
Ultimate Pressure: 0.003 Torr without gas ballast
0.03 Torr with gas ballast
Manufacturer: Leybold-Heraeus Inc.

Orifice Diameter: 0.4, 0.6, 0.8, 1.0 , or 5.0 cm
Thickness: 0.32 cm

Duct 1 Diameter (ID) x Length = 5.0 x 7.5 cm
Duct 2 Diameter (ID) x Length = 5.0 x 27.5 cm (flexible bellows)

Figure 2-1 Experimental apparatus for performing vacuum pump-down in the large chamber.

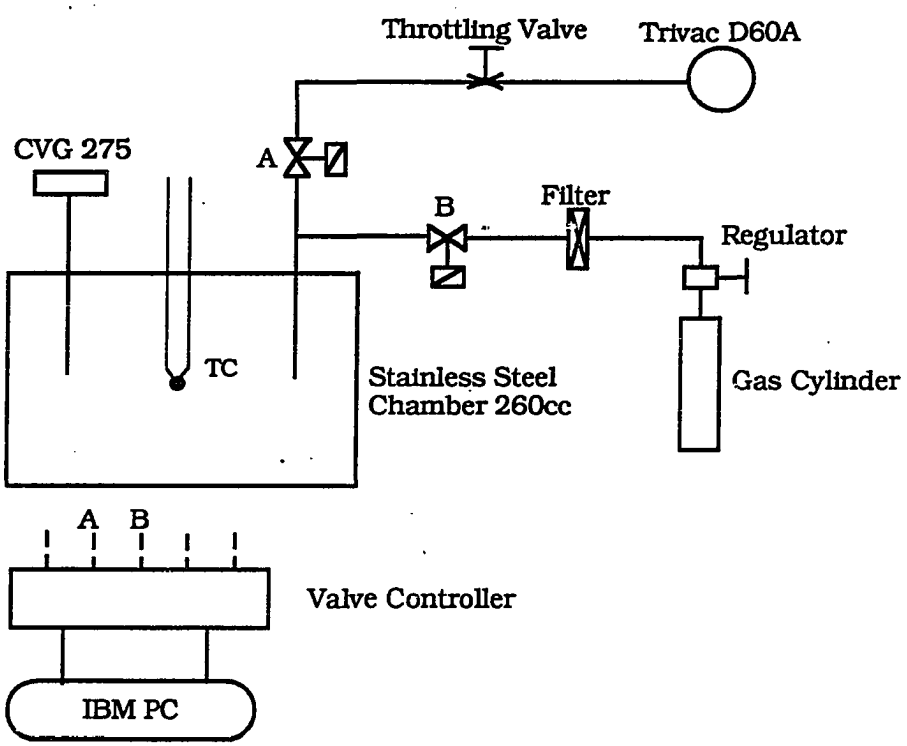

A, B: Nupro Air Activated Valve (SS-BNS4-C)
Vavle Orifice = 0.396 cm
Estimated Maximum Flow Rate = 148 lpm

Figure 2-2 Experimental apparatus for performing vacuum pump-down in the small chamber

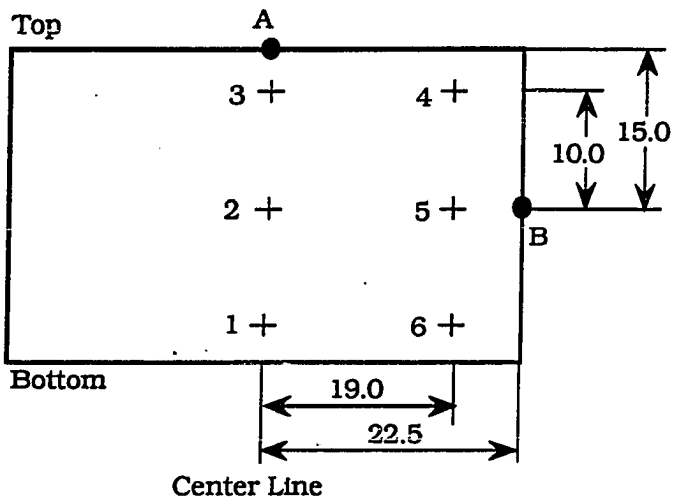

Dimensions in cm.

● Wall temperature measured (marked as A and B)

+ Gas temperature measured (numbered as 1 to 6)

Figure 2-3 Temperature measurement locations in the large chamber

2.2.1 Apparatus for the Large Chamber

As shown in Fig.2-1, the experimental setup for performing pump-down and measurement consists of a vacuum chamber; pumping control devices including a manually operated gate valve, a mechanical vacuum pump, and a flow restricting orifice; gas cylinders containning dry nitrogen or argon; feedthroughs on the top and bottom of the chamber for feeding TCs, connecting vacuum gauge, and venting gas; and a measurement system consisting of a vacuum gauge, two pair of TCs, a data acquisition system, and a personal computer. Details of the major elements are described below.

Orifice Assembly: Fig.2-4 shows the assemblies and dimensions of the circular orifices that were used for restricting the pumping rate. The orifices are made of stainless steel. Since their dimensions are in accordance with the ISO-KF and Universal Flanging System, these orifices can be easily installed by using a toggle clamp.

Vacuum Gauge: As shown in Fig.2-5, the pressure signal is sensed by a Convectron Vacuum Gauge (CVG), conditioned by a Vacuum Gauge Controller (VGC), and then collected by the data acquisition system. The CVG is a type of Pirani (thermal) gauge which measures pressure by measuring the heat loss from a heated wire. The wire forms one arm of a Wheatstone bridge and is maintained at a constant temperature (120°C for CVG 275). As the pressure decreases, the heat loss from the sensor wire decreases and therefore the bridge voltage reduces. The bridge voltage is conditioned by the VGC. The analog output has been calibrated against pressure by the manufacturer.

The advantage of the CVG is its wide measurement range (from 10^{-3} to 10^{3} Torr) and continuous reading which is suitable in measuring transient pressure. The disadvantage is that the CVG is calibrated under steady pressure, and it is accurate only below 30 Torr

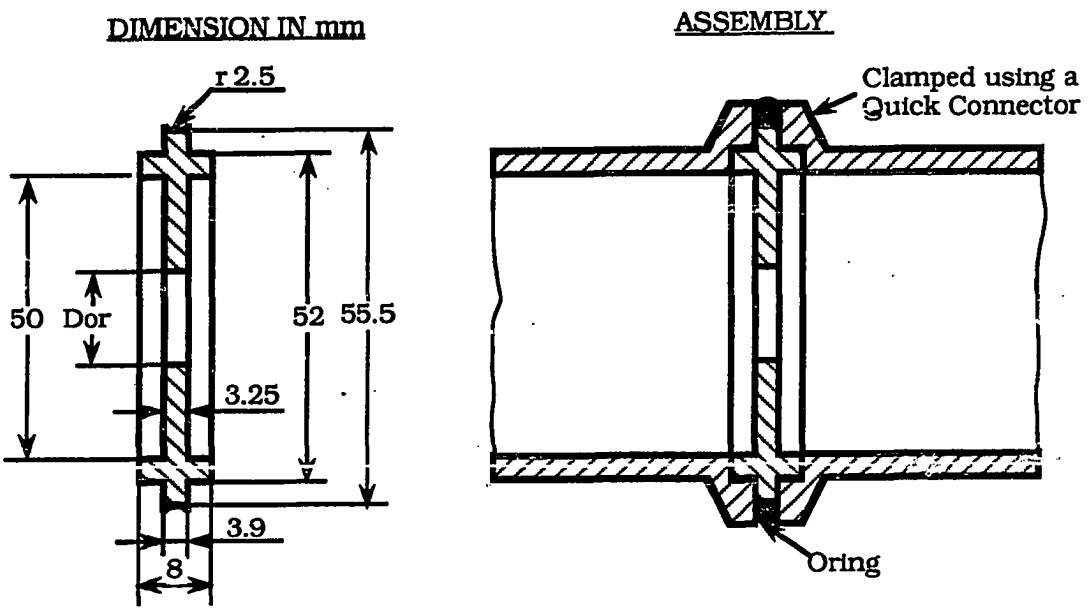

Dor = 4, 6, 8, 10, or 50 mm
All the other dimensions in the figure are in accordance with ISO-KF and Universal Flanging System.

Figure 2-4 Orifice dimension and assembly.

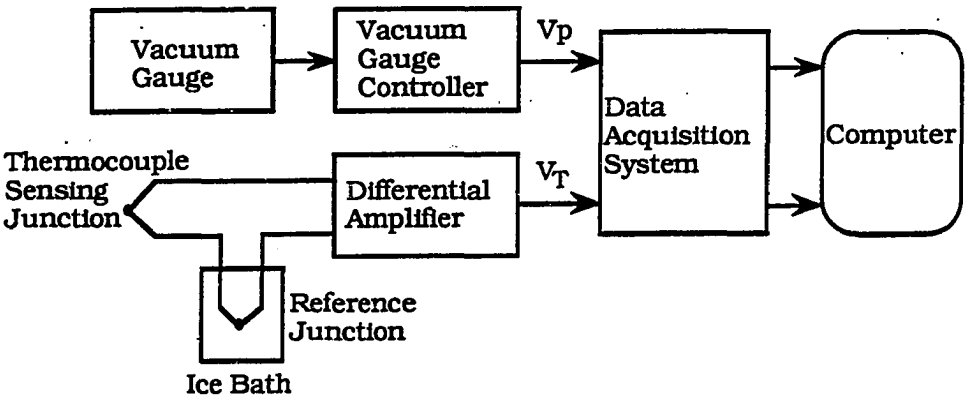

Measurement System Specifications

Vacuum Gauge
Convectron Vacuum Gauge (CVG 275)
Range: 1 mTorr to 1000 Torr
Vacuum Gauge Controller (VGC 316):
0 to 7 Volt (±5%) analog output
linearly increasing with pressure in log scale
Manufacturer: Granville-Phillips Co., Colorado

Thermocouple Type E
Sensitivity: 61 micro V/°C
Size: 0.001" (40 Gauge)
Time Constant: < 0.03 sec (estimated)
Manufacturer: Omega Engineering

Differential Amplifier
Gain: 400 (±2%)
Output Offset: 5 mv

Data Acquisition System DT2801
A/D Channel: 16SE/8DI
A/D Thruput: 13,000 sps
D/A resolution: 12 bits
Manufacturer: Data Translation Co., Marlborough, MA

In measurement
A/D Channels Used: 3
Programmable Gain: 1
Full Sampling Range: ±10 v

Figure 2-5 Data acquisition system and transducers

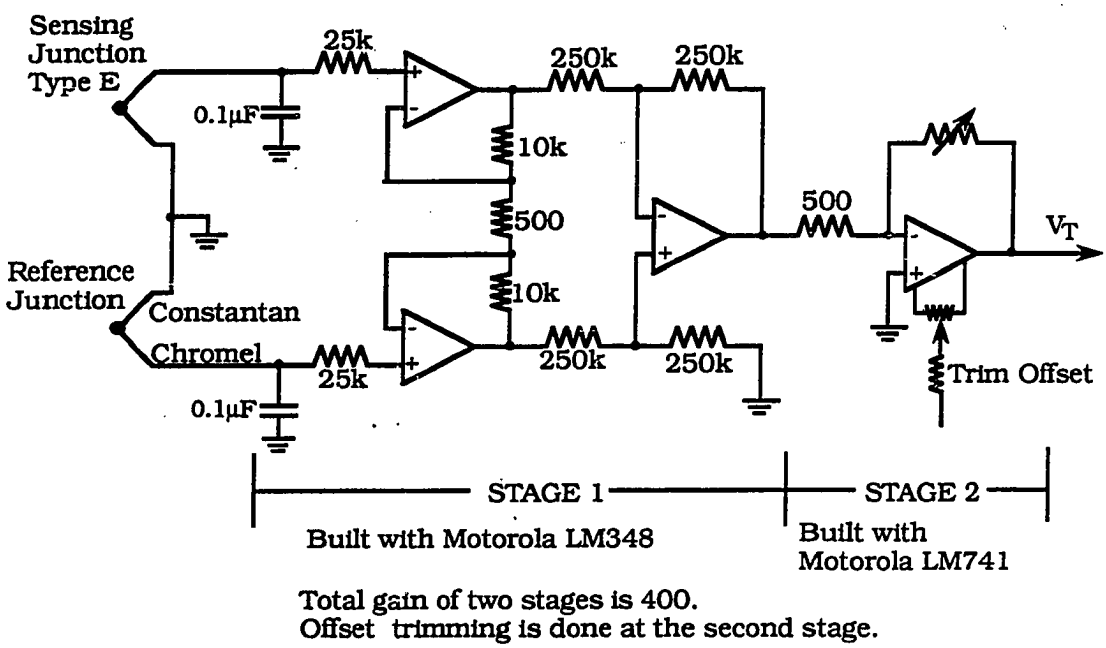

Figure 2-6 Thermocouple amplifier circuitry.

in transient pressure measurement. (Appendix B explains the CVG operation principle and its performance in detail.)

Thermocouples and Circuitry: The temperature signals are measured by E-type TCs with wire diameter of 0.0025 cm and estimated time constant of 0.03 seconds or less. The TC circuitry, shown in Fig.2-6, is built by referencing the circuitries given in Horowitz and Hill (1986). The reference junction is immersed in an ice bath, and the sensing junction is inserted into the chamber in a feedthrough. The differential electromotive force of these two junctions is then sent to an amplifier which consists of two stages. The first stage is a standard three-op-amp instrumentation amplifier with a gain of 41 (this stage has high differential gain and unity common-mode gain without any close resistor matching). The second stage is an ordinary op-amp whose adjustable resistor is set such that the total gain of the two stages is 400 (±2%). The output of the amplifier is then collected by the data acquisition system. When both the sensing junction and the reference junction are placed into the ice bath, the offset of the output of the applifer is adjusted to zero (actually within ±5 mV corresponding to temperature offset ±0.2°C). Two identical TC circuits have been built, one for gas temperature and one for wall temperature.

Data Acquisition System: Voltages for temperature and pressure are collected by DT2801 which consists of an interfacing board to a personal computer (IBM AT) and a terminal panel for connecting signals. The DT2801 provides eight differential input analog to digital (A/D) channels with throughput 13,000 sample per second. The A/D resolution is 12 bits. When the programmable gain is set to unity, the full sampling range (FSR) is ±10 V, and accuracy is ±0.03% FSR. In the measurements, three A/D channels are used: one for pressure, two for temperature.

A computer program, developed by using Microsoft Basic, controls the data acquisition sequences and data storage. Total sampling time, t_F, and sampling period, t_p, are the most important

parameters in collecting data. In our experiments, t_F is set to be equal to, or a little larger than, 9τ which is the approximate time required for the pressure to reduce from 760 to 0.1 Torr. Since τ ranges from 0.7 to 25 seconds, t_F ranges from 7 to 235 seconds in this work. After t_F is set, t_p determines total number of data to be collected, $N = t_F/t_p$. In our experiments, t_p ranges from 2 to 6 ms.

The program reads three channels sequentially for gas temperature, wall temperature, and pressure respectively. Therefore, the sampling period is $3t_p$ for a specific signal. For instance, if t_p is 2 ms, the program will read gas temperature at time of 0 ms, wall temperature at 2 ms, pressure at 4 ms, and gas temperature again at 6 ms, etc. Thus the time between two consecutive readings for gas temperature is 6 ms. Typically, the total data taken is 22,500 (7,500 for each signal).

2.2.2 Measurement Procedures

The measurement procedures in a pump-down are as follows:

1) Pumping rate restriction: An orifice is assembled between the chamber and the pump by using a quick connector.

2) Temperature measurement preparation: Two TCs are fed into the chamber through top feedthroughs to the desired location. Contact between the TC and the chamber wall (aluminum plate) is checked with a volt meter.

3) Pressure measurement preparation: The VGC is adjusted so that its reading of atmospheric pressure agrees with that of an accurate barometer.

4) Leak test of the vacuum system: This is done by evacuating the chamber to the lowest pressure possible, about 5×10^{-3} Torr,

closing the gate valve, and reading the gauge to see if the pressure increases.

5) Initial gas pressure setting: If no leaks are present, the test gas is vented to a desired initial pressure.

6) Data collection: First, run the data acquisition control program to set t_p and t_F, then open the gate valve to start pump-down. The data are then collected and stored in the computer.

2.2.3 Experimental Method for the Small Chamber

As shown in the Fig.2-2, the pump-down sequences are controlled by two solenoid-pneumatic valves named A and B. In the pumping period, A is open and B is closed. In the venting period, B is open and A is closed. The IBM AT controls, via a valve controller, the on/off timing of both valves with 0.1 seconds accuracy. A throttling valve between valve A and the vacuum pump sets the pumping rate. The measurement system for the small chamber is the same as that for the large chamber. The procedure to perform pump-down for the small chamber is the same as that for the large chamber except the pumping rate is adjusted using a throttling valve instead of orifices.

2.3 PRESSURE MEASUREMENT RESULTS AND DISCUSSIONS

Fig.2-7 shows typical measured voltage of pressure V_p and temperature V_T versus time during pump-down. Under the same experimental conditions (pump, chamber, orifice, gas, and initial pressure), these measured voltages are very repeatable. V_p is converted to the indicated pressure according to the CVG calibration. V_T is converted to temperature according to the thermocouple calibration. The results are shown in Fig.2-8. The details of pressure characteristics, conversion, and accuracy are discussed first.

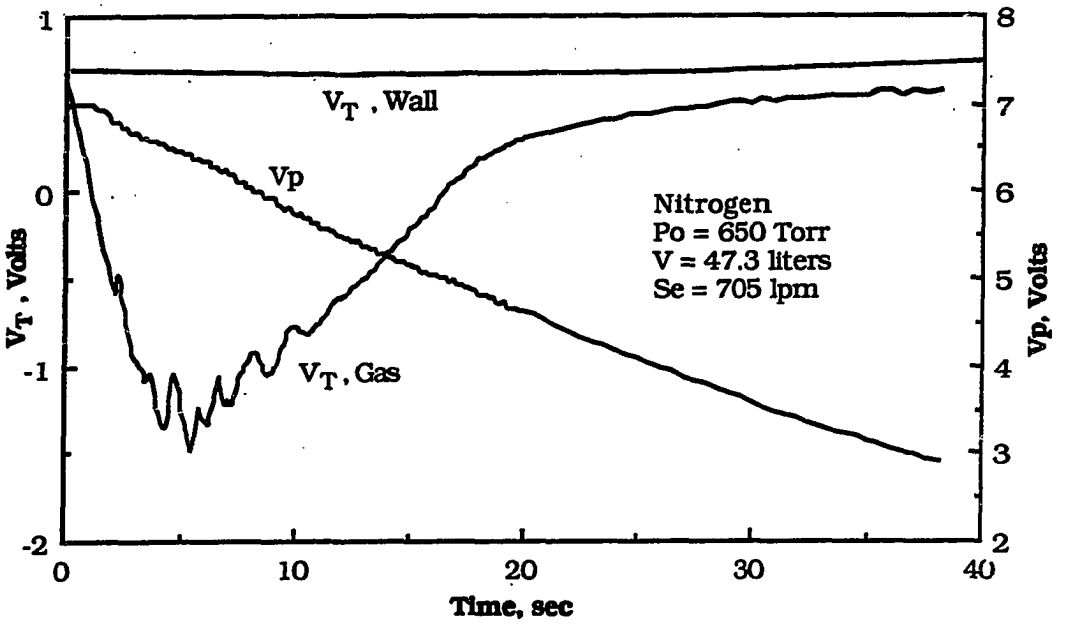

Figure 2-7 Typical analog output of the thermocouples and the vacuum gauge vs. time during pump-down

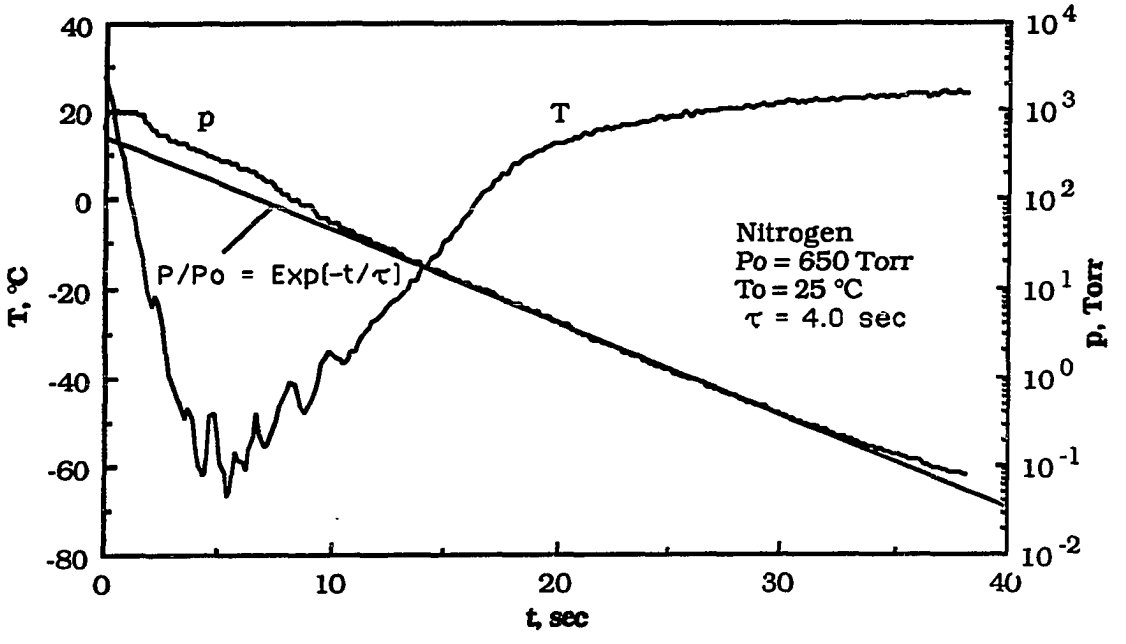

Figure 2-8 Typical gas temperature and pressure vs. time during pump-down

2.3.1 Characteristics of Pressure History

It has been commonly accepted in vacuum work that the pressure p during pump-down in the viscous flow regime decays exponentially with a time constant τ, i.e.,

$$\frac{p}{p_o} = e^{-t/\tau} \tag{2.1}$$

where

$$\tau = \frac{V}{S_e} \tag{2.2}$$

The conditions for Eq.(2.1) are that (i) the vacuum system is leak-free or that leaks are negligible, (ii) the pump oil backstreaming is negligible, (iii) the pump-down process is isothermal, and (iv) the effective pumping speed S_e is constant. The first two conditions are usually satisfied when $p \geq 0.1$ Torr. However, the third condition is not met -- temperature decreases in the initial pump-down, as shown in Fig.2-8, which leads to the following consequences:

1) Eq.(2.1) is not exactly correct and the interpretation of τ as the time constant of pressure decay is not precise. For this reason, τ is referred to as the pumping time constant in this thesis.

2) Decrease in temperature has two effects on the pressure. First, it reduces the kinetic energy and therefore the pressure of the gas: Consider that S_e remains constant regardless of the temperature change, one can find that the density instead of the pressure decays exponentially, i.e., $\rho/\rho_o = e^{-t/\tau}$. According to the perfect gas law,

$$\frac{p}{p_o} = \frac{T}{T_o} e^{-t/\tau} \tag{2.3}$$

Secondly, it may slow down the pumping speed and therefore the rate of pressure decrease. For example, if a critical orifice is used to restrict pumping rate S_e, then S_e is found to be proportional to $\sqrt{T}$ (see Chapter 3).

3) The accuracy of Eq.(2.1) depends on τ, and on pressure. The larger the τ, the more accurate Eq.(2.1) becomes because the larger τ results in a lower temperature drop. For p_o = 760 Torr and τ = 4.0 seconds (corresponding to the fastest pumping rate used in the large chamber), the simultaneous calculation of pressure and temperature, made in Chapter 3, shows that Eq.(2.1) may over-predict the pressure by 35% in the worst case in the period of $0 < t/\tau < 3$; Eq.(2.1) is accurate when $t/\tau > 3$, i.e., the pressure does decay nearly exponentially below certain pressures (< 40 Torr in this experiment) where $T \approx T_o$.

4) Viewing the pressure history in pump-down as a whole, it is found that the temperature effect is minor. Note that the ratio of pressure, p/p_o, varies over nearly 4 orders of magnitude while the ratio of temperature, T/T_o, varies form 1 to 0.65, as shown in Fig.2-8. Eq.(2.2) indicates that it takes approximately 9τ for the pressure to reduce from 760 to 0.1 Torr. Eq.(2.1) is accurate enough from an engineering point of view.

2.3.2 Indicated Pressure of the CVG

Gas pressure is measured with CVG. The indicated pressure of the gauge, p', is found from measured voltage V_p. According to the calibration for the CVG

$$V_p = \log(p') + 4 \qquad (2.4)$$

where p' is in Torr and V_p is measured voltage in Volts.

For steady pressure, p' equals the true pressure from 10^3 to 10^{-3} Torr. However, for transient pressure, p' equals the true pressure only when p' ≤ 30 Torr, above which p' is higher than the true pressure. As seen in Fig.2-8, an overshoot in p' above 760 Torr is observed. This phenomena has also been observed by Chen et al. (1989). Appendix B analyzes the gauge operation principle in detail, and shows that the false reading in pressure above 30 Torr is caused by the disturbance of gas temperature drop and the gas flow near the sensor wire inside the CVG.

2.3.3 Determination of τ and S_e

If Eq.(2.1) is true at all times, τ is the time when $p/p_0 = 0.368$ -- if p_0 = 760 Torr, τ is the time when pressure reaches 280 Torr. Error will occur if one directly uses this interpretation to find τ because, as has been indicated, the temperature decreases in the period $0 < t/\tau < 3$. Taking the temperature drop into account, Eq.(2.3) shows that it only takes 0.64τ to reach $p/p_0 = 0.368$ if $T/T_0 = 0.7$ at the pressure. Therefore, care must be taken in using Eq.(2.1) to determine τ. An alternate method, which is more accurate, is used to determine τ, as described below.

Both Eq.(2.1) and Eq.(2.3) is accurate for pressure below 30 Torr where true pressure is equal to gauge indicated pressure (p = p'). Substituting Eq.(2.1) to Eq.(2.3),

$$V_p = \frac{-0.4343}{\tau} t + V_{po} \qquad (2.5)$$

where V_{po} is the gauge voltage at initial pressure, a constant for a pump-down process. Therefore below 30 Torr, V_p decreases linearly with time t (see Fig.2-8). The slope is $\frac{-0.4343}{\tau}$, from which τ is identified. This method is equivalent to the "constant volume method"

(Lewin, 1965) except that we have taken the advantage of Eq.(2.3) which varies linearly with pressure on a log scale.

For pump-down of nitrogen in the large chamber with D_{or} = 5.0 cm, τ is identified to be 4.0 seconds which makes Eq.(2.1) fit the pressure below 30 Torr extremely well, shown in Fig.2-8.

Table 2-1 Measured effective pumping speed for different orifice sizes[a]

D_{or}, cm	Nitrogen or Air		Argon	
	τ, sec	S_e, lpm	τ, sec	S_e, lpm
5.0[b]	4.05	705	5.05	562
1.0	5.10	556	6.05	469
0.8	6.50	437	8.00	355
0.6	10.50	270	12.80	222
0.4	20.50	138	30.50	93

a. Test condition: Chamber volume V = 47.3 liter, T = 25°C.
b. Same as the pipe tube size. In this case, the S_e is the same as the intrinsic pumping speed of D60A.

In the large chamber experiments, S_e and thus τ is controlled by circular orifices with diameter D_{or} = 0.4, 0.6, 0.8, 1.0, or 5.0 cm respectively. Table 2-1 lists τ and S_e determined for each orifice for room air, nitrogen, and argon. Note $S_e = \frac{V}{\tau}$ where V = 47.3 liters. These data agree with the calculation in Chapter 3 to within ±5%. The results are summarized as follows:

1) Nitrogen and air have the identical S_e under the same pumping conditions (chamber, pump, and orifice) because they have almost the same physical properties.

2) The S_e of argon is less than that of nitrogen by approximate 20% under the same pumping conditions. The reason is that argon molecules are heavier and thus are more difficult to be pumped out.

3) The S_e identified for D_{or} = 5.0 cm can be regarded as intrinsic pumping speed S_p because the flow resistance through this orifice is negligible. Therefore, S_p = 705 lpm for nitrogen and S_p = 562 lpm for argon for the vacuum pump used.

4) After τ is determined, Eq.(2.3) is used to determine the pressure from 760 to 30 Torr, where T/T_0 is obtained from the measurements.

2.4 GAS TEMPERATURE DETERMINATION

The gas temperature is obtained from the measured thermocouple voltage, V_T. To be more exact, V_T is an indication of the TC junction temperature T_j. It must be realized that T_j may not be equal to the gas temperature because of the thermal inertia of the TC, wall radiation, and condensation or evaporation at the TC junction (if condensable species are present). If these effects are negligible, the junction temperature can be regarded as the gas temperature. Otherwise corrections must be made. In this section, the conversion from V_T to T_j and its uncertainty analysis are first carried out, and then the correction of the measured gas temperature is discussed.

Note: temperature is in units of K and pressure is in units of Torr in all the following equations unless otherwise noted.

2.4.1 Thermocouple Junction Temperature

The principle of using a thermocouple to measure temperature is well known. When two dissimilar materials are joined to form a junction, an electromotive force (emf), will be induced. The induced emf is a function of the junction temperature. By measuring the emf, the junction temperature is measured. For the E-type of TC, whose composition and physical properties are listed in Appendix A, the relationship between the junction temperature T_j in °C and the emf, e, in Volts is expressed as a polynomial

$$T_j = a_1 e + a_2 e^2 + a_3 e^3 + a_4 e^4 \qquad (2.6)$$

where the coefficients a_i (i=1, 4) are listed in Table A-2. The emf is found from V_T in Volts according to

$$e = \frac{1000\ V_T}{G_{A/D}\ G_A} \qquad (2.7)$$

where $G_{A/D}$ and G_A are the gain of the A/D conversion and the differential amplifier respectively. In the measurements, $G_{A/D}$ = 1 and G_A = 400. With Eq.(2.6) and (2.7), T_j can be determined from V_T.

The total uncertainties in determining the junction temperature can be estimated by

$$\Delta T_j = \frac{dT_j}{de}\,\Delta e \qquad (2.8)$$

where $\frac{dT_j}{de}$ is about constant which can be found from e = 0, i.e., $\frac{dT_j}{de}$ = 17.3 °C/mV. The uncertaintly in determining e is

$$\frac{\Delta e}{e} = \sqrt{\left(\frac{\Delta G_{A/D}}{G_{A/D}}\right)^2 + \left(\frac{\Delta G_A}{G_A}\right)^2 + \left(\frac{\Delta V_T}{V_T}\right)^2} = \pm 3.2\%$$

where $\left(\frac{\Delta V_T}{V_T}\right) = \pm 0.1\%$, $\left(\frac{\Delta G_{A/D}}{G_{A/D}}\right) = \pm 1\%$, $\left(\frac{\Delta G_A}{G_A}\right) = \pm 3\%$ are the uncertainty of V_T, $G_{A/D}$, and G_A respectively. The maximum e measured is about 4 mv, corresponding to $\Delta e = 0.12$ mV. Thus the uncertainty in determining the junction temperature is within ± 2°C.

2.4.2 Gas Temperature Correction

The TC junction temperature T_j determined above is equal to the gas temperature T only when the junction and the surrounding gas is in thermal equilibrium. However, this condition may not be satisfied since both T and T_j are both changing during pump-down. The energy balance equation for the TC junction yields

$$T - T_j = \tau_j \frac{dT_j}{dt} - \frac{(T_w^3 - T_j^3)\,\kappa\, d_j}{k_g\, Nu} + \frac{D_v\, M\, L_v}{R\, k_v}\left(\frac{p_{vj}}{T_j} - \frac{S\, p_{sg}}{T}\right) \quad (2.9)$$

I II III

Each term in the right side of equation (RSE) will be explained and estimated below.

A. Response of Thermocouple

The first term in the RSE of Eq.(2.9) represents the delay of the TC response to the gas temperature.

$$I = \frac{\tau_j\, dT_j}{dt} \quad (2.10)$$

where dT_j/dt is the rate of the junction temperature change and τ_j is the time constant of TC response

$$\tau_j = \frac{\rho_j c_{pj} d_j^2}{6 Nu k_g} \qquad (2.11)$$

where d_j, ρ_j, c_{pj} are the junction diameter, density and specific heat respectively; k_g, the thermal conductivity of the gas medium; and Nu, the Nusselt number of convective heat transfer at the junction. For a spherical object in the continuum regime

$$Nu = 2 + 0.376\, Re^{1/2}\, Pr^{0.6} \qquad (2.12)$$

where Re is the Reynolds number and Pr is the Prandtl number. The junction used in our measurement can be reasonably approximated as a sphere of 0.005 cm, and thus the above formula is valid when the pressure is above 1 Torr (Kn < 0.1). The first term in the RSE of Eq.(2.12) is the heat transfer due to heat conduction and the second term is the enhancement of heat transfer due to convection.

The junction temperature tends to fall behind the change of gas temperature because of its thermal inertia. If the gas temperature is decreasing, $T_j > T$ and vice versa. This effect becomes significant when a large TC (large τ_j) is used in a fast temperature changing environment (large dT/dt). In the following discussion, τ_j and dT_j/dt in this measurement are estimated.

Since the gas velocity inside the chamber is usually low and the junction size is small, the enhancement of heat transfer due to convection is negligible, and thus Nu = 2. Using the air and junction properties listed in Appendix A, the τ_j for our TC is estimated to be less than 0.03 seconds.

The dT_j/dt depends on the change rate of gas temperature dT/dt. As shown in Chapter 3, the maximum dT/dt occurs at the

beginning of pump-down where the expansion cooling dominates and the wall heating can be neglected.

$$\frac{dT}{dt} = - \frac{(\gamma - 1)\, T}{\tau} \qquad (2.13)$$

where T is in the unit of K. The smallest τ for the 47.3 liter chamber is 4 seconds. Then dT/dt is about 30 K/s. The dT_j/dt is less than but close to dT/dt. Thus the maximum error caused by the response delay is estimated to be less than -1°C. For the 260 cc chamber, the smallest τ used is 0.7 seconds, and thus the maximum dT_j/dt is 150 K/s. The response error in this case can be as high as -4.5°C and thus needs to be corrected.

B. Wall Radiation

The second term in the RSE of Eq.(2.7) represents the effect of the wall radiation which tends to enhance the junction temperature during pump-down:

$$II = \frac{(T_w^3 - T_j^3)\, \sigma'\, d_j}{k_g\, Nu} \qquad (2.14)$$

where T_w is the wall temperature and σ' is the Stefan-Boltzmann constant. The lowest junction temperature T_j detected in pump-down is about 203 K, while the wall temperature T_w remains almost at 298 K. Using the values listed in Appendix A, we find that the maximum junction temperature elevation due to the wall radiation is approximately 0.005°C, which is negligible.

C. Condensation and Evaporation at the Thermocouple Junction

When water vapor is present, the thermocouple junction may become a condensation site when the junction diameter is larger than the Kelvin diameter

$$d^* = \frac{4\sigma M}{\rho' R T \ln(S)} \tag{2.15}$$

where M is the molecular weight of vapor; R, the universal gas constant; S, the vapor saturation ratio; σ, the surface tension of the liquid; and ρ', the density of the liquid. Alternatively, if the condensate is already on the junction, and its total size (condensate plus the junction bead) is smaller than the Kelvin diameter, the condensate will evaporate. Actually, for the TC used in our measurement (d_j = 50 μm), condensation will occur when $S > 1$ and evaporation will occur when $S < 1$. The condensation tends to elevate the junction temperature to cause $T_j > T$ and evaporation does just the opposite.

The third term in the RSE of Eq.(2.9) represents the elevation (or depression) of the junction temperature due to vapor condensation (or evaporation). Its magnitude can be estimated by neglecting term I and II in the equation, i.e.,

$$T - T_j = \frac{D_v M L_v}{R k_g}\left(\frac{p_{vj}}{T_j} - \frac{S p_{sg}}{T}\right) \tag{2.16}$$

where L_v is the latent heat of vaporization; D_v, the diffusion coefficient of the vapor; p_{sg}, the saturation vapor pressure at T:

$$\log(p_{sg}) = A + \frac{B}{T} \tag{2.17}$$

where A and B are the vapor constants; and p_{vj}, the vapor pressure at the junction surface. Since the Kelvin effect can be neglected, p_{vj} can be regarded as the saturation pressure at T_j:

$$\log(p_{vj}) = A + \frac{B}{T_j} \qquad (2.18)$$

Eq.(2.16) has the same form for the condensation on a liquid droplet, which is derived by assuming a uniform junction temperature and quasi-steady mass and heat transfer processes (Davies, 1978). For the given T and S, the only unknown in Eq.(2.16) is T_j which can be solved by iteration. The result is shown in Fig.2-9.

As an example, let us consider an adiabatic pump-down of clean air of 55% RH. Using the adiabatic relationship, one can find that the saturation ratio S will be 8 when T is cooled to -20°C. As shown in Fig.2-9, T_j will be 13°C higher than T. This estimation shows that the effect of water vapor is rather significant for the humid air. However, it is difficult to find the actual difference between T and T_j caused by the water vapor condensation. The reason is the uncertainties in determining the saturation ratio because: (i) the water vapor condensing onto foreign nuclei and the chamber wall cause a depression in the saturation ratio (this process has large uncertainties), and (ii) the pump-down can not be completely regarded as an adiabatic expansion process because of wall heat transfer.

2.4.3 Summary

The total uncertainty in determining the TC temperature is within ±2°C. The effect of wall radiation on temperature measurement is negligible. The effect of TC response delay is negligible for the measurement in the large chamber, but it needs to be considered for the measurement in the small chamber. The effect of water vapor on gas temperature measurement is small for dry nitrogen and argon, but it may be significant for moist air.

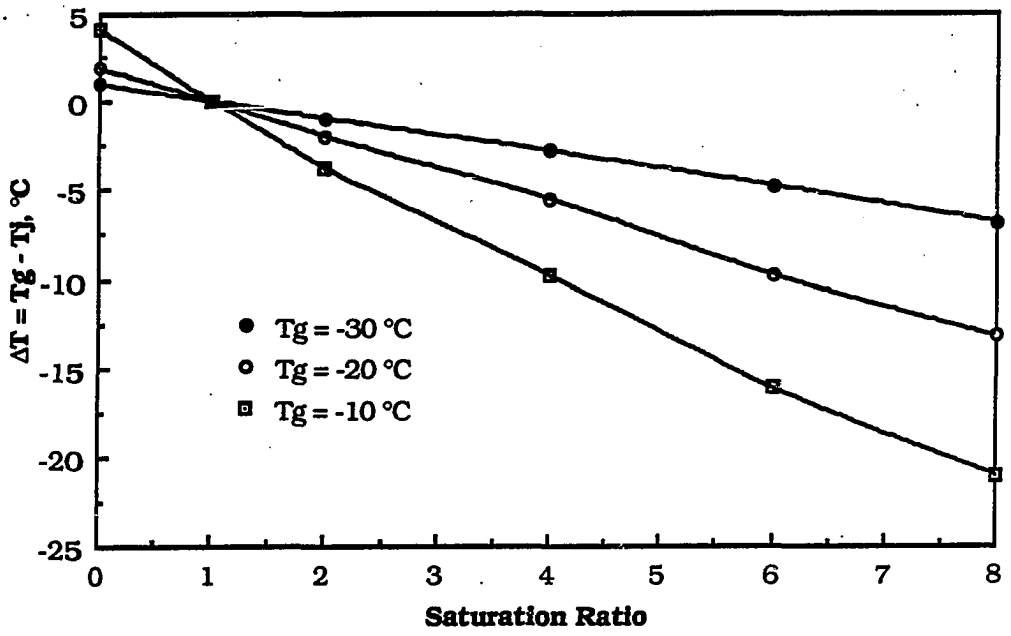

Figure 2-9 Effect of water vapor condensation or evaporation on gas temperature measurement

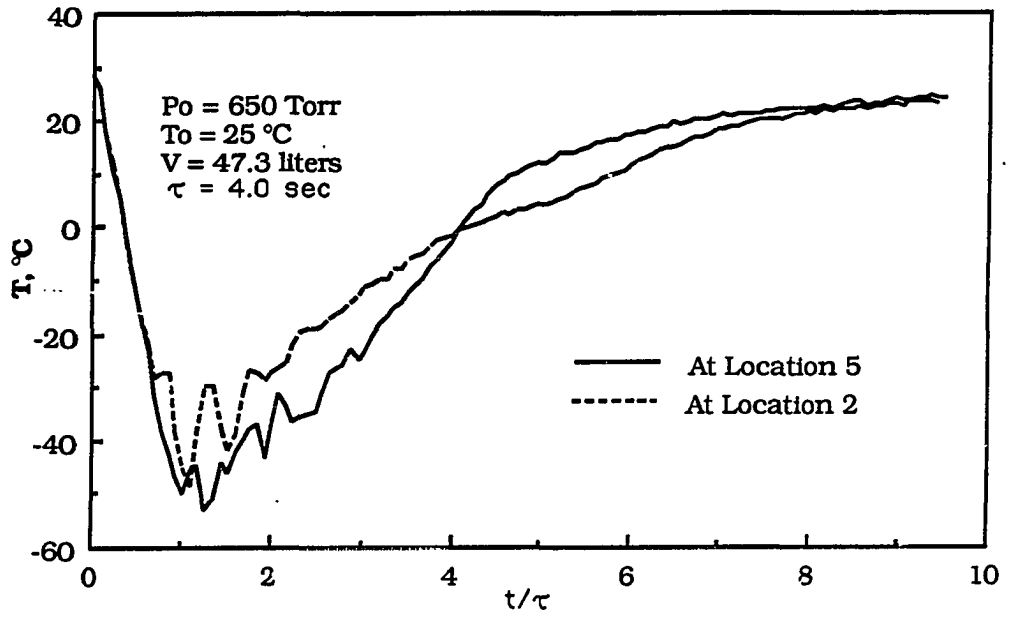

Figure 2-10 Comparison of nitrogen temperature at different locations

2.5 TEMPERATURE MEASUREMENT RESULT AND DISCUSSION

Because the wall temperature at the internal gas-wall interface varies less than 2°C during pump-down (see Fig.2-7), we will emphasize the data for gas temperature. Fig.2-8 and Figs. 2-10 to 2-16 show typical gas temperature during pump-down. All the temperature data presented are at the location 6 in the large chamber unless otherwise noted. The measured data for dry nitrogen have been reported in detail, and the data for argon and room air are presented for the comparison purposes.

2.5.1 General Features of Transient Temperature

Fig.2-8 shows general features of transient temperature during pump-down. The nitrogen temperature starts with 25°C, decreases dramatically to -70°C, and then recovers to 25°C in the later period. The temperature valley is caused by two competing processes: the cooling due to the gas expansion and heating due to the heat transfer from the chamber wall. As it will be derived in Chapter 3, the rate of temperature change can be predicted by

$$\frac{dT}{dt} = \frac{h A_s T}{p (\gamma - 1) V} (T_w - T) - \frac{(\gamma - 1) T}{\tau} \qquad (2.19)$$

where h is the average heat transfer coefficient at the chamber walls; A_s, the surface area of the chamber; and γ, the ratio of specific heat. The first term in the right hand side of this equation represents wall heating and the second term represents adiabatic expansion cooling. The cooling term is more or less constant for a given τ. The heating term is proportional to the temperature difference $(T_w - T)$ and is inversely proportional to the pressure. For the time being, the average wall heat transfer coefficient h is assumed to be constant.

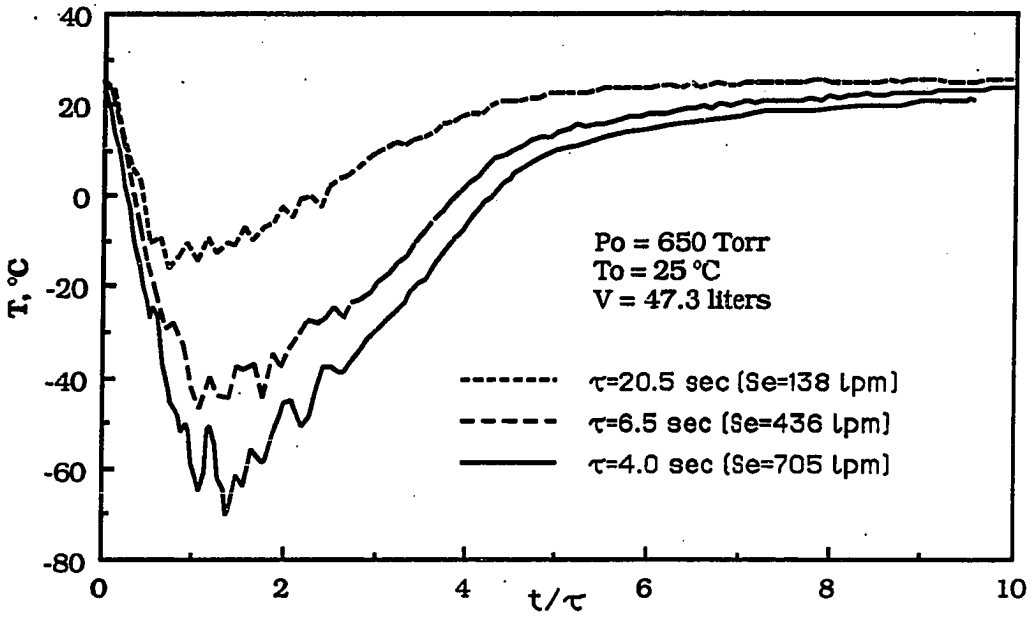

Figure 2-11 Nitrogen temperature histories under different pumping rates

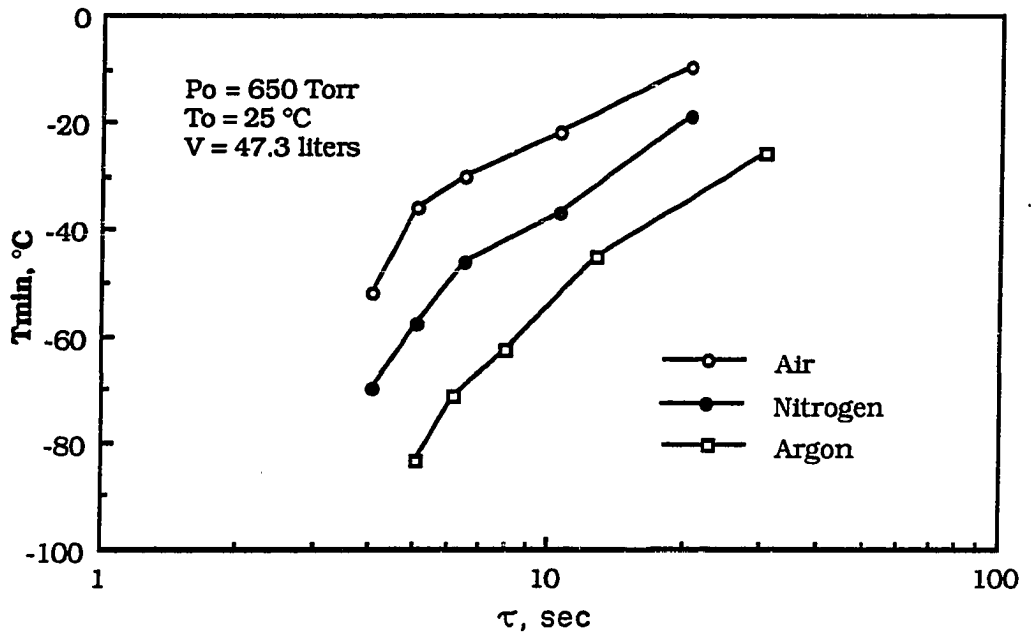

Figure 2-12 Minimum gas temperature as a function of pumping time constant

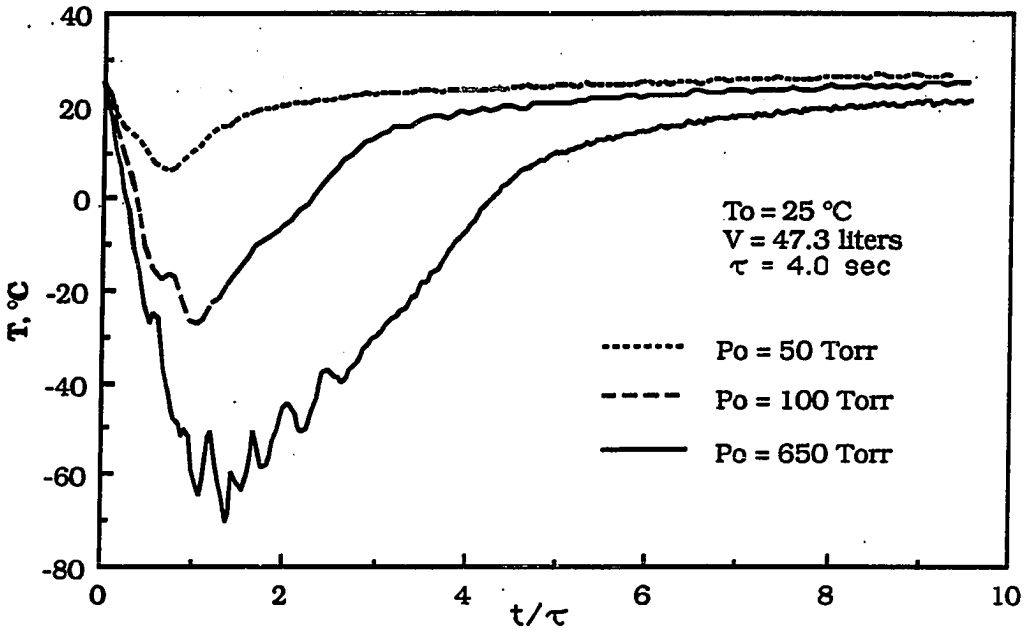

Figure 2-13 Comparison of nitrogen temperature histories when pump-down starts with different initial pressures

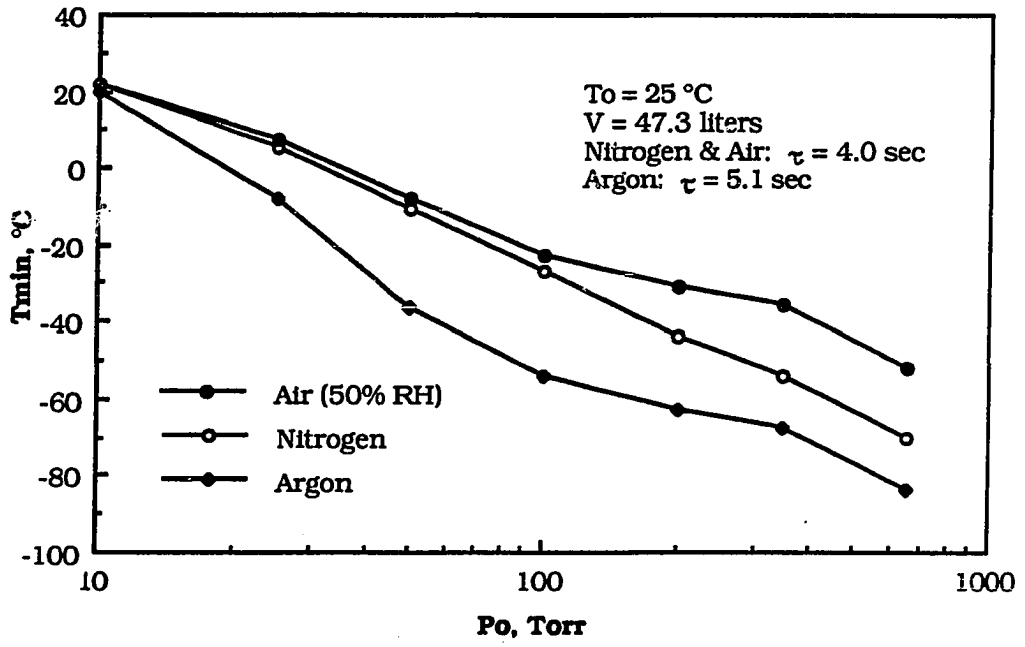

Figure 2-14 Minimum gas temperature as a function of initial pressure

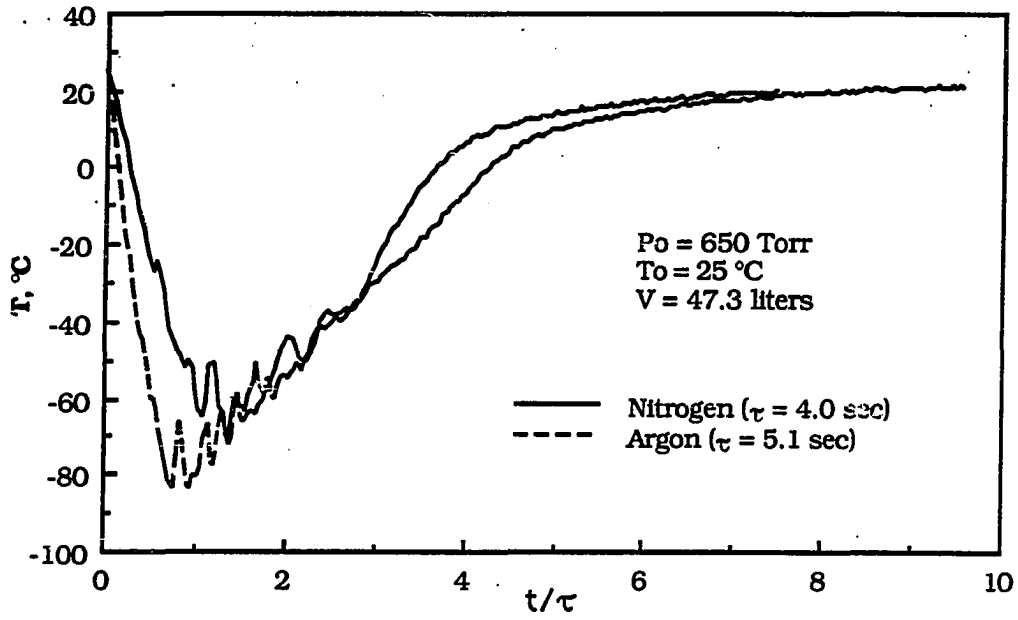

Figure 2-15 Comparison between nitrogen and argon temperature under the same pumping conditions

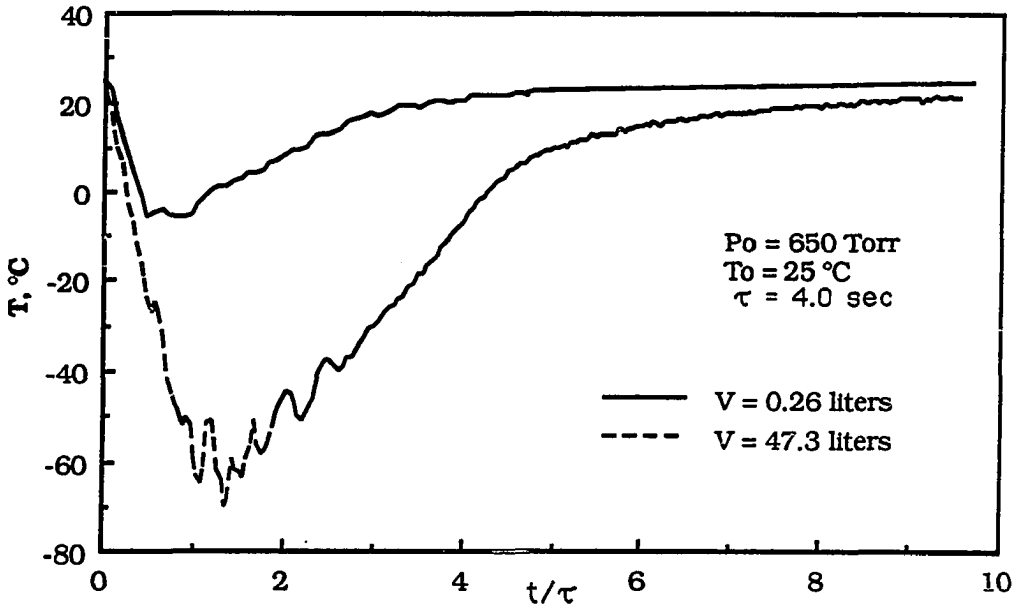

Figure 2-16 Comparison of nitrogen temperatures in the large chamber and the small chamber under the same pumping time constant

Three distinguishing periods in gas temperature history can be observed in Fig.2-8. (i) $0 < t/\tau < 0.5$ (where $\tau = 4.0$ seconds): In this beginning period, the temperature difference is small and the adiabatic cooling dominates. (ii) $0.5 < t/\tau < 5$: Both wall heating and expansion cooling are important. The significant temperature difference has built up. At the point of minimum temperature, the effects of the cooling and the heating are equal. (iii) $t/\tau > 5$: In this later period, the gas temperature almost recovers, the pressure becomes very small, and wall heating prevails. Pump-down can be regarded as an isothermal process hereafter.

It is also found in Fig.2-8 that the gas temperature decreases smoothly up to -22 °C at 350 Torr, and then starts to fluctuate with approximately a 10°C magnitude. The fluctuation is believed to be caused by turbulent natural convection. Turbulence may occur in two situations. The first is when the Reynolds number Re > 2300 corresponding to the onset of turbulent flow inside the pipe. The second is when the Grashof number $Gr > 10^7$ corresponding to onset of the turbulent natural convection. Calculations show that the mean maximum Re (occurring in the initial pressure 650 Torr) in our experiments is about 925 which is below the onset of turbulent flow. The Grashof number at -22°C and 350 Torr is 8×10^7 which is above the onset for turbulent natural convection. When turbulence occurs, the hot gas near the wall will mix with the cold gas inside the chamber causing the gas temperature at a fixed location to fluctuate.

2.5.2 Spatial Variation of Gas Temperature

Fig.2-10 shows spatial variations of gas temperature. For a fixed τ, the nitrogen temperatures at different locations are recorded. It is found that temperature histories at location 2 and 5 are identical when $0 < t/\tau < 0.5$ (where $\tau = 4.0$ seconds) while the temperature decreases from 25 to -22°C. After 0.5τ, the temperatures at two locations become different. It is interesting to note that the onset of

nonuniform temperature field coincides with the onset of temperature fluctuation. Temperatures at six different locations have been measured. They show the behavior as discussed above. Detailed information about the flow and temperature fields can be obtained by numerically solving the compressible Navier-Stokes equations and energy equation in two or three dimensions or by more detailed measurements.

2.5.3 Effect of Pumping Speed

The effect of effective pumping speed on temperature is shown in Fig.2-11, where τ = 20.5, 6.5, and 4.0 seconds corresponding to S_e = 138, 436, and 705 lpm respectively. It is found that for a given chamber the smaller the τ (fast pumping), the more the gas is cooled because fast pumping reduces the time for heat transfer. It is also found that before 0.5τ, the gas temperature histories are similar because adiabatic cooling dominates in this period regardless of what pumping speed is used. Fig.2-12 shows the minimum temperature during pump-down for dry nitrogen, air, and argon at different τ. Data for the figures are listed in Table 2-2.

Table 2-2 Measured minimum temperature and associated pressure at different pumping speeds (V = 47.3 liters)

	Nitrogen		Air	
τ, sec	T_{min}, °C	p_{min}/p_o	T_{min}, °C	p_{min}/p_o
4.0	-70	0.165	-52	0.156
5.1	-58	0.191	-36	0.192
6.5	-46	0.224	-30	0.201
10.5	-37	0.301	-22	0.237
20.5	-19	0.370	-10	0.335

p_o = 650 Torr, T_o = 25 °C.

2.5.4 Effect of Initial Pressure

Fig.2-13 shows the effect of initial pressure on the gas temperature. For a fixed pumping rate of 705 lpm, the gas temperature T decreases less if the pump-down is initiated at low pressure. Fig.2-14 shows the minimum of T as a function of the initial pressure p_0. The data for the figure are listed in Table 2-3. When $p_0 < 10$ Torr, T varies less than 5°C.

It is noted that the lower the initial pressure, the smaller the drop in the temperature. The reason is that (i) the heat diffusion coefficient of the gas, which is inversely proportional to pressure, becomes higher at the low pressure and thus enhance the heat transfer; and (ii) the lower the pressure, the less gas is inside the chamber so that less heat is required to maintain a constant temperature. In order to reduce the temperature drop and thus to avoid possible water vapor condensation, one can first uses slow pumping to reduce pressure to a lower level, say below 10 Torr, then use fast pumping thereafter. This is the procedure that some companies use in vacuum pump-down processes.

2.5.5 Effect of Gas Medium

Fig.2-15 illustrates the temperature histories of dry nitrogen and argon under the same pumping conditions (same pump, orifice, and chamber). Although the argon pressure decays more slowly than nitrogen under the same pumping conditions (see Section 2.3), its temperature decreases more because Argon has a higher γ and thus can be cooled more while it expands.

Table 2-3 Measured minimum temperature and associated pressure at different initial pressures (V = 47.3 liters)

	Nitrogen		Air		Argon	
p_o,Torr	T_{min}, °C	p_{min}/p_o	T_{min}, °C	P_{min}/p_o	T_{min}, °C	P_{min}/p_o
650	-70	0.165	-52	0.156	-83	0.207
350	-54	0.191	-36	0.190	-68	0.266
200	-52	0.223	-31	0.216	-63	0.304
100	-27	0.318	-23	0.323	-54	0.346
50	-11	0.434	-11	0.422	-36	0.406
25	6	0.496	8	0.486	-8	0.617
10					20	0.786

$\tau = 4.0$ sec, $T_o = 25$ °C

Table 2-4 Measured minimum temperatures and associated pressuresof dry nitrogen at different pumping speeds (V = 0.26 liters)

τ, sec	T_{min}, °C	p_{min}/p_o
0.6	-58	0.204
1.0	-46	0.239
1.9	-26	0.344
2.7	-17	0.383
3.6	-10	0.423
4.0	-7	0.444
15.6	10	0.603

$p_o = 760$ Torr, $T_o = 25$ °C.

2.5.6 Effect of Chamber Size

Fig.2-16 shows a comparison of the nitrogen temperature history in the 47.3 liter chamber with that in the 0.26 liter chamber. For the same τ, the gas temperature in the small chamber decreases much less than that in the large chamber because it is easier for the gas to be heated in the small chamber which has higher surface to volume ratio. The measured minimum dry nitrogen temperatures during pump-down for this chamber at different τ are shown in Table 2-4.

2.5.7 Effect of Water Vapor

During pump-down of moist air, water vapor in air may condense to become droplets or even ice crystals. Fig.2-17 shows the measured temperature of air with 50% initial relative humidity. Based on assumptions that water vapor and air are in thermal equilibrium and the vapor pressure is proportional to the total pressure (see Chapter 3), the potential saturation of the water vapor during pump-down, S, is calculated and shown in Fig.2-17. The peak potential saturation is about 16. The critical saturation ratio of homogeneous nucleation for water is about 8. This estimation indicates that homogeneous nucleation will occur if foreign nuclei are absent. With the presence of foreign nuclei, heterogeneous nucleation (condensation on existing particles) will also occur. Water droplets will form and grow due to these nucleation processes. If the gas temperature is below -30°C, all the droplets greater than 5 μm will become ice crystals (Mason, 1971). The details of nucleation processes and particle formation during vacuum pump-down will be covered in Chapter 6.

A clue of the water vapor condensation or ice formation during pump-down may be observed from the comparison of the temperature history of dry nitrogen with that of room air. Condensation of water

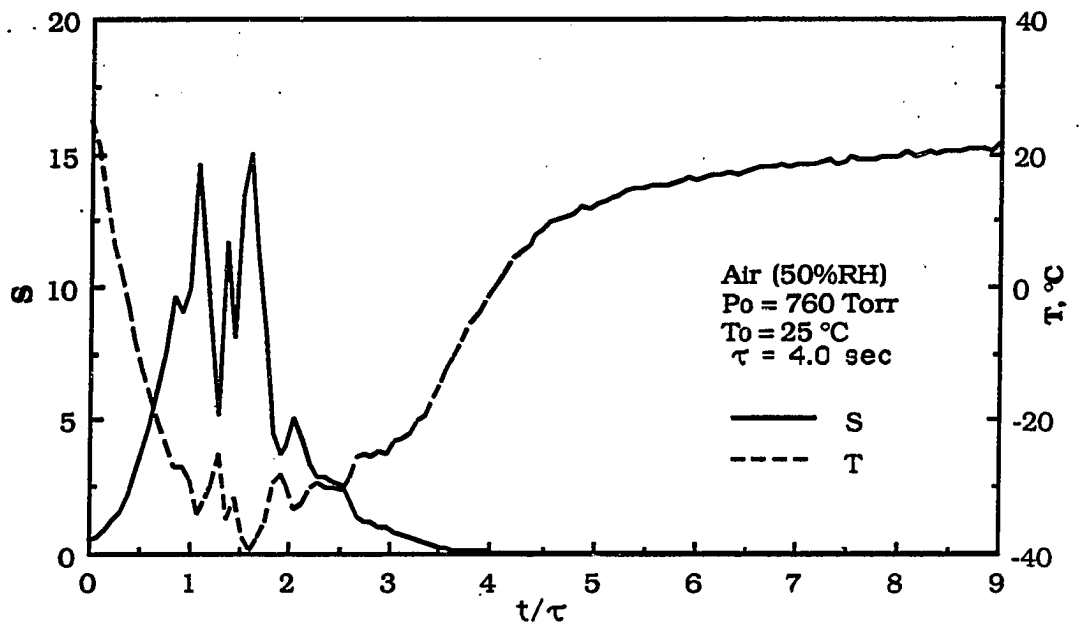

Figure 2-17 Potential saturation ratio of water vapor during pump-down

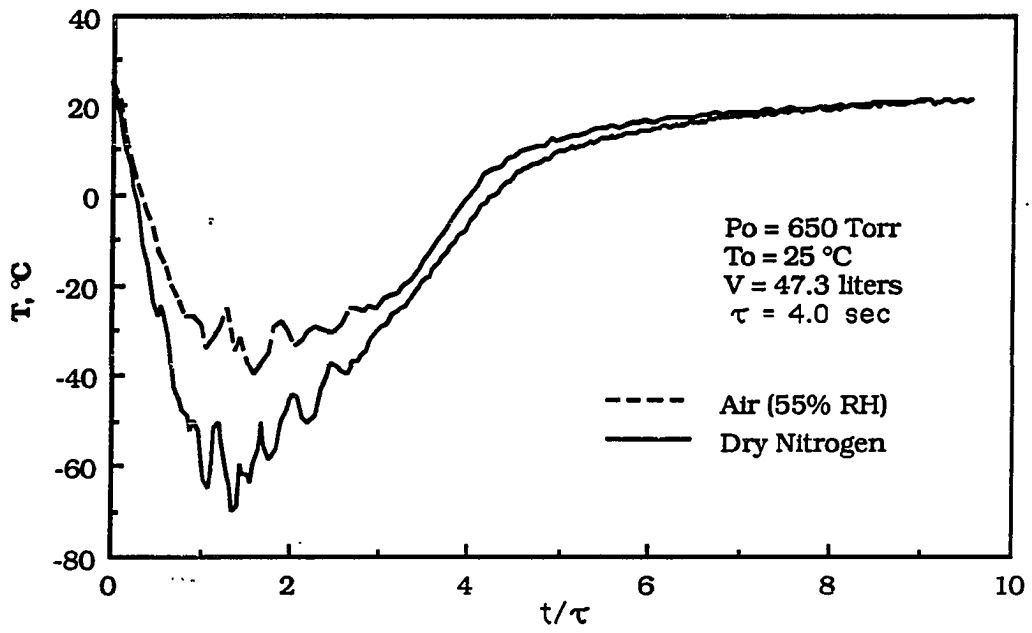

Figure 2-18 Comparison of temperatures of room air and dry nitrogen under the same pumping conditions

vapor or crystallization of water droplets will release latent heat which will heat the air. The estimation in Chapter 3 shows that the heating effect due to latent heat release can be very significant. Room air contains a significant amount of water vapor while dry nitrogen may be regarded as "water vapor free air" (0% RH) (dry nitrogen and air have almost identical physical properties such as molecular weight, heat diffusion coefficient, and specific heat). The possibility of water vapor condensation or ice formation is excluded in dry nitrogen. Under the same pumping conditions, if the temperature of air is significantly higher than that of dry nitrogen which is an indication of latent heat release and thus formation of water droplets or ice crystals.

Four distinctive period can be observed in Fig.2-18 where τ = 4.0 seconds. (i) $0 \leq t/\tau \leq 0.25$: The air and dry nitrogen temperature are almost identical, decreasing from 25 to 5°C. No water vapor condensation occurs in this period. (ii) $0.25 < t/\tau \leq 0.75$: The air temperature decreases with slower rate to -30°C, while dry nitrogen decreases with faster rate to -50°C. Some water vapor may start to condense to existing nuclei, and the latent heat release slows down the decrease in air temperature. (iii) $0.75 < t/\tau \leq 3$: The air temperature stays at about -30°C, while the dry nitrogen decreases further down to -70°C and then recovers to -30°C. Large scale condensation or nucleation may occur. Ice crystals may also evolve. Large quantities of latent heat released prevents the air temperature from decreasing further. (iv) $t/\tau > 3$: The air temperature is close to but slightly higher than the dry nitrogen temperature. The condensation and ice formation processes stop when the temperature recovers and when water vapor has been consumed or pumped out.

2.6 CONCLUSIONS

The gas temperature during vacuum pump-down from 760 to 0.1 Torr has been systematically measured for dry nitrogen, high purity argon, and room air in two cylindrical chambers of volume 47.3 liter and 0.26 liter respectively. The pumping speed and initial pressure have been carefully controlled with uncertainties less than ±2°C. The chamber wall temperature measured varies less than 2°C during pump-down. The following effects on gas temperature measurement have been considered: the time response of the thermocouple, wall radiation, and water vapor condensation or evaporation on the TC junction. Total uncertainty for nitrogen and argon temperature is less than 5% of the absolute temperature, while larger uncertainties exists for air temperature because of the uncertainties in determining the actual saturation ratio. The measurement data have clearly shown that:

1) When the pressure is reduced from 760 to 0.1 Torr during vacuum pump-down, the gas temperature first decreases because of gas expansion cooling and then recovers because of wall heating. If the pump-down is started from atmospheric pressure, the time span of temperature variation lasts approximate 5 to 6τ, with significant variation occurring in $0 < t < 3\tau$. The degree of temperature variation depends on gas medium, chamber geometry, effective pumping speed, initial gas pressure, and quantities of condensable vapor.

2) In the measurement mades in the 47.3 liter chamber, the gas temperature decreases smoothly and almost uniformly from the beginning of pump-down to approximately 0.5τ, after which the fluctuations of gas temperature at a fixed location and the nonuniformity in the temperature field are observed. These phenomena are believed to be caused by the onset of turbulent natural convection. The measurements inside the 0.26 liter

chamber do not show fluctuations in gas temperature because of its smaller size.

3) The effect of water vapor on gas temperature history is significant. Nucleation or condensation of water vapor or even ice formation may occur during pump-down due to the presence of water vapor. The latent heat released from condensation or crystallization reduces the temperature drop.

CHAPTER 3
SIMULATION OF THE VACUUM PUMP-DOWN PROCESS

ABSTRACT

A mathematical model for the process of vacuum pump-down, based on fundamental thermodynamics and processes of heat and mass transfer in the continuum regime, has been developed to predict the temperature and pressure of the gas, and the saturation ratio of the condensable species. The inputs to the model include the physical properties of the gas and vapor, their initial states, the chamber geometry, and the pumping conditions. Numerical calculations based on the model have been carried out for various pump-down conditions, and the predictions are in good agreement with the experimental data.

Along with the development of the model, an order-of-magnitude analysis in this chapter has lead to the following conclusions regarding the pump-down process: (i) natural convection is the predominant process affecting heat transfer to and from the chamber walls, (ii) the chamber wall temperature remains nearly constant during pump down, and (iii) the latent heat released from water vapor condensation or ice formation may be a significant heat source affecting the gas temperature.

3.1 GENERAL CONSIDERATIONS

The thermodynamics and the heat and mass transfer processes in the continuum regime for the vacuum pump-down process will be studied in this chapter. By continuum regime, we mean that the gas can be treated as a continuum fluid, rather than as discrete molecules in the studying of gas flow and heat transfer.

From the standpoint of thermodynamics, the condition of a vacuum is defined by its thermodynamic state -- gas temperature, pressure, and vapor saturation ratio (if condensable species are present). The changes in the thermodynamic state are determined by (i) gas flow through pipes, valves, pumps, and other vacuum components, and (ii) the heat exchange between the chamber wall and the internal gas. If the gas is treated as a continuum medium, the governing equations for gas flow and heat transfer are a set of continuum equations expressing the laws of conservation of momentum, mass, and energy. These are:

1) Navier-Stokes equations

$$\frac{\partial(\rho\vec{u})}{\partial t} + (\vec{u}.\nabla)(\rho\vec{u}) = -\nabla p + \nabla.(\mu\nabla\vec{u}) + \vec{f} \qquad (3.1)$$

where ρ is the density; p, the pressure; μ, the dynamic viscosity; $\vec{u}$, the velocity; $\vec{f}$, the external body force; and ∇, the gradient operator. In Cartesian coordinates

$$\nabla = \vec{i}\frac{\partial}{\partial x} + \vec{j}\frac{\partial}{\partial y} + \vec{k}\frac{\partial}{\partial z}$$

with $\vec{i}$, $\vec{j}$, $\vec{k}$ being the unit vector in x, y, z directions respectively.

2) Continuity equation

$$\frac{\partial(\rho\vec{u})}{\partial t} + \nabla.(\rho\vec{u}) = m_s \qquad (3.2)$$

where m_s is the mass source rate.

3) Energy equation

$$\frac{\partial(\rho\, c_v T)}{\partial t} + \vec{u}.\nabla(\rho\, c_v T) = \nabla.(k\nabla T) + h_s \qquad (3.3)$$

where c_v is the specific heat at constant volume; k, the thermal conductivity; T, the gas temperature; and h_s, the heat source rate.

The validity of Eqs. (3.1) to (3.3) is determined by the magnitude of the Knudsen number

$$Kn = \frac{\lambda}{D_n} \tag{3.4}$$

where λ is the gas mean free path and D_n is the nominal dimension of a vacuum component. In studying gas flow through a pipe, for instance, D_n is the pipe diameter. In studying heat transfer between the gas and a cylindrical chamber, D_n may be either the diameter or the height of the chamber, whichever is smaller. The continuum description is valid when the gas mean free path is small compared to the nominal dimension of a vacuum component. According to Bird (1976), $Kn \leq 0.1$ is the limit for the continuum regime. For convenience, we may also express Kn in terms of pressure. It is noted that for a specific gas at a given temperature, $p\lambda$ is constant. For air at 20°C, $p\lambda = 0.0046$ Torr.cm. In terms of p in Torr and D_n in cm,

$$Kn = \frac{0.0046}{p\, D_n} \tag{3.5}$$

As pressure increases, Kn decreases. Therefore, the continuum assumption is more valid at high pressures, which is exactly what we are interested in because of the following two reasons:

1) Variation of gas temperature occurs only at high pressure, and so far there is no model available to predict the transient temperature. As shown by the measurements in Chapter 2, inside the 47.3 liter chamber, the transient gas temperature takes place only at pressures above 1 Torr, below which variation in gas temperature is negligible. The minimum gas temperature and maximum vapor saturation ratio occurs near 100 to 300 Torr. If we are interested in

finding what happened above 1 Torr during pump-down, the continuum description is valid as long as the smallest dimension of all the vacuum components is greater than 0.05 cm. This condition is usually satisfied.

2) At low pressure, the gas temperature is almost time invariant, only pressure varies with time which can be well predicted by existing theories, such as Dushman (1962, Section 2.6), and Lewin (1965, Section 4.1).

Two approaches may be used to study the thermodynamic processes of pump-down in the continuum regime. The first is to solve the partial differential Eqs. (3.1) to (3.3) numerically with proper boundary conditions. An advantage of this approach is that it yields spatial information of pressure, temperature, and flow fields. The disadvantage is that it is usually time consuming, and involves too much detail which makes the process hard to characterize. Moreover, the uncertainties in turbulent conditions inside the chamber makes the problem even more difficult to deal with.

The second approach is to use a lumped model by taking the chamber, pipes, valves, or other vacuum components as discrete, individual objects, the properties of gas and vapors within each object are assumed to be uniform. An integro-differential equation can then be applied to these individual, lumped objects. Analytical or empirical formulas are used for calculating the gas flow and heat transfer. This approach will yield a set of ordinary differential equations for the pump-down process. Although this approach does not provide spatial information, it is simple and easy to apply. It enables dimensional analysis to be used, and provides more insight to the physical phenomena involved. For this reason, the lumped model is used in this study.

3.2 A LUMPED MODEL FOR THE VACUUM SYSTEM

As shown in Fig. 3-1, a lumped model is proposed for a typical vacuum system which is composed of a vacuum chamber with volume V and surface area A; a vacuum pump with an intrinsic pumping speed S_p; and a restricting orifice with conductance C_{or}, representing the combined flow conductance of the throttling valve, pipes and baffle and other obstructions between the chamber and the pump.

Before pump-down starts, the chamber contains a mixture of gas and condensable vapor at temperature T_o, the initial gas pressure being p_o and the initial vapor pressure, p_{vo}. If leaks are present, the room air with temperature T_o will leak into the chamber during pump-down. This situation is shown in Fig. 3-2.

The objective of the model is to predict the transient thermodynamic variables of gas pressure p, gas temperature T, gas density ρ, and vapor saturation ratio S with a given vacuum system (A, V, S_p, C_{or}) and initial conditions (p_o, T_o, p_{vo}).

3.3 FUNDAMENTAL EQAUTIONS

Since gas is regarded as a continuum fluid, the control volume approach and integro-differential equations are applied. The control volume is the mixture (gas plus condensable species) inside the chamber. the control surface is the boundary of the chamber. There are two ports on the control surface: room air is leaking through port 1 and the mixture is pumped out through port 2. Variables associated with the control volume and the control surface are shown in Fig. 3-2. The governing equations are the mass conservation equation

$$0 = \frac{d}{dt}\int_{CV}\rho\, dV + \int_{CS}\rho\, \vec{u}\cdot d\vec{A} \qquad (3.6)$$

and the energy equation

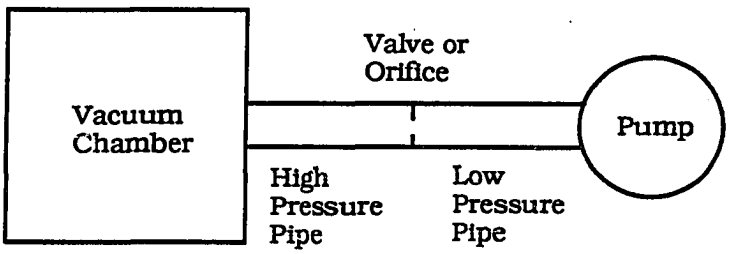

Figure 3-1 A lumped model for a vacuum system.

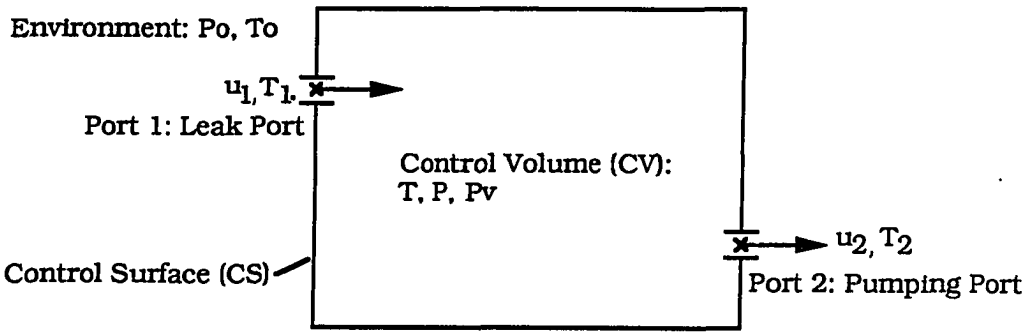

The variables at each port are defined at point x on the CS.
At port 1, T1 has stagnation temperature To.
At port 2, T2 has stagnation temperature T.

Figure 3-2 Control volume formulation for pump-down process.

$$\dot{Q} + \dot{W} + \dot{S} = \frac{\partial}{\partial t}\int_{CV}\left(c_v T + \frac{u^2}{2} + gz\right)\rho dV + \int_{CS}\left(c_p T + \frac{u^2}{2} + gz\right)\rho \vec{u}.d\vec{A} \tag{3.7}$$

where CV stands for control volume; CS, control surface; dV, differential volume; $d\vec{A}$, differential surface area with positive outside normal; $\dot{Q}$, rate of heat transfer to the mixture; $\dot{W}$, rate of external work done on the mixture; $\dot{S}$, rate of energy generation within the mixture; c_v, specific heat of the mixture at constant volume; c_p, specific heat of the mixture at constant pressure; c_vT, internal energy of the mixture; c_pT, enthalpy of the mixture; $\vec{u}$, velocity vector; u, magnitude of velocity vector; $u^2/2$, kinetic energy of the unit mass; g, gravitational constant; and gz, gravitational potential energy of unit mass.

3.4 BASIC ASSUMPTIONS

In this section, several assumptions are made to simplify the general equations (3.6) and (3.7). The limitations of these assumptions are discussed first.

Assumption 1: The gas and vapor inside the chamber are perfect gases, always in thermal equilibrium, and pumped out with at the same speed. No vapor condensation or nucleation is allowed.

The perfect gas assumption is nearly always valid for a gas inside a vacuum system because the gas (including vapor) is usually rarefied and its thermodynamic state is far away from the critical point. The assumption of no vapor condensation or nucleation is valid before the onset of condensation or nucleation. Based on this assumption, we have

$$p = \rho R T \tag{3.8}$$

$$p_v = \rho_v R_v T_v \tag{3.9}$$

$$T_v = T \tag{3.10}$$

$$p_v = \frac{p_{vo}}{p_o} p \tag{3.11}$$

where p, p_o, and T are the pressure, initial pressure, and temperature of the gas respectively; p_v, p_{vo}, and T_v are the pressure, initial pressure, and temperature of the vapor.

Equations (3.8) to (3.10) are a direct consequence of the perfect gas assumption. Eq. (3.11) states that the pressure ratio of the vapor to the gas during pump-down remains constant at the initial value. This results from the assumptions that vapor condensation is not allowed, and that vapor and gas are pumped out at the same speed. It follows that the density ratio of the vapor to the gas during pump-down is also constant, since $T_v = T$.

Based on this assumption, only two independent thermodynamic variables are left among the original six (p, ρ, T, p_v, ρ_v, T_v). The best choice for these independent variables are either (ρ, T) or (p, T). In this chapter, (ρ, T) are used in deriving the equations because of convenience and the fact that the derivation can be made more clear. The final results are then put in terms of (p, T), which are the independent vaiables customarily used in vacuum science and technology.

The total pressure and density of the mixture are $p_t = p + p_v$ and $\rho_t = \rho + \rho_v$. It should be noted that the vapor concentration is usually quite small compared to that of the gas and is usually less than 1%. We can thus take the partial pressure (or density) of the gas as the total

pressure (or density) of the mixture without much error. This means that the physical properties of the gas can also be taken as the properties of the mixture. Since the mixture is assumed to be a perfect gas, its thermophysical properties such as thermal conductivity and viscosity are functions of temperature only and independent of pressure. The following equations can be used,

$$\frac{k}{k_o} = \left(\frac{T}{T_o}\right)^{1/2} \tag{3.12}$$

$$\frac{\mu}{\mu_o} = \left(\frac{T}{T_o}\right)^{1/2} \tag{3.13}$$

where k_o and μ_o are the thermal conductivity and dynamic viscosity evaluated at the initial temperature T_o. The specific heats, c_v, c_p, and the ratio $\gamma = c_p / c_v$, are assumed to be independent of both temperature and pressure.

Assumption 2: All thermodynamic variables and gas properties are assumed to be uniform inside the chamber and the internal energy is assumed to be much larger than the kinetic and gravitational energies of the gas in the volume, i.e., $c_vT >> \frac{u^2}{2} + gz$. With these assumptions, the volume integrals of Eqs. (3.6) and (3.7) can be evaluated:

$$\frac{d}{dt}\int_{CV} \rho \, dV = V \frac{d\rho}{dt} \tag{3.14}$$

$$\frac{d}{dt}\int_{CV} (c_vT + \frac{u2}{2} + gz)\, \rho dV = c_vV\frac{d(\rho T)}{dt} = c_v\rho V \frac{dT}{dt} + c_vTV \frac{d\rho}{dt} \tag{3.15}$$

Since the ratio of kinetic to internal energy is $0.5(\gamma-1)Ma^2 / \gamma$ and the gas velocity in the chamber is much less than the speed of sound i.e. the Mach number, Ma << 1, the kinetic energy can indeed

be neglected. Also, the typical chamber dimension is quite small. Consequently, the changes in gravitational energy are also negligible when compared with the internal energy.

Assumption 3: The gas flow at the ports 1 and 2 are uniform and isentropic, i.e.,

$$\left\{ c_p T_2 + \frac{1}{2} u_2^2 \right\} = c_p T \tag{3.16}$$

$$\left\{ c_p T_1 + \frac{1}{2} u_1^2 \right\} = c_p T_o \tag{3.17}$$

where T_1 is the local temperature at port 1 with the corresponding stagnation temperature of T_o, and T_2 is the local temperature at port 2 with the corresponding stagnation temperature of T. The assumption of isentropicity is valid when the viscous dissipation and heat transfer at these ports can be neglected. With this assumption, the surface integrals in Eqs. (3.6) and (3.7) can be evaluated:

$$\int_{CS} \rho \vec{u} \cdot d\vec{A} = \rho_2 u_2 A_2 - \rho_1 u_1 A_1 = \dot{m}_2 - \dot{m}_1 \tag{3.18}$$

$$\int_{CS} (cpT + \frac{u^2}{2} + gz)\, \rho \vec{u} \cdot d\vec{A} = \left\{ c_p T_2 + \frac{1}{2} u_2^2 \right\} \dot{m}_2 - \left\{ c_p T_1 + \frac{1}{2} u_1^2 \right\} \dot{m}_1$$

$$= c_p T\, \dot{m}_2 - c_p T_o\, \dot{m}_1 \tag{3.19}$$

In the above derivations, the kinetic energy, $\rho u^2 / 2$, at the two ports has been taken into account since it is comparable with the corresponding enthalpy at each port. Flow at the two ports usually has a high velocity because (i) the ports have small cross-sectional area, and (ii) the ratio of the down stream pressure to the upstream pressure is often less than the critical pressure ratio and the flow is

usually sonic or choked. The ratio of the kinetic energy to enthalpy is $0.5Ma^2(\gamma-1)$. For air $\gamma = 1.4$ at sonic flow (Ma = 1) so the kinetic energy is 20% of the gas enthalpy at the ports.

Assumption 4: Energy generation within the gas is zero, i.e.,

$$\dot{S} = 0. \tag{3.20}$$

Possible energy generation during vacuum pumping include (i) viscous dissipation, (ii) latent heat release from condensation or crystallization, and (iii) chemical reaction. The magnitude of chemical reaction cannot be estimated without knowing the specific reaction involved. The magnitude of the viscous dissipation and the latent heat, however, can be estimated.

Viscous dissipation comes from flow friction which generates heat of $\mu(\nabla\vec{u})^2$ per unit time and volume, where $\nabla\vec{u}$ is the velocity gradient. The rate of temperature change (dT/dt) due to viscous dissipation is then $\frac{\mu(\nabla\vec{u})^2}{c_v\rho}$. Consider the following example: pump-down of air with a pumping rate of 705 lpm inside a chamber with diameter D = 45 cm (for one of the pump-down experiments reported in Chapter 2). The mean velocity in the chamber is u = 7.4 cm/s, corresponding to Re = 2160. The maximum velocity gradient occurs near the wall which has the magnitude of u/δ, where δ is the boundary layer thickness, and is on the order of $D/\sqrt{Re}$. The maximum velocity gradient is on the order of $u\sqrt{Re}/D$. Using the properties of air, one can find that the heating rate due to viscous dissipation is on the order of 10^{-6} °C/s, which is negligible.

Latent heat released from water vapor condensation or ice formation will now be estimated. The rate of latent heat generation depends on the rate of vapor condensation or ice formation, which is usually difficult to determine exactly. Let us consider the limiting case where all the vapor condenses to form liquid and then freezes

instantaneously (infinite rate). The gas would see a sudden temperature rise due to latent heat release of $\frac{\rho_v}{\rho}\frac{L_v + L_s}{c_v}$ where ρ_v/ρ is mass fraction of the vapor, Lv is the latent heat of vaporization, and Ls is the heat of fusion. For water vapor, Lv = 2.25 x 10^{10} erg/g, and Ls = 2.549 x 10^{10} erg/g. For 50% relative humidity air at 20°C, ρ_v/ρ is about 1%. With these values, one can find that the air temperature rise due to latent heat release is 90°C. In practice, infinite rate of condensation or ice formation cannot be achieved. However, homogeneous or heterogeneous condensation of water vapor or ice formation may occur with a significant rate because of the sharp temperature decrease in the beginning of pump-down. Effects of latent heat on temperature history will be studied in conjunction with the study on particle formation processes in Chapter 5.

Assumption 5: External work done to the internal gas medium is zero, i.e.,

$$\dot{W} = 0. \tag{3.21}$$

Since the chamber walls are rigid, no work is done on the gas by its surroundings. Actually, gas inside the chamber has expanded during pump-down and work has been done on the surroundings, which is the reason for the drop in gas temperature. But this drop in temperature and work done has already been taken into account in Eq.(3.6).

3.5 EQUATIONS FOR PUMP-DOWN

With assumptions 1 to 5, one can simplify the integral equations (3.6) and (3.7) into a pair of ordinary differential equations. Substituting Eqs. (3.16) to (3.21) into Eqs. (3.6) and (3.7), one can find

$$\frac{d\rho}{dt} = \frac{\dot{m}_2 - \dot{m}_1}{V} \tag{3.22}$$

$$\frac{dT}{dt} = \frac{h A (T_w - T)}{c_v \rho V} + \frac{(c_p - c_v)}{c_v \rho V} T \dot{m}_2 + \frac{(c_p T_o - c_v T)}{c_v \rho V} \dot{m}_1 \tag{3.23}$$

By means of equations (3.22) and (3.23), ρ and T can be solved provided the mass leaking rate $\dot{m}_1$, mass pumping rate $\dot{m}_2$ and wall temperature T_w are known.

For a pump-down process, $\dot{m}_2$ can be controlled by adjusting a throttling valve or by using a restricting orifice. But the leak rate $\dot{m}_1$ is usually unpredictable. One way to know $\dot{m}_1$ is to measure it. The effect of a leak can be studied by using a numerical simulation technique; in the absence of experimental data, one may assume a leak function χ

$$\frac{\dot{m}_1}{\dot{m}_2} = \chi \tag{3.24}$$

where χ is a function of pressure which varies from 0 to 1 when the gas pressure varies from one atmosphere to the ultimate pressure. With this definition of χ, using $\dot{m}_2 = \rho S_e$ and $c_p/c_v = \gamma$, one can simplify equations (3.22) and (3.23) to

$$\frac{d\rho}{dt} = -\rho(1 - \chi) \frac{S_e}{V} \tag{3.25}$$

$$\frac{dT}{dt} = \frac{hA}{\rho V c_v} (T_w - T) - (\gamma - 1) \frac{S_e}{V} T + \chi (\gamma T_o - T) \frac{S_e}{V} \tag{3.26}$$

with initial conditions $\rho = \rho_o$, $T = T_o$ at $t = 0$.

By further assuming that the wall temperature is a constant equal to the initial gas temperature ($T_w = T_o$) and no leak ($\chi = 0$), one can find the simplest model for the pump-down process:

$$\frac{d\rho}{dt} = -\rho \frac{S_e}{V} \tag{3.27}$$

$$\frac{dT}{dt} = \frac{hA}{\rho c_v V}(T_o - T) - (\gamma - 1)T \frac{S_e}{V} \tag{3.28}$$

with initial condition $\rho = \rho_o$,$T = T_o$, at $t = 0$.

3.6 GAS FLOW CALCULATION

The rate of mass flow out of the chamber can be calculated by

$$\dot{m}_2 = \rho S_e \tag{3.29}$$

where S_e is the effective pumping speed -- the volumetric flow rate at the outlet of the chamber. Assuming that the throughput -- the internal energy flow -- is continuous in the vacuum system, one can find that

$$S_e = \frac{S_p C}{S_p + C} \tag{3.30}$$

where S_p is the intrinsic pumping speed of the vacuum pump and C is the combined conductance of the obstructions such as pipes, baffle, orifice, and elbows in the pumping line. Details of the derivation and the terminology commonly used in vacuum technology are given in Appendix C. Calculations for conductance of a variety of vacuum components can be found in standard reference texts on vacuum technology (see for example, Dushman, 1962; O'Hanlon, 1980; or Lewin, 1965). Generally speaking, S_p and C depend on both pressure and temperature, and the procedure used to calculate S_e is usually complicated. However, if an orifice or a throttling valve is used to restrict the pumping rate in the viscous flow regime, S_e is determined mostly by the orifice and the pump, and the effects of other obstructions may be neglected.

For the configuration shown in Fig. 3-2, $C = C_{or}$, the conductance of the orifice. By further assuming that S_p is constant independent of pressure, one can find that (see Appendix D):

$$S_e = \begin{cases} Q_{or} & \frac{Q_{or}}{S_p} \le r^* \text{ (choked flow)} \\ r\,S_p & \frac{Q_{or}}{S_p} > r^* \text{ (unchoked flow)} \end{cases} \tag{3.31}$$

In the above formula, r^* is the critical pressure ratio below which the flow at the orifice is choked

$$r^* = \left(\frac{2}{\gamma+1}\right)^{\gamma/(\gamma-1)} \tag{3.32}$$

and Q_{or} is the choked volumetric flow rate

$$Q_{or} = C_d' \left\{ \gamma \left(\frac{2}{\gamma+1}\right)^{(\gamma+1)/(\gamma-1)} \right\}^{1/2} A_{or} \sqrt{RT} \tag{3.33}$$

where A_{or} is the area of the orifice, and C_d' is the discharge coefficient for the choked flow, and C'_d is a constant depending on specific heat ratio γ and orifice shape. For a square edged orifice (Liepmann, 1961), $C' = 0.824$ for nitrogen or air, and $C' = 0.812$ for argon.

In Eq. (3.31) for unchoked flow, r is the ratio of gas pressure at the pump inlet to that inside the chamber.

$$r = \left\{ 0.5B\left(\sqrt{1+\frac{4}{B}} - 1\right)\right\}^{\gamma/(\gamma-1)} \tag{3.34}$$

and

$$B = \left\{ \left(\frac{2\gamma}{\gamma-1}\right)^{1/2} \frac{C_d'' A_{or} \sqrt{RT}}{S_p} \right\}^2 \tag{3.35}$$

where C_d" is the discharge coefficient for unchoked flow which is a function of Re, the Reynolds number for the orifice, and β, the ratio of the Vena contracta diameter to the upstream pipe diameter. For thin, square-edged orifice with small β (< 0.1), C_d" increases from 0.3 to 0.7 as Re increases from 4 to 200, and C_d" decreases form 0.7 to 0.62 as Re further increases from 200 to 10^5 (Miller, 1983).

In summary, the orifice controlled flow under the condition that S_p is constant has the following characteristics: (i) For choked flow, S_e is independent of p but depends on gas temperature to $\sqrt{T}$, (ii) For unchoked flow, S_e depends on pressure and temperature, but rather weakly.

3.7 HEAT TRANSFER CALCULATON

The rate of heat transfer from the chamber wall to the internal gas can be calculated by

$$\dot{Q} = h A (T_w - T) \qquad (3.36)$$

where A is the internal surface area of the chamber; T_w, the wall temperature; and h, the heat transfer coefficient at the gas-wall interface. It is the key issue to find an appropriate expression for h for heat transfer calculations.

3.7.1 Natural Convection Heat Transfer Coefficient

A natural convection heat transfer coefficient will be used in the calculation of the heat added to the gas from the chamber wall. The reason is that natural convection prevails during vacuum pump-down, as will be shown below.

Effects of radiation on gas temperature are negligible because gas is usually transparent to the infrared radiation involved in radiant heat exchange and absorbs very little radiation energy. Conduction is negligible when convection prevails. Both forced and natural convection may occur during pump-down. Forced convection is caused by the gas continually being pumped out. The natural convection results from the buoyancy force due the temperature gradient near the wall. During pump-down, natural convection prevails over forced convection because the condition given below is almost always valid

$$\frac{Gr}{Re^2} > 10 \tag{3.37}$$

where

$$Gr = \frac{g \rho^2 D_{ch}^3}{\mu^2} \frac{T_w - T}{T_w} \tag{3.38}$$

$$Re = \frac{\rho u D_{ch}}{\mu} \tag{3.39}$$

Criterion (3.37) is obtained by an order-of-magnitude analysis to the natural convection boundary-layer equation (Holman, 1986). The criterion can be further expressed as

$$\frac{g D_{ch}}{u^2} \frac{T_w - T}{T} > 10 \tag{3.40}$$

Let us use an example to check the validity of Eq. (3.40). Consider that air is pumped out with S_e = 705 lpm, D_{ch} = 45 cm, and T = 300 K. Calculation shows that Eq.(3.40) will be true provided $(T_w - T) > 4°C$. The measured data in Chapter 2 show that $(T_w - T)$ can be as as high as about 100°C which indicates that natural convection in pump-down is of primary importance.

For natural convection,

$$h = \frac{Nu\, k}{D_{ch}} \tag{3.41}$$

where Nu is the natural convection Nusselt number which is a dimensionless number representing the ratio of convective heat transfer to pure heat conduction. For natural convection inside a closed enclosure, the general expression for Nu is (Holman, 1986)

$$Nu = c(GrPr)^n (L/D)^m \tag{3.42}$$

where coefficients c, n, and m depend on the nature of the flow (laminar or turbulent) and geometry of the enclosure. Since natural convection in an enclosure is a very complex physical phenomena, determination of these coefficients is usually based on empirical correlations based on experiments.

For a cylindrical chamber in which turbulent natural convection occurs, experiments of Ulrich et al (1969) show that

$$Nu = 0.13\ (GrPr)^{1/3} \tag{3.43}$$

and the turbulent heat transfer coefficient becomes

$$h_T = 0.13\ k \left(\frac{\rho^2\, g\, Pr}{\mu^2} \frac{T_w - T}{T} \right)^{1/3} \tag{3.44}$$

Note that h_T is independent of D_{ch} and thus independent of the chamber geometry.

If laminar natural convection occurs, experiments of Evans and Stefany (1965) show that

$$Nu = 0.55\ (GrPr)^{1/4} \tag{3.45}$$

and the laminar heat transfer coefficient becomes

$$h_L = 0.55\, k \left(\frac{\rho^2 g\, Pr}{\mu^2} \frac{T_w - T}{T} \frac{1}{D_{ch}} \right)^{1/4} \qquad (3.46)$$

Note that h_L is proportional to $D_{ch}^{-1/4}$, and thus is not very sensitive to the value of D_{ch}. In Eqs. (3.43) and (3.45), the Grashof number is based on the length of the cylinder (i.e. $D_{ch} = L$).

The Nusselt number versus GrPr for natural convection inside an enclosure is plotted in Fig.3-3. It is found that at GrPr = 3.3×10^7, the Nusselt number for turbulent and laminar natural convection has the same value and therefore $h_T = h_L$ at this point. To ensure the continuity in computation, the condition for the onset of turbulence is GrPr = 3.3×10^7. According to Holman (1986), the onset for turbulent natural convection inside an enclosure occurs at GrPr on the order of 10^7.

In pump-down processes, eigher laminar or turbulent natural convection may occur. Since GrPr is proportional to $D_{ch}^3 p^2$, convection tends to be more turbulent inside the large chamber and at high pressure. Transition from laminar to turbulent conditions or vice versa may also occur. If natural convection has started with turbulent flow at high pressures, it will eventually become laminar at low pressures.

3.7.2 Constant Wall Temperature

In the heat transfer calculations, the chamber wall temperature at the wall-gas interface is assumed to remain constant during pump-down. Generally speaking, the wall temperature T_w varies as the internal gas temperature varies. Additional differential equations for the wall must be solved in conjunction with the equations governing the gas. The problem becomes much more complicated.

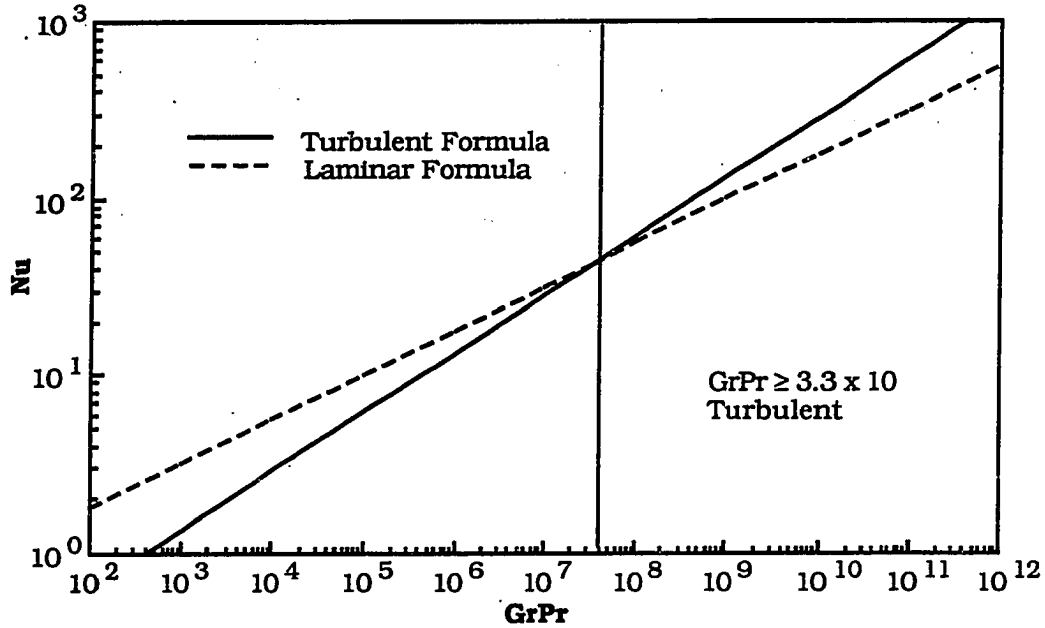

Figure 3-3 Nusselt number as a function of GrPr for natural convection heat transfer inside enclosures

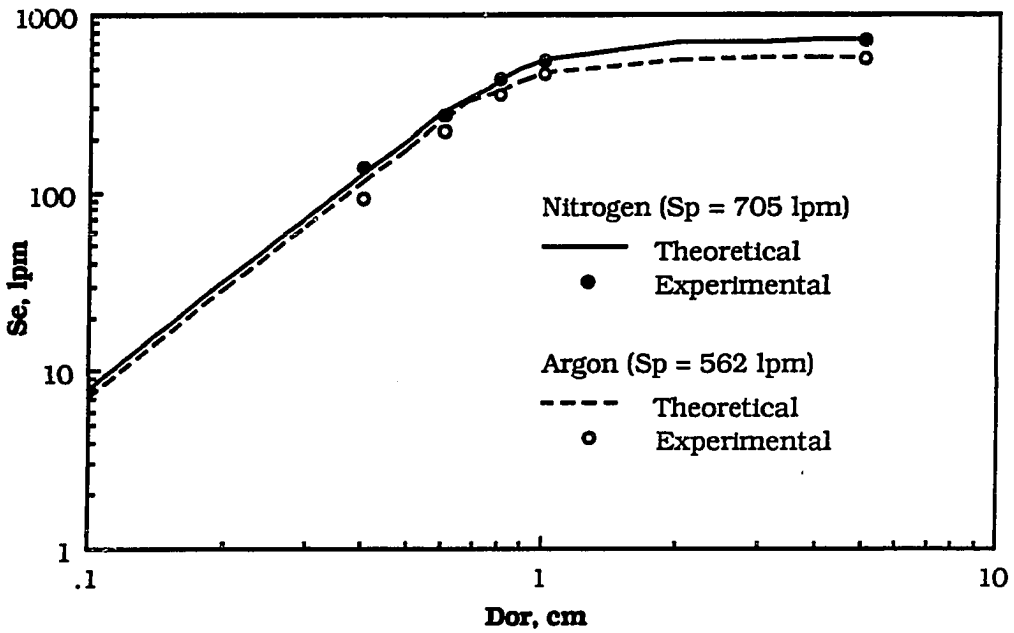

Figure 3-4 Effective pumping speed as a function of orifice size for vacuum pump D60A

Measured temperatures given in Chapter 2 show that the temperature at the gas-wall interface remains almost constant (varying by less than 2°C), while the gas temperature varies nearly 100°C. There are two reasons for this phenomena.

The first reason is that the heat capacity of the chamber wall is usually much greater than that of the gas. Consider air inside a spherical aluminum chamber with diameter D = 50 cm and thickness t_w = 1 cm. The ratio of the heat capacity of the chamber wall to the internal gas is $6\left(\frac{t_w}{D}\right)\frac{(\rho c_v)_{al.}}{(\rho c_v)_{air}}$ which is calculated to be 262. This means that the heat released due to 1°C temperature change in the chamber wall will increase the gas temperature by 262°C. Thus the chamber wall behaves like a large heat source to the gas during pump-down.

The second reason is that the wall temperature is nearly uniform due to its large thermal conductivity, which prevents the surface of the wall from being cooled while the internal solid remains at constant temperature. When the Biot number Bi = $ht_w/k_w \ll 1$, the wall temperature will be uniform. In studying heat transfer from a solid object, the Biot number is the ratio of heat conductance of surface convection to internal conduction of the object. Small Biot number indicates a uniform temperature inside the object. Consider the same example as that for calculating the heat capacity. Assume $(T_w-T)/T$ = 0.2 and turbulent natural convection, h is calculated to be 0.05 erg/K.cm^2.s by Eq.(3.44), and Bi = 2 x 10^{-4}, which is indeed very small.

3.8 POTENTIAL VAPOR SATURATION RATIO

If condensable species such as water vapor is present in the vacuum system, vapor saturation during pump-down is an important parameter that must be taken into account. When saturation reaches its critical value for nucleation, vapor to particle conversion will take place. Saturation ratio is defined as

$$S = \frac{p_v}{p_s} \tag{3.47}$$

where p_S is the saturation pressure of the vapor which is only a function of temperature given by the Clausius-Clapeyron equation

$$\log(p_S) = A + \frac{B}{T} \tag{3.48}$$

where A and B are constants for a specific vapor.

Both p_V and p_S vary during pump-down. It has been assumed that the vapor and the gas are in thermal equilibrium and the partial pressure of the vapor is proportional to the gas pressure (Assumption 1 in Section 3.4). Substituting Eqs. (3.11) and (3.48) into Eq. (3.47), the saturation ratio can be expressed in terms of the gas pressure and temperature

$$S' = \frac{p_{vo}}{p_o} \frac{p}{10^{(A + \frac{B}{T})}} \tag{3.49}$$

S' is used to distinguish it from the actual vapor saturation ratio S, defined by Eq. (3.47). It should be noted that S' only accounts for the vapor reduction resulting from pumping and S' = S only when $S' \leq S_c$, the critical saturation for nucleation in the absence of foreign nuclei or for condensation in the presence of foreign nuclei. If $S' \geq S_c$, nucleation or condensation will occur which will, in addition to the

vapor being pumped out, consume extra vapor by condensation. As a consequence, $S < S'$. The actual saturation S, after the onset of condensation, must be determined by studying the thermodynamics of pump-down in conjunction with particle formation, which is a more complicated phenomena.

In this thesis, we refer to S' as the potential vapor saturation ratio (PVSR) which is the maximum achievable saturation (neglecting any condensation) at a given p and T during pump-down. PVSR has its own physical significance -- it is a measure of the ability of a pump-down to saturate a vapor. By calculating PVSR, we can predict whether condensation or nucleation will occur during pump-down.

3.9 SUMMARY ON MODELING AND SOLUTION APPROACH

In the continuum regime, the thermodynamics of a pump-down process can be described, based on assumption 1, in terms of only two independent thermodynamic variables (ρ, T). Others variables such as gas pressure and vapor saturation ratio are dependent on these variables. With assumptions 2 to 5, a pair of ordinary differential equations are derived from mass and energy conservation for solving (ρ, T).

In the case of a system with no leaks, Eqs. (3.27) and (3.28) must be solved. In these equations, the effective pumping speed S_e is calculated by Eqs. (3.31) to (3.35) and the heat transfer coefficient h is calculated by Eqs. (3.41) to (3.46). The preliminary conditions for solving these ordinary differential equations are the initial conditions (ρ_o, T_o), chamber geometry (A, V), orifice cross-section area A_{or} (if an orifice is used to control the effective pumping speed, otherwise assume S_e to be known), and thermophysical properties of the gas (γ, Pr, k etc). If leaks are present, one needs to solve the ordinary differential Eqs. (3.25) and (3.26). In addition to the conditions mentioned above, the mass leak rate must be given or assumed.

After the independent variables (ρ, T) become known, the gas pressure is calculated from the perfect gas law. The PVSR is then calculated using Eq. (3.49) for a given initial vapor pressure p_{vo}.

3.10 SIMULATIONS AND EXPERIMENTAL COMPARISONS

In this section, numerical calculations for vacuum pump-down are carried out for dry nitrogen, room air, and argon. The results are compared with the experimental data reported in Chapter 2. We will use the same parameters in the numerical calculation or simulation as those in the experiments: the volume of the chamber is 47.3 liters (diameter D = 45 cm, height H = 30 cm, made of aluminum); the vacuum pump is the D60A pump manufactured by Laybold; and the effective pumping speeds are controlled by orifices with diameters of 0.4, 0.6, 0.8, 1.0 and 5.0 cm respectively. It is assumed that there is no leak in all the calculations.

3.10.1 Calculation of Effective Pumping Speed

For the vacuum pump used, the intrinsic pumping speed S_p = 705 lpm for nitrogen or air, and S_p = 562 lpm for argon, assuming that the gas temperature is 25°C. Fig. 3-4 shows the calculated S_e for different orifices. The results agree with the experimental data to within ±5%. For the particular pump used, the calculation indicates that choked flow occurs at the orifice when $D_{or} < 0.75$ cm for nitrogen or air and when $D_{or} < 0.68$ cm for argon.

3.10.2 Simulated Pressure

The accuracy of pressure prediction is mainly determined by how accurately S_e the calculated. If T and S_e remain constant, Eqs. (3.25) and (3.26) show that pressure will decay exponentially with time constant $\tau = V/S_e$, i.e.,

$$p/p_o = e^{-t/\tau} \qquad (3.50)$$

Note that both T and S_e vary during pump-down. However, calculations indicate that these variations would cause only minor, if not negligible, changes to the values given by Eq. (3.50). Comparison of calculated pressure using Eq. (3.50) with values are shown in Fig. 3-5. For τ = 5.0 seconds (D_{or} = 1.0 cm under STP condition), and in the period of 0 < t/τ < 3, the calculated pressure based on the more exact Eq. (3.50) is lower than that predicted by Eq. (3-50) by 25%, in the worst case; and for t/τ > 3, the difference becomes negligible. For τ = 20.5 seconds (D_{or} = 0.4 cm under STP condition), very small difference between the calculated value and that given by Eq. (3.50) is found.

3.10.3 Calculation of Gas Temperature

Typical calculated gas temperatures for dry nitrogen and high purity argon and their experimental comparisons are presented in Figs. 3-7 to 3-9. Generally speaking, the calculation results agree well with the experimental data. The agreement is particularly good during the initial stages of the pump down process, i.e. from the beginning of pump-down to the time that the gas temperature reaches a minimum--the agreement between the theoretical and experimental temperatures is nearly perfect. However, beyond minimum in temperature, the measured temperature increases at a faster rate than that calculated, suggesting that the numerical model under-estimates the heat transfer from the wall at low pressures--however, only by a small amount.

The calculation based on numerical simulation has revealed two important features of the pump-down process. The first is that the rate of gas temperature decrease is the highest at the start of pump-down. At t = 0, Eq. (3.28) gives

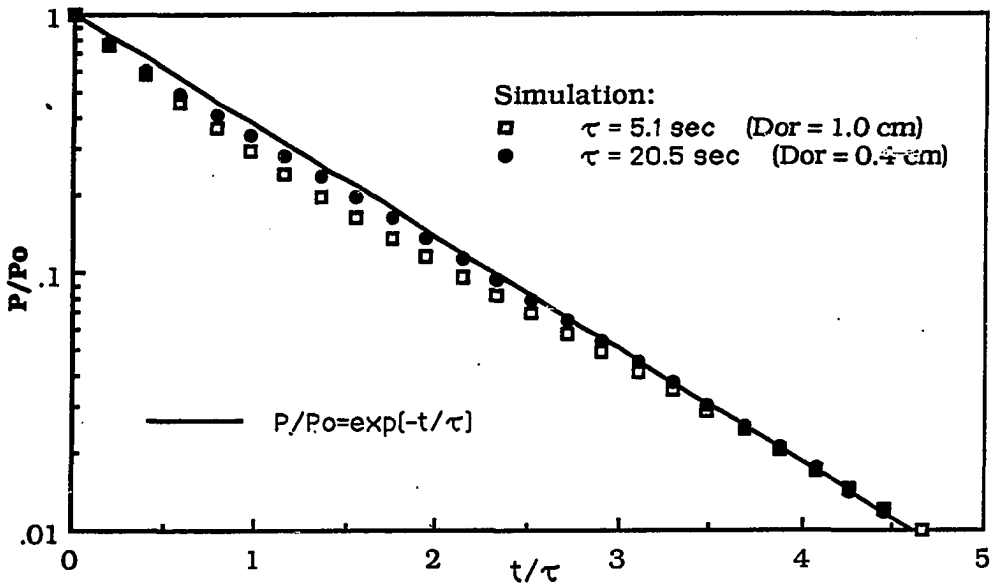

Figure 3-5 Comparison between simulated pressure and equation (3.50)

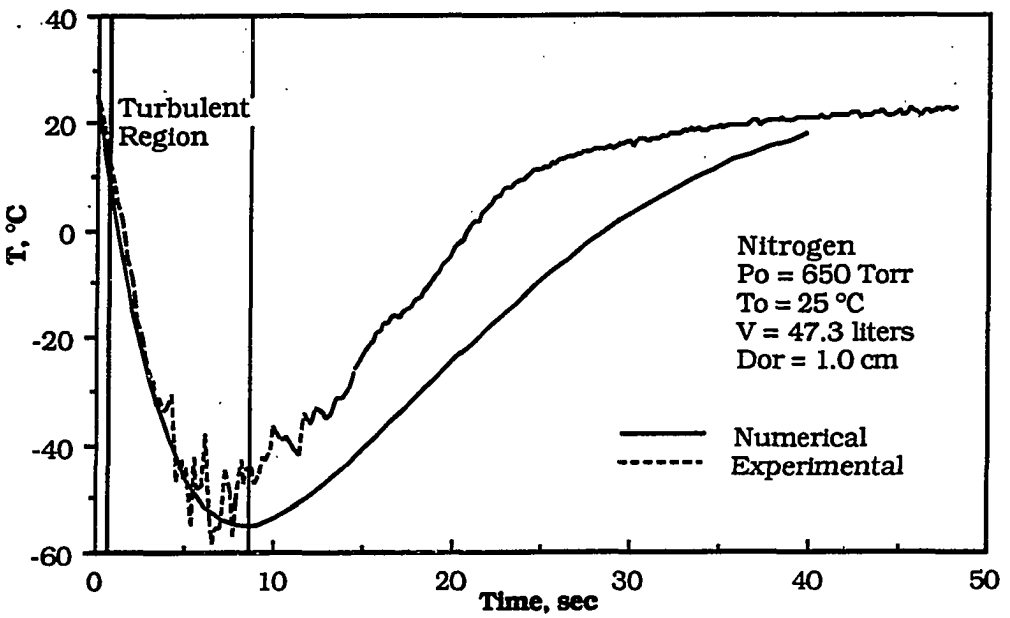

Figure 3-6 Gas temperature simulation: Agreement is best during the cooling dominant period; the predicted turbulent region cioncides with measured fluctuation

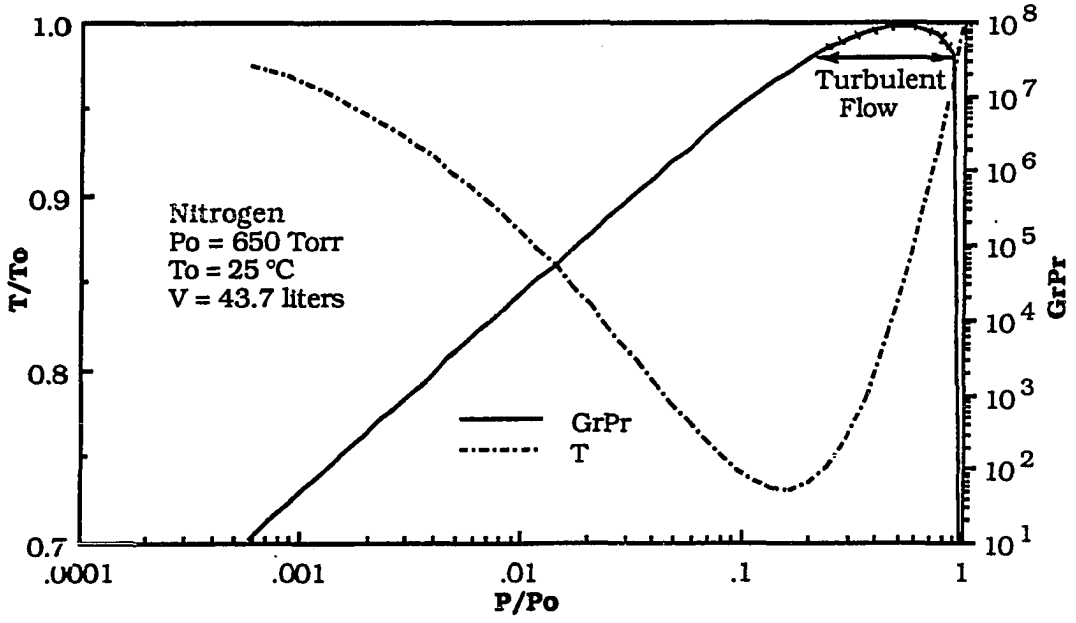

Figure 3-7 Simulation of GrPr during pump-down: Natural convection transition from laminar to turbulent flow, then returning to laminar flow

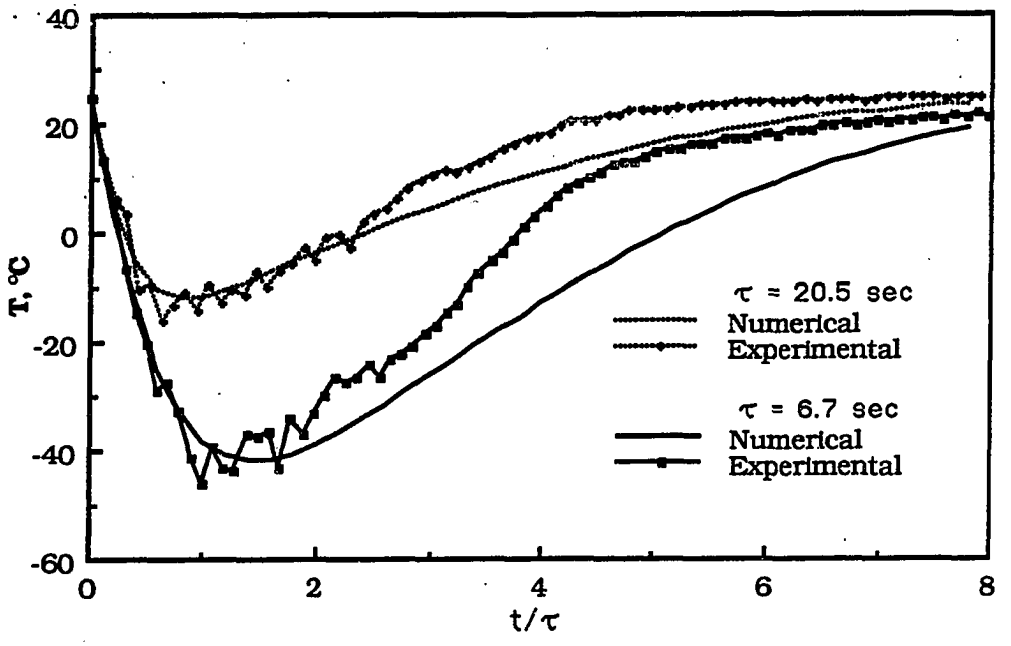

Figure 3-8 Nitrogen temperature during pump-down: Comparison between simulation and experiment

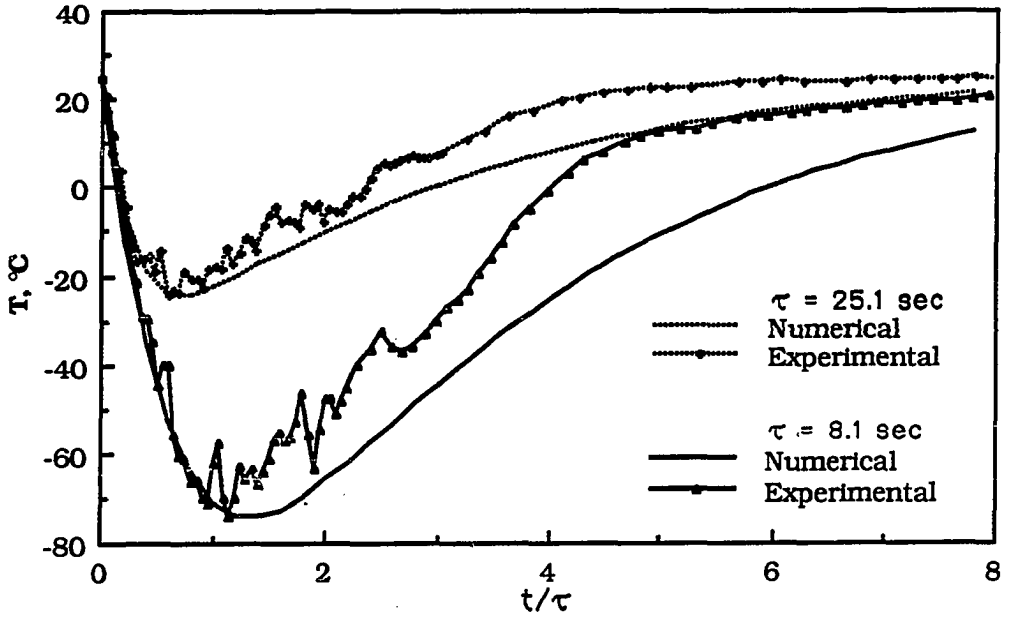

Figure 3-9 Argon temperature during pump-down: Comparison between simulation and experiment

$$\left(\frac{dT}{dt}\right)_{t=0} = -\frac{(\gamma - 1)\, T_o}{\tau} \qquad (3.51)$$

In Fig. 3-6, τ = 5.1 seconds and T_o = 298 K. Thus the initial rate of temperature change is -23 K/s which agrees with the measured value closely. The second is that natural convection in the chamber may change from laminar to turbulent flow, and then return to laminar. The onset of turbulent natural convection is generally assumed to be GrPr > 3.3 x 10^7. Fig. 3-7 shows the calculated GrPr during pump-down. For nitrogen in the given chamber,

$$\text{GrPr} = 1.1 \times 10^9 \left(\frac{p}{p_o}\right)^2 \left(\frac{\Delta T}{T}\right) \left(\frac{T_o}{T}\right)^3 \qquad (3.52)$$

where $\Delta T = T_o - T$. In this expression, the Grashof number is based on the equivalent sphere diameter, D_{ch} = 6V/A = 38.6 cm for the chamber used. As shown in Fig. 3-7, GrPr is zero at t = 0. The value quickly increases to 3.3 x 10^7 at t = 0.4 seconds (p = 600 Torr and T = 18°C) which may signify the transition from laminar to turbulent flow. However, the value of GrPr will decrease as the gas temperature recovers and the pressure decreases further. After t = 6 seconds (p = 130 Torr, T = -50°C), the value of GrPr will be lower than 3.3 x 10^7 and natural convection will again become laminar. The period of turbulent conditions revealed in the calculation coincides with the period of significant fluctuation in the measured temperature. The fluctuation in measured temperature is undoubtedly caused by fluid turbulence. The transition from laminar to turbulent conditions, or vice versa, is a very complex physical phenomena which is not amenable to exact theoretical analysis. The above discussion only shows the possible existence of such transitions during pump-down.

3.10.4 Potential Saturation Ratio of Water Vapor

Fig. 3-10 show the value of S' for water vapor during pump-down of room air with 50% initial relative humidly. In the numerical

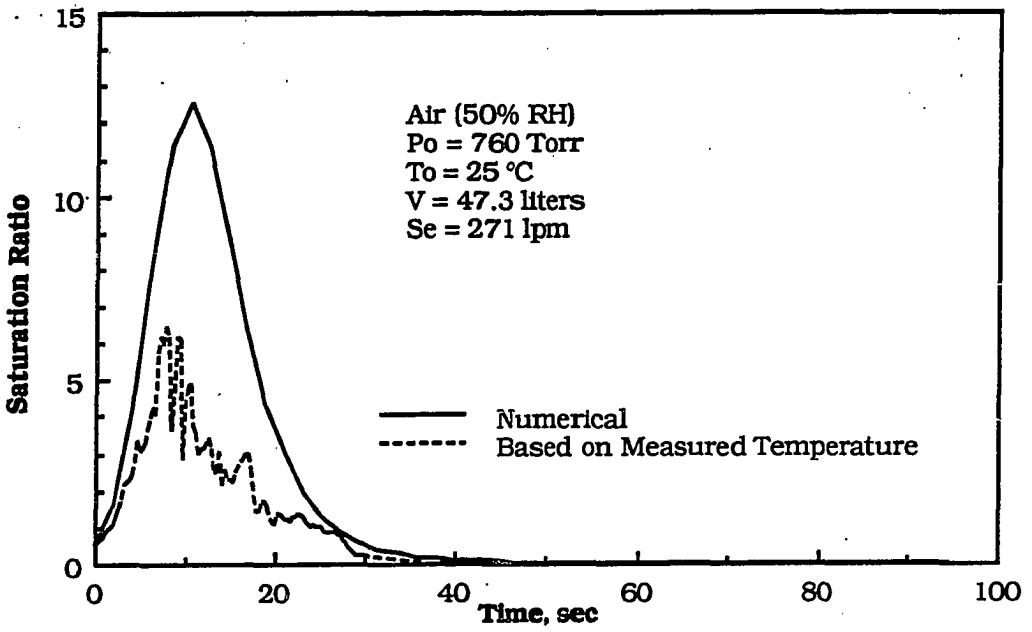

Figure 3-10 Potential saturation ratio of water vapor which indicates the occurrence of water vapor condensation

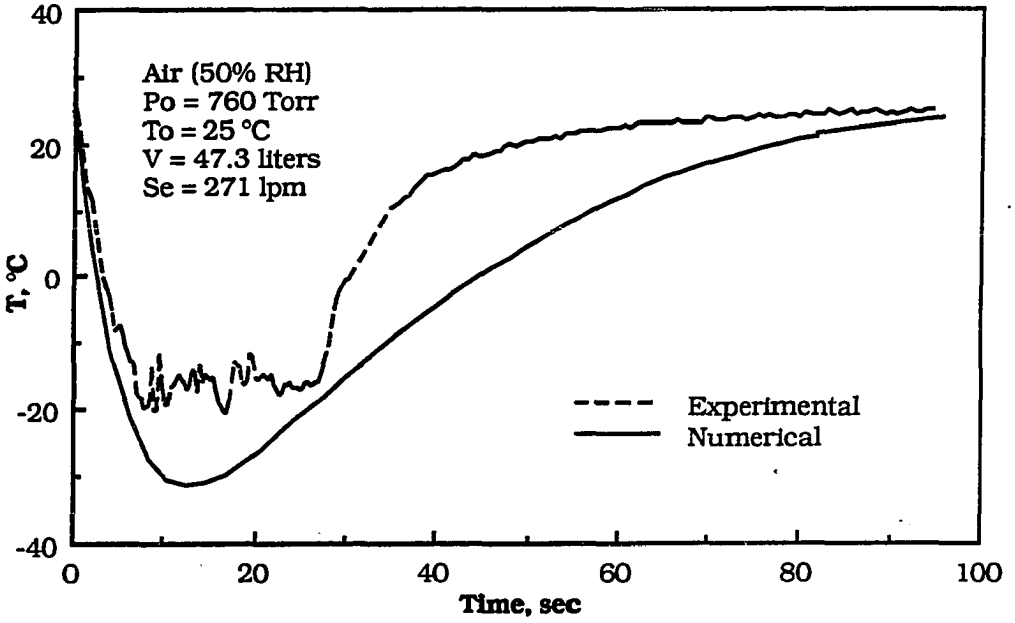

Figure 3-11 Air temperature during pump-down: Difference between simulation and measurement indicates latent heat release from water vapor condensation

simulation study, the maximum value of S' calculated is 13 indicating that water vapor will condense on existing nuclei. Since room air contains a large number of particles of diameter larger than 1 μm, about 10^4/cc. In this case, the critical saturation for condensation is only slightly higher than 1. However, if room air does not contain particles, the value of S' indicates that homogeneous nucleation of water vapor (S_c is in the range of 6 to 8) will occur. The S' value based on measured temperature is also shown in Fig. 3-10, and it shows a maximum value of 6.

More evidence of the occurrence of water vapor condensation can be seen from the temperature curves of Fig. 3-11. The measured air temperature remains almost constant over a period of time, which is believed to be the result of latent heat release from water vapor condensation. In the numerical simulation the effect due to latent heat release has been neglected. Consequently, the calculated air temperature is significantly lower than that measured during the period of water vapor condensation.

3.11 CONCLUSIONS

A thermodynamic model for vacuum pump-down in the continuum regime has been developed to predict the temperature, pressure, and vapor saturation ratio during pump down. The model can be used for various given initial conditions and properties of gas and vapor, different chamber geometries, and various pumping conditions. The model consists of a pair of ordinary differential equations which can be solved by numerical integration.

The predications made on the basis of the model have been compared with experimental data obtained with dry nitrogen, high purity argon, and room air. In all cases, the model is capable of predicting the effective pumping speed, and therefore the pressure, accurately. Effect of the temperature variation on pressure has been

taken into account in the model. For nitrogen and argon, the prediction of gas temperature agrees well with measured values. For room air, significant difference exists between the predicted and measured temperatures mainly because the effect of latent heat release has been neglected in the model. This difference can be taken as proof that water vapor nucleation and condensation have occurred during pump-down.

Along with the development of the model, order-of-magnitude analysis in this chapter has revealed other physical phenomena taking place during pump-down. These are: (i) natural convection prevails, (ii) the chamber wall temperature remains nearly constant, and (iii) the latent heat release from water vapor condensation or ice formation may be a significant heat source.

CHAPTER 4

SIMILARITY AND CHARACTERISTICS OF PUMP-DOWN PROCESSES

ABSTRACT

A generalized theory based on continuum thermodynamics is developed to describe paths along which the gas temperature (T) and pressure (p) change during pump-down. A path can be expressed in a functional form as $T/T_0 = f(Z, \gamma, p/p_0)$, where T_0 and p_0 are the initial temperature and pressure respectively; γ, the gas insentropic coefficient; and Z, a dimensionless number which is determined for a given gas, chamber, pumping rate, and initial pressure and temperature. The physical significance of Z is that it is a measure of the degree of adiabaticity of the pump-down process. When $Z = 0$, pump-down is adiabatic, and when $Z = \infty$, it is isothermal. The conditions for the expression of the path are that (i) turbulent natural convection prevails inside the chamber, (ii) pumping rate is constant.

4.1 INTRODUCTION

Experimental measurements and numerical simulations of a pump-down process in previous chapters have revealed the essential features of the physical phenomena which include change in thermodynamic state, gas flow, heat transfer, and water vapor condensation. Although factors that determine these phenomena have been systematically investigated, the solution is limited to specific gases, chambers, pumping rates, and initial conditions used in the experiment or simulation. It is the objective of this chapter to find a general solution which can apply to all cases.

In this chapter, dimensional analysis is first carried out to show the time and length scale of physical phenomena involved in pump-down. Following this the derivations of the dimensionless governing ordinary differential equations (ODEs) and interpretations of important parameters are given. Numerical simulations of these ODEs and their experimental verification are then presented.

The study in this chapter is limited to a vapor-free gas. Vapor behavior in vacuum systems during pump-down will be discussed in detail in the next two chapters.

4.2 DIMENSIONAL ANALYSIS

Pump-down is a transient thermodynamic process which involves gas flow and heat transfer. The task of dimensional analysis includes finding dimensionless quantities, the time scale of pump-down, and the length scale and characteristics of heat transfer and gas flow phenomena.

4.2.1 Dimensionless Quantities

Dimensionless temperature, density, and pressure are introduced as follows:

$$T^* = \frac{T}{T_o}; \quad \rho^* = \frac{\rho}{\rho_o}; \quad \text{and } p^* = \frac{p}{p_o} \tag{4.1}$$

The subscript "$_o$" designates the initial value of each variable. The perfect gas law in terms of dimensionless variables becomes

$$p^* = \rho^* T^* \tag{4.2}$$

Other thermophysical properties are related to these dimensionless variables as

$$\frac{\mu}{\mu_o} = T^{*1/2}; \quad \frac{k}{k_o} = T^{*1/2}; \quad \text{and} \quad \frac{\alpha}{\alpha_o} = \rho^{*-1} T^{*1/2} \tag{4.3}$$

where μ_o, k_o, and α_o are the dynamic viscosity, thermal conductivity, and thermal diffusively respectively evaluated at T_o and p_o.

4.2.2 Time Scale of Pump-Down and Dimensionless Time

The time span of pump-down in the continuum regime can be well scaled by

$$\tau = \frac{V}{S_{eo}} \tag{4.4}$$

where V is the chamber volume and S_{eo} is the effective pumping speed at initial pump-down. It takes approximate 9τ for the pressure to reduce from 760 to 0.1 Torr. Based on such a defined τ, the dimensionless time can be expressed as

$$t^* = \frac{t}{\tau} \tag{4.5}$$

4.2.3 Characteristic Chamber Dimension

In order to study heat transfer and gas flow phenomena inside the vacuum chamber, the characteristic dimension of the chamber, D_{ch}, must be defined. For a spherical chamber, it is logical to chose the diameter as D_{ch}. For a cylindrical chamber, D_{ch} may be chosen as its diameter, or height, or equivalent spherical diameter. Generally, D_{ch} can be expressed as

$$D_{ch} = \left(\frac{V}{\Gamma}\right)^{1/3} \tag{4.6}$$

where Γ is a dimensionless shape factor whose value depends on chamber geometry and choice of D_{ch}. Table 4-1 lists possible choices for D_{ch} and corresponding to Γ for vacuum chambers with simple geometries.

Table 4-1 Shape factor Γ for vacuum chambers with simple geometry

Chamber Shape	D_{ch}	Γ
Sphere With Diameter d	d	$\frac{\pi}{6}$
Cube With Edge a	a	1
Rectangular With Dimension a x b x c	a	$\frac{bc}{a^2}$
Cylindrical With	d	$\frac{\pi H}{4d}$
Diameter d and Height H	H	$\frac{\pi d^2}{4H^2}$
All Shapes	D_{ch}	$\frac{\pi}{6}$

In this work, D_{ch} is chosen to be the equivalent spherical diameter; for this choice, $\Gamma = \pi/6$ for all chambers regardless of their shape. As will be shown below, the calculation of heat transfer and gas flow is not very sensitive to the choice of Γ as long as the aspect ratio of the vacuum chamber -- the ratio of the longest to the shortest dimension -- is less than 2 (not too thin).

4.2.4 Heat Transfer Characteristics

During pump-down, natural convection governs the heat transfer from the chamber wall to the internal gas (see Chapter 3). The heat transfer coefficient at the gas-wall interface, h, depends on the Nusselt number

$$Nu = \frac{h\,(V/\Gamma)^{1/3}}{k} = C(GrPr)^N \qquad (4.7)$$

where Gr and Pr are the Grashof and Prandtl number respectively, C and N are experimentally determined constants. In terms of dimensionless variables, GrPr can be expressed as:

$$GrPr = \frac{g\,Pr\,(V/\Gamma)}{\nu_o^2}\,\frac{\rho^{*2}\,(1 - T^*)}{T^{*2}} \qquad (4.8)$$

Depending on the value of GrPr, the natural convection can be either laminar or turbulent. If GrPr is on the order of, or greater than, 10^7, turbulent natural convection occurs. Since the exact onset condition for turbulence is unknown, GrPr $\geq 3.3 \times 10^7$ is assumed in this work (at GrPr = 3.3×10^7, the turbulent Nu and thus h is the same as the laminar value which ensures continuity in heat transfer calculations).

The natural convection tends to be turbulent inside a large chamber at high pressure because the large chamber gives less constraint to the gas motion, and the buoyancy force -- the driving force for natural convection -- is important at high pressure. Details on natural convection during pump-down have been discussed in Chapter 3. Here important features of natural convection are summarized.

1) For a given gas and initial conditions, there is a critical chamber volume, denoted as V_c, for natural convection to become turbulent. V_c can be estimated by finding $(GrPr)_{max}$ -- the maximum value of GrPr during pump-down. Eq.(4.8) indicates that $(GrPr)_{max}$ occurs when the time-dependent term $\frac{\rho^{*2}\,(1 - T^*)}{T^{*2}}$ reaches a maximum. Assuming pump-down is adiabatic (this is a good approximation at the very beginning of pump-down where significant temperature difference has

not yet occurred), $T^* = \rho^{*(\gamma-1)}$ and the time-dependent term becomes $\frac{\rho^{*2}(1 - \rho^{*(\gamma-1)})}{\rho^{*2(\gamma-1)}}$ which has the maximum value of 0.1055 at $\rho^* = 0.49$ when $\gamma = 1.4$. Then

$$(GrPr)_{max} = 0.1055 \frac{g\,Pr\,(V/\Gamma)}{\nu_o^2} \tag{4.9}$$

Turbulence will occur if $(GrPr)_{max}$ exceeds the onset value. Consider air under STP conditions: $\nu_o = 0.156$ cm^2/s, Pr = 0.71. Eq.(4.9) shows that $(GrPr)_{max}$ will exceed 3.3×10^7 if V > 6 liters.

The actual chamber volume required for turbulence may be larger than just estimated because (i) the estimation is based on adiabatic assumptions (corresponding to infinite pumping rate) and (ii) larger chamber volume is required in order for turbulence to sustain for a period of time. Under normal pumping conditions, as a rule of thumb, V_c is about, or little larger than, 10 liters. V_c = 15 liters is assumed in this work.

2) If the chamber volume $V > V_c$, natural convection starts with laminar flow in the very beginning of pump-down where $(1 - T^*)$ is nearly zero, changes to turbulent flow as $(1 - T^*)$ becomes large, then returns to laminar flow as pressure further decreases and the gas temperature recovers. If $V < V_c$, the natural convection will remain laminar during the entire pump-down period.

3) In turbulent natural convection, the experimentally determined coefficients are C = 0.13 and N = 1/3. The average heat transfer coefficient is obtained from Eq.(3.44)

$$h_T = 0.13 \left\{ \left(\frac{g\,Pr\,k_o^3}{\nu_o^2} \right) \left(\frac{1 - T^*}{T^*} \right) T^{*1/2}\, \rho^{*2} \right\}^{1/3} \tag{4.10}$$

Here, h_T is independent of chamber volume and shape factor. As seen in Eq.(4.10), the term (V/Γ) cancels out because Nu depends on GrPr to the 1/3 power.

4) In laminar natural convection, C = 0.55 and N = 1/4. The average heat transfer coefficient is obtained

$$h_L = 0.55 \left(\frac{V}{\Gamma} \right)^{-1/12} \left\{ \left(\frac{g \, Pr \, k_o^4}{\nu_o^2} \right) \frac{\rho^{*2} (1 - T^*)}{T^*} \right\}^{1/4} \qquad (4.11)$$

h_L depends on V and Γ only to -1/12 power. If the aspect ratio of chamber (for example diameter/height) ranges from 0.5 to 2, the choice of Γ only cause h_L to differ approximately ±5%.

4.2.5 Characteristics of Gas Flow

To evacuate a chamber from atmospheric pressure to 0.1 Torr (so called roughing period), mechanical vacuum pumps are usually utilized. For this kind of pump, the intrinsic pumping speed S_p is nearly a constant independent of pressure when pressure great than 0.1 Torr.

Gas flow may occur in the following two situations: (i) No flow restricting device, such as a throttling valve or an orifice, is present in the pumping line. In this situation, the conductance of the pumping line in the viscous flow regime (including pipes, gate valves, elbows, etc.) is usually large in comparison with S_p. Then the effective pumping speed S_e is mostly determined by S_p. Therefore,

$$S_e = S_{eo} \qquad (4.12)$$

(ii) Restricting device is present in the pumping line. In this situation, S_e depends on the conductance of this device. If gas flow is controlled

by an orifice and choked, S_e is independent of pressure but dependent on gas temperature:

$$\frac{S_e}{S_{eo}} = \sqrt{T^*} \tag{4.13}$$

If $T^* = 0.7$, the actual S_e will be 16% lower than S_{eo}.

4.3 DIMENSIONLESS EQUATIONS

Depending on the situation of natural convection and pumping rate, pump-down may be modeled in the following cases:

Natural Convection	Pumping Rate
Turbulent	Constant
"	Variable
Laminar	Constant
"	Variable

In the subsequent derivations, the case of turbulent natural convection and constant pumping rate (TNC-CPR) is considered. The other cases can be derived similarly.

4.3.1 Equations in Time Space

Substituting all the dimensionless variables, Eq.(4.1) and Eq.(4.3) into Eq.(3.27) and Eq.(3.28), one can find the following dimensionless ordinary differential equations:

$$\frac{d\rho^*}{dt^*} = -\rho^* \tag{4.14}$$

$$\frac{dT^*}{dt^*} = \left\{ 0.13\, Z \left(\frac{1 - T^*}{T^*} \right)^{4/3} T^{*1/5}\, \rho^{*2/3} - (\gamma - 1) \right\} T^* \tag{4.15}$$

The initial conditions are $\rho^* = 1$ and $T^* = 1$ at $t^* = 0$. Therefore, under the condition of TNC-CEPS,

$$\rho^* = \exp(-t^*) \quad \text{and} \quad T^* = f(Z, \gamma, t^*) \tag{4.16}$$

Here γ is the ratio of specific heat at constant pressure to that at constant volume. Z is a dimensionless number and defined as

$$Z = \frac{\tau \omega}{\xi} \tag{4.17}$$

where

$$\tau = \frac{V}{S_{eo}}$$

$$\xi = \frac{V}{A_s} \tag{4.18}$$

$$\omega = \left(\frac{g \alpha_o}{Pr} \right)^{1/3} \tag{4.19}$$

It is noted that Z is determined only by the chamber size, initial gas properties, and initial effective pumping speed. Therefore, Z is a time-independent constant for a pump-down. The physical significance of τ, ω, ξ and Z will be explained later.

4.3.2 Equation in Thermodynamic Space

In all the previous studies, pump-down processes have been described in time space, where time is the independent variable, and gas temperature and pressure are dependent variables. This approach uses two equations, for example Eqs.(4.14) and (4.15), to describe change of gas temperature and pressure during pump-down. This section will present a single equation which describes a path in thermodynamic space along which gas temperature and pressure change during pump-down.

From the standpoint of thermodynamics, the pair number (p, T) at any instance defines the thermodynamic state of the gas. During pump-down, this state changes, and the loci of the state in a temperature-pressure diagram scribes a path, which will be referred to as a thermodynamic state path (TSP). When the condition of pump-down changes, the TSP changes. There are two advantages in using TSP to describe pump-down. First, it is more concise. Second, it represents a general solution to the gas state during pump-down.

In dimensionless quantities, the state of a gas can be defined by either (T^*, p^*) or (T^*, ρ^*). In terms of T^* and ρ^*, the TSP can be described by the following ordinary differential equation:

$$\frac{dT^*}{d\rho^*} = \left\{ -0.13\, Z \left(\frac{1 - T^*}{T^*} \right)^{4/3} T^{*1/6} \rho^{*-1/3} + (\gamma - 1) \right\} \frac{T^*}{\rho^*} \qquad (4.20)$$

with an initial condition $T^* = 1$ at $\rho^* = 1$. This ODE is derived by solving dt^* in terms of $d\rho^*$ in Eq.(4.14), and then substituting it into Eq.(4.15). The solution to the Eq. (4.20) is in the form of

$$T^* = f(Z,\ g,\ \rho^*) \qquad (4.21)$$

If T^* and p^* are used to specify the TSP, the equation is

$$\frac{dT^*}{dp^*} = \left\{ \frac{-0.13\, Z \left(\frac{1 - T^*}{T^*} \right)^{4/3} T^{*1/2} p^{*-1/3} + (\gamma - 1)}{-0.13\, Z \left(\frac{1 - T^*}{T^*} \right)^{4/3} T^{*1/2} p^{*-1/3} + \gamma} \right\} \frac{T^*}{p^*} \qquad (4.22)$$

with an initial condition $T^* = 1$ at $p^* = 1$. This ODE is derived by substituting $p^* = \rho^* T^*$ into Eq. (4.20). The solution to Eq. (4.22) is in the form of

$$T^* = f(Z, \gamma, p^*) \tag{4.23}$$

It is noted that Eq.(4.21) or (4.23) represents the similarity solution to the thermodynamic state of gases in pump-down. Pump-down processes can be performed with different combinations of gases, chambers, pumping rates, and initial conditions. However, the TSP is the same as long as these processes have the same γ and Z.

Compared with Eq.(4.22), Eq. (4.20) is simpler; therefore the pump-down processes will be analyzed based on this equation. The final results will be presented in terms of (p^*,T^*), which are the variables customarily used in vacuum science and technology.

4.3.3 Condition for Minimum Gas Temperature

A key point along a TSP is the one at which the minimum temperature occurs. Before this point, expansion cooling dominates; after it, wall heating dominates. The minimum temperature occurs when $dT^*/dt^* = 0$, or $dT^*/dp^* = 0$. Designate the minimum temperature as $\tilde{T}$ and associated pressure as $\tilde{p}$ (both are dimensionless). When $dT^*/dp^* = 0$, Eq.(4.23) yields relationship among $\tilde{T}$, $\tilde{p}$, γ, and Z

$$\tilde{p}^{-1/3}\left(\frac{1-\tilde{T}}{\tilde{T}}\right)^{4/3}\tilde{T}^{1/2} = \frac{(\gamma - 1)}{0.13\,Z} \tag{4.24}$$

Since $\tilde{T}$ and $\tilde{p}$ must also satisfy Eq.(4.23), they must have a solution in the form of

$$\tilde{T} = f_1(Z, \gamma) \quad \text{and} \quad \tilde{p} = f_2(Z, \gamma) \tag{4.25}$$

4.4 PHYSICAL SIGNIFICANCE OF Z NUMBER

This section describes the physical significance of Z and its constituents (τ, ξ, and ω) in detail. For a given gas (γ is known), Z is the only parameter required to specify a TSP for a pump-down.

4.4.1 Interpretation of τ

The term τ has the unit of time. Under the assumption that both effective pumping speed and gas temperature remains constant, one can find that

$$p^* = e^{-t/\tau} \tag{4.26}$$

This means that τ is the time constant of pressure decay (i.e. if a pump-down starts at initial gas pressure of 760 Torr, τ is the time period when the pressure reaches 280 Torr). Small τ indicates fast pumping and a small chamber. This concept has been conventionally accepted in vacuum work.

However, regarding τ as the time constant of pressure decay is not precise because gas temperature changes during pump-down. If we only assume the effective pumping speed to be a constant and allow the temperature to vary, the solution for ρ^* is

$$\rho^* = e^{-t^*} = e^{-t/\tau} \tag{4.27}$$

In this case, τ is the time constant of gas density decay. According to the perfect gas law

$$p^* = T^* e^{-t/\tau} \tag{4.28}$$

The ratio of Eq.(4.26) to Eq.(4.28) is $1/T^*$. As shown by the experimental measurements in Chapter 2, T^* can be as low as 0.7.

Therefore, Eq.(4.26) predicts pressure that is 40% higher (in the worst case) than Eq.(4.28). However, since p* varies over several orders of magnitude, the effects of temperature on overall pressure history may be minor. Eq.(4.28) may be accurate enough for engineering purposes.

4.4.2 Interpretation of ξ

The term ξ is the ratio of chamber volume-to-surface area, and it has units of length. Table 4-2 lists values of ξ for four simple chamber geometries. Generally speaking, large ξ indicates a large chamber. For example, $\xi = d/6$ for a spherical chamber. In a processing chamber, wafer holders and other apparatus inside the chamber reduce the gas volume and contribute more surface area. As a result, ξ will be reduced.

Table 4-2 Volume to surface area ratio for simple chamber geometries

Chamber shape	ξ
Sphere with diameter d	$\frac{d}{6}$
Cube with edge length a	$\frac{a}{6}$
Rectangular with dimension a x b x c	$\frac{abc}{2(ab+bc+cd)}$
Cylindrical with diameter d and height H	$\frac{Hd}{2(d+2H)}$

During a pump-down process, ξ has a significant effect on heat transfer between the chamber wall and the internal gas. Although gas temperature decreases, the wall temperature remains nearly constant, and the wall acts like a heat source to the internal gas. Large ξ means less heat can be transferred from the wall to the gas because of (i) less exposure of gas to the wall and (ii) a longer heat transfer path from the surface to the internal gas.

4.4.3 Interpretation of ω

The term ω represents the effect of gas properties on heat transfer, and it has units of length/time. In the definition of ω, the Prandtl numbers for different gases are very much the same (about 0.7). Large ω corresponds to a large heat diffusion coefficient, α_o. Thus, ω may be interpreted as the heat-penetrating rate of the chamber wall to the internal gas. The values for ω for typical gases at one atmosphere pressure and 300 K are shown in Table 4-3.

It is noted that ω is a function of initial pressure and temperature. If pump-down starts at initial conditions other than 760 Torr and 300 K, then ω must be modified according to

$$\omega = \omega_{ref} \left(\frac{T_o}{300} \right)^{1/6} \left(\frac{p_o}{760} \right)^{1/3} \qquad (4.29)$$

where ω_{ref} is the value given in Table 4-3.

Table 4-3 Heat-penetrating rate of gases[a]

Gas	ω, cm/s	α_o, cm^2/s[b]	Pr[b]	γ
Air	6.743	0.220	0.708	1.400
Argon	7.877	0.349	0.700	1.667
Helium	14.500	2.190	0.705	1.667
Hydrogen	12.867	1.540	0.706	1.409
Oxygen	6.733	0.220	0.709	1.400
Nitrogen	6.724	0.220	0.710	1.400

(a) Pressure p=760 Torr, and gas temperature T=300K.
(b) α_o and Pr are interpolated from Holman, 1986, p643-645 .

4.4.4 Interpretation of Z

The meaning of Z can be easily understood by considering two limiting cases: $Z = 0$ and $Z = \infty$.

When $Z = 0$, pump-down is an adiabatic expansion process. Setting $Z = 0$ in ODE(4.22), one finds that temperature and pressure during pump-down obey the adiabatic relationship, i.e.,

$$T^* = p^{*(\gamma-1)/\gamma} \tag{4.30}$$

The case of $Z = 0$ corresponds to one of the three limiting situations: an infinite rate of pumping ($\tau = 0$), a near-zero rate of heat transfer ($\omega = 0$), or an extremely large chamber ($\xi = \infty$).

When $Z = \infty$, pump-down is an isothermal process. This can be proved using Eq.(4.24). When $Z = \infty$, Eq.(4.24) equals zero, and $\tilde{T}$ must be equal to 1 ($\tilde{T}$ is the minimum temperature that occurs during pump-down). $\tilde{T} = 1$ indicates that the temperature is constant. This case corresponds to one of the three limiting situations: a near-zero rate of pumping ($\tau = \infty$), an infinite rate of heat transfer ($\omega = \infty$), or an extremely small chamber ($\xi = 0$).

In practice, Z is neither zero nor infinity, but between them. Correspondingly, pump-down is neither adiabatic nor isothermal. The smaller the Z number, the more likely the pump-down will be adiabatic. Thus Z is a measure of degree of adiabaticity of the pump-down process.

4.5 THERMODYNAMIC STATE PATH OF PUMP-DOWN

This section presents numerical predicted and measured TSPs for nitrogen ($\gamma = 7/5$) and argon ($\gamma = 5/3$). The TSPs for limiting cases $Z = \infty$ and $Z = 0$ are two straight lines (on a log-log plot), which are identified as isothermal and adiabatic curves respectively in Fig.4-1. TSPs for other Z numbers fall between these two limits. Since it is hard to find an analytical solution of TSP for these intermediate value of Z, numerical simulation techniques will be used.

4.5.1 Numerical Calculation

For a given γ and Z, TSP can be found by numerically integrating Eq.(4.22). A fourth order Runge-Kutta integration method is used in this work. The $\tilde{T}$ and $\tilde{p}$ associated with the TSP are also found during the integration.

Fig.4-1 shows calculated TSPs for nitrogen under different Z numbers. The following features are revealed by this figure:

1) When Z equals neither zero nor infinity, a valley exists in a TSP. As pressure or density decreases, the gas temperature first decreases, reaches a minimum, and then recovers. This temperature valley is caused by two competing factors: gas expansion cooling and wall heating. As seen in Eq.(4.20), the cooling effect is represented by

$$E_c = (\gamma - 1)$$

The heating effect is represented by

$$E_h = 0.13\, Z \left(\frac{1 - T^*}{T^*}\right)^{4/3} T^{*1/6} \rho^{*-1/3}$$

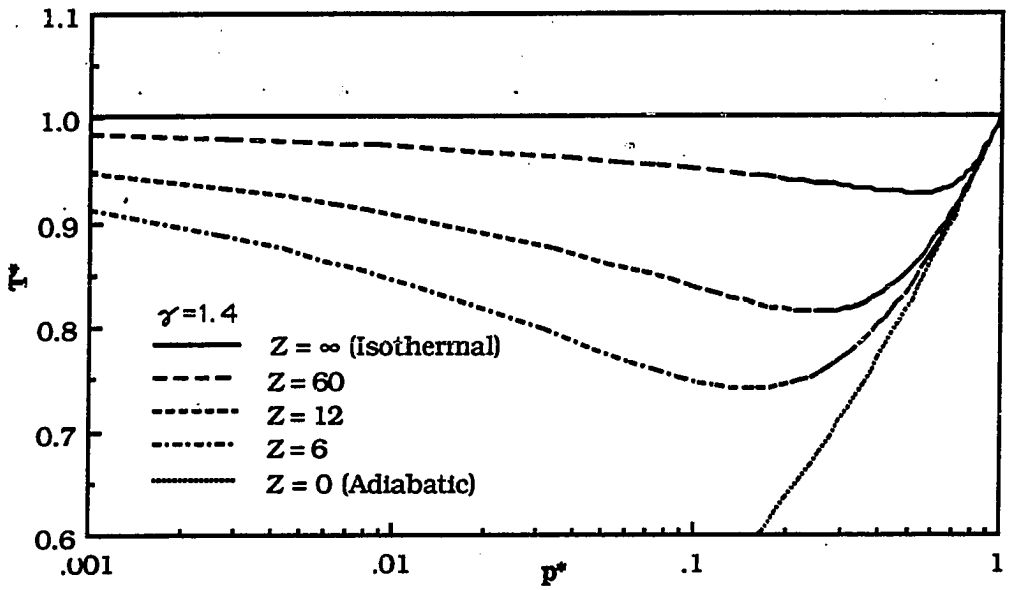

Figure 4-1 The path of thermodynamic states during vacuum pump-down for different Z numbers: Numerical simulation for nitrogen

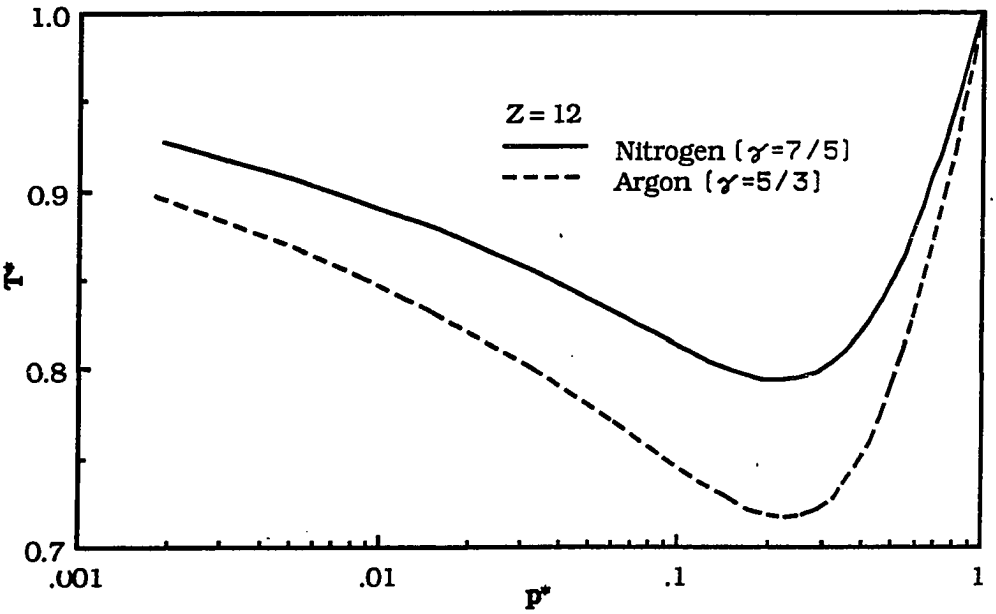

Figure 4-2 Effect of γ on thermodynamic path of vacuum pump-down: Comparison between nitrogen and argon

Here E_c is a constant for a given gas, but E_h increases as T^* and ρ^* decrease. In the initial pump-down, E_h is zero and cooling dominates. As temperature and density decrease, the heating effect becomes increasingly important. At the minimum temperature, the two effects are equal. As the density further decreases, heating prevails and eventually the gas temperature recovers to its initial temperature (equal to the wall temperature).

2) The smaller the Z, the more the gas temperature would decrease. This is due to the fact that a small Z number corresponds to fast pumping, large chamber, or a gas with a lower thermal diffusivity.

Fig.4-2 compares the TSP of argon with that of nitrogen. For a given Z, the temperature of argon drops more than that of nitrogen because argon has a higher value of γ. Note that the expansion cooling is proportional to $(\gamma - 1)$.

$\tilde{T}$ and $\tilde{p}$ for argon and nitrogen as functions of Z are plotted in Fig.4-3 and Fig.4-4. The overall picture of TSP for a pump-down process can be easily outlined with the help of $(\tilde{T}, \tilde{p})$. Fig.4-5 shows the outline for dry nitrogen with T_o = 298 K, p_o = 760 Torr. The line that connects the initial point (1,1) to $(\tilde{T}, \tilde{p})$ may represent cooling dominant period. The line that connects $(\tilde{T}, \tilde{p})$ and $(1, 0.01\,\tilde{p})$ may represent heating dominant period. When Z = 12, calculation shows that $\tilde{T}$ = 0.823 (T = 241 K) and $\tilde{p}$ = 0.272 (p = 207 Torr).

4.5.2 Experimental Verification (Large Chamber)

Experimental data reported in Chapter 2 are used to verify the numerical results presented above. Since the numerical simulation is based on turbulent natural convection, we will first take a look at the experimental data in a large chamber (a cylindrical chamber with a diameter of 45 cm, a height of 30 cm, and a volume of 47.3 liters).

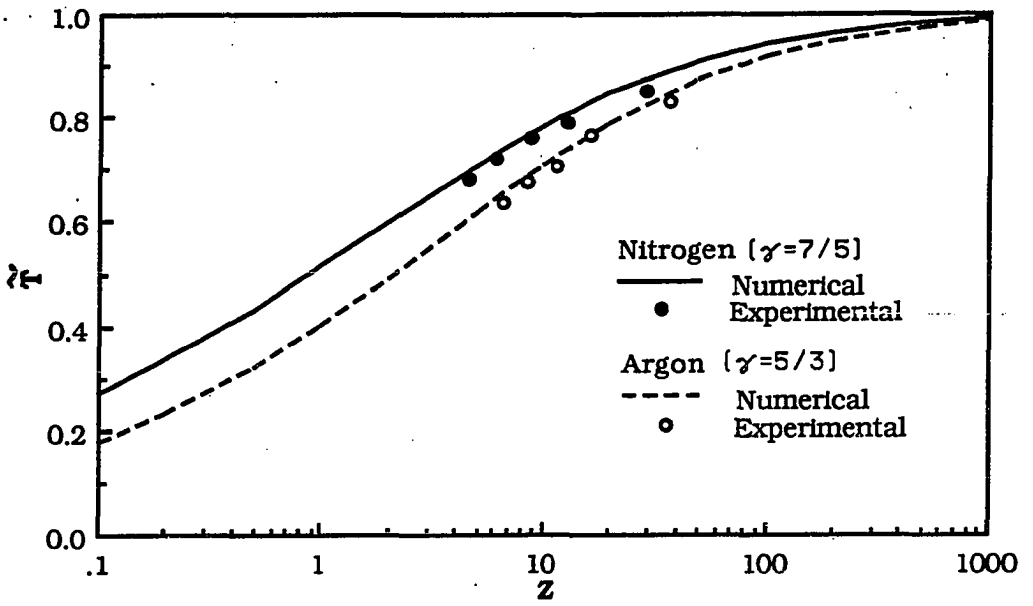

Figure 4-3 Dimensionless minimum gas temperature as a function of Z number in the case of turbulent natural convection

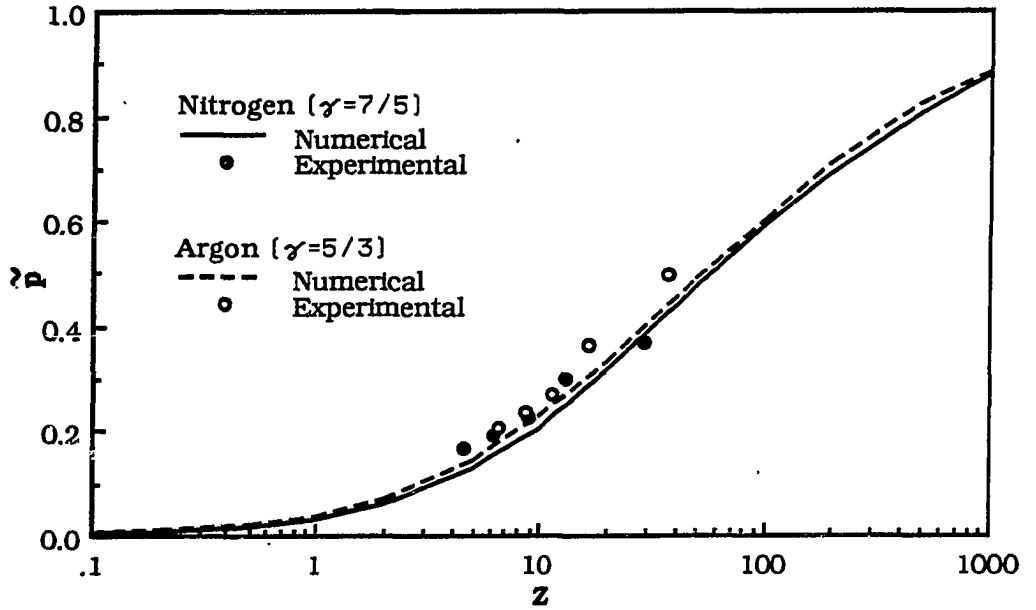

Figure 4-4 Dimensionless pressure at which the minimum temperature occurs as a function of Z number in the case of turbulent natural convection.

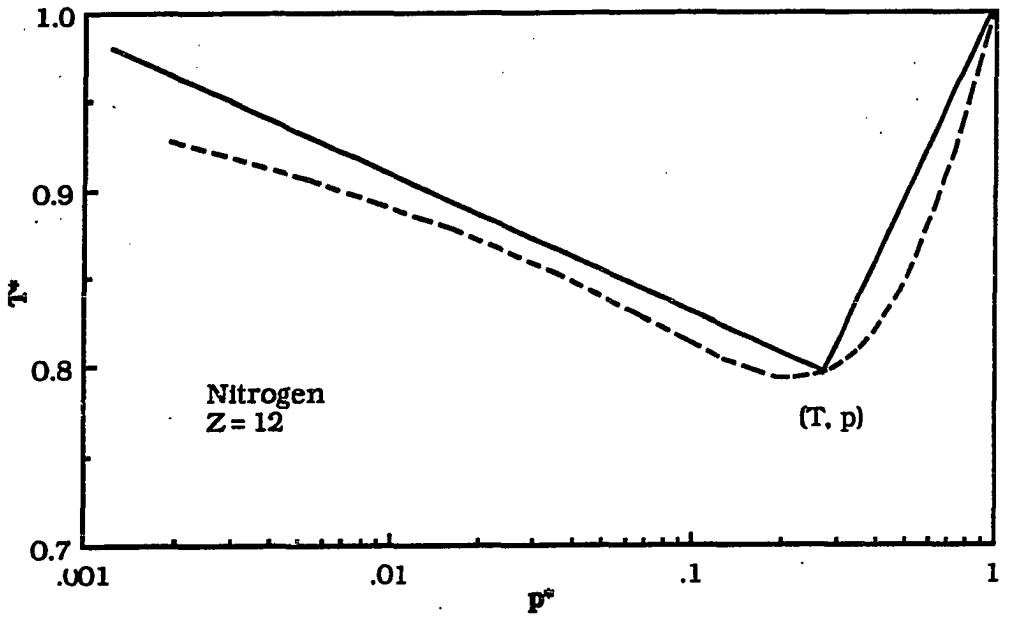

Figure 4-5 Outline the termodynamic path by connecting point (1,1) to (T, p) to (1, 0.01p) in the plane of (T*, p*)

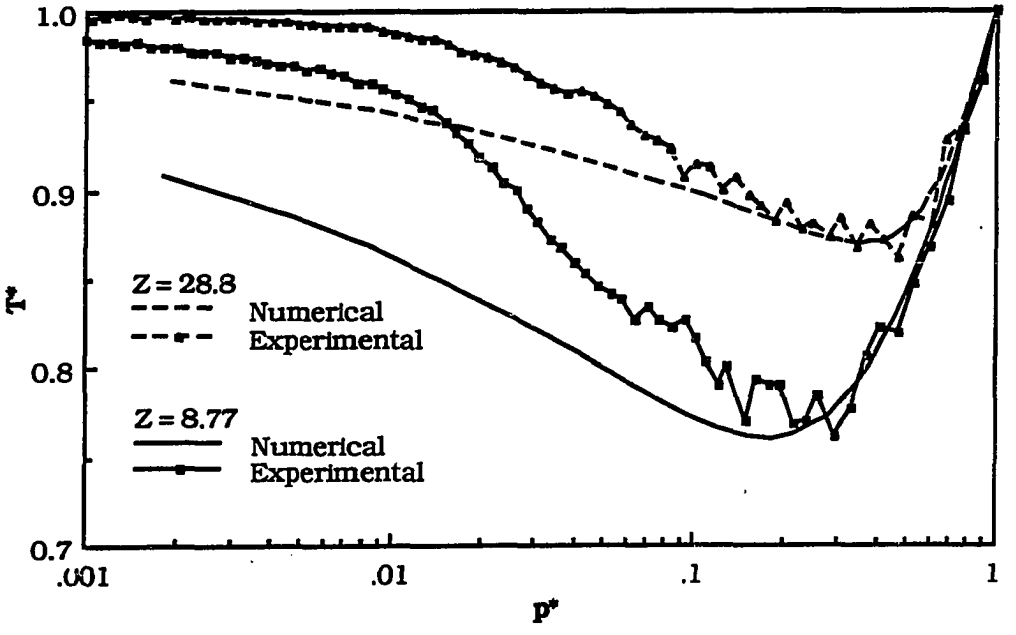

Figure 4-6 Comparison between simulated and measured thermodynamic path of nitrogen

The volume-to-surface area ratio ξ for this chamber is calculated to be 6.43 cm. Nitrogen and argon have been tested at 650 Torr and 298 K. The corresponding ω = 6.40 cm/s for nitrogen and ω = 7.48 cm/s for argon. With each gas, five values of pumping time constant τ have been tested.

Fig.4-6 compares the simulated and measured thermodynamic paths for nitrogen. Good agreement is observed. Especially in the cooling period, the simulated paths are almost identical. At low pressure, the simulated temperature at a given pressure is lower than that measured. The reason is that at low pressure ($GrPr < 3.3 \times 10^7$), natural convection is laminar. Using the turbulent heat transfer coefficient given by Eq.(4.10) underestimates the heat transfer from the chamber wall.

The measured $\tilde{T}$ and $\tilde{p}$ for nitrogen and argon are listed in Table 4-4 and Table 4-5. It is found that numerical results agree with measured data, as seen in Fig.4-3 and Fig.4-4.

4.5.3 Experimentation and Simulation in the Small Chamber

Experiments have also been carried out in a small chamber with a volume of 0.26 liters (a cylindrical chamber with a diameter of 8 cm, and height of 5.2 cm). ξ for this chamber is calculated to be 1.13 cm. Only nitrogen is tested (p_0 = 760 Torr, T_0 = 298 K, and ω = 6.743 cm/s). Z is varied by adjusting τ. The measured $\tilde{T}$ and $\tilde{p}$ are listed in Table 4-4.

Numerical calculations have also been carried out for this chamber. Since the chamber volume is small ($V < V_c$), natural convection remains laminar during the entire period of pump-down. The laminar heat transfer coefficient h_L should be used. All the ODEs derived in Section 4.2 keep the same form except that Z is replaced with $(h_L/h_T)Z$, and

$$\frac{h_L}{h_T} = \frac{0.55\,(V/\Gamma)^{-1/12}}{0.13}\left\{\left(\frac{g\,Pr}{\nu_o^2}\right)\left(\frac{1-T^*}{T^*}\right)\rho^{*-2}\right\}^{-1/12} T^{*-1/6} \quad (4.31)$$

Fig.4-7 and Fig.4-8 show the numerical results for $\tilde{T}$ and $\tilde{p}$ which agree well with experimental data.

Table 4-4 Dimensionless minimum temperature and associated pressure: experimental data for nitrogen[a]

ξ= 6.43 cm [b]				ξ= 1.13 cm [c]			
τ,sec	Z	$\tilde{T}$	$\tilde{p}$	τ,sec	Z	$\tilde{T}$	$\tilde{p}$
4.0	4.482	0.681	0.165	0.6	3.58	0.723	0.204
5.1	6.168	0.723	0.191	1.0	5.97	0.763	0.239
6.5	8.766	0.761	0.224	1.9	11.34	0.828	0.344
10.5	12.798	0.793	0.301	2.7	16.11	0.858	0.383
20.5	28.800	0.852	0.370	3.6	21.48	0.881	0.423
				4.0	23.87	0.894	0.444
				15.6	93.09	0.948	0.603

(a) γ= 1.4
(b) Cylindrical Chamber: d = 45 cm, H = 30 cm; p_o = 650 Torr; T_o = 298 K; ω_o = 6.40 cm/s.
(c) Cylindrical Chamber: d = 8 cm, H = 5.2 cm; p_o = 760 Torr; T_o = 298 K; ω_o = 6.14 cm/s.

Table 4-5 Dimensionless minimum temperature and associated pressure: experimental data for argon[a]

τ, sec	Z	$\tilde{T}$	$\tilde{p}$
5.1	5.93	0.636	0.207
6.1	7.10	0.676	0.236
8.1	9.43	0.706	0.273
12.8	14.89	0.764	0.367
25.1	29.20	0.830	0.498

(a) γ= 5/3; Cylindrical Chamber: d = 45 cm, H = 30 cm; ξ = 6.43 cm; p_o = 650 Torr; T_o = 298 K; ω_o = 7.48 cm/s.

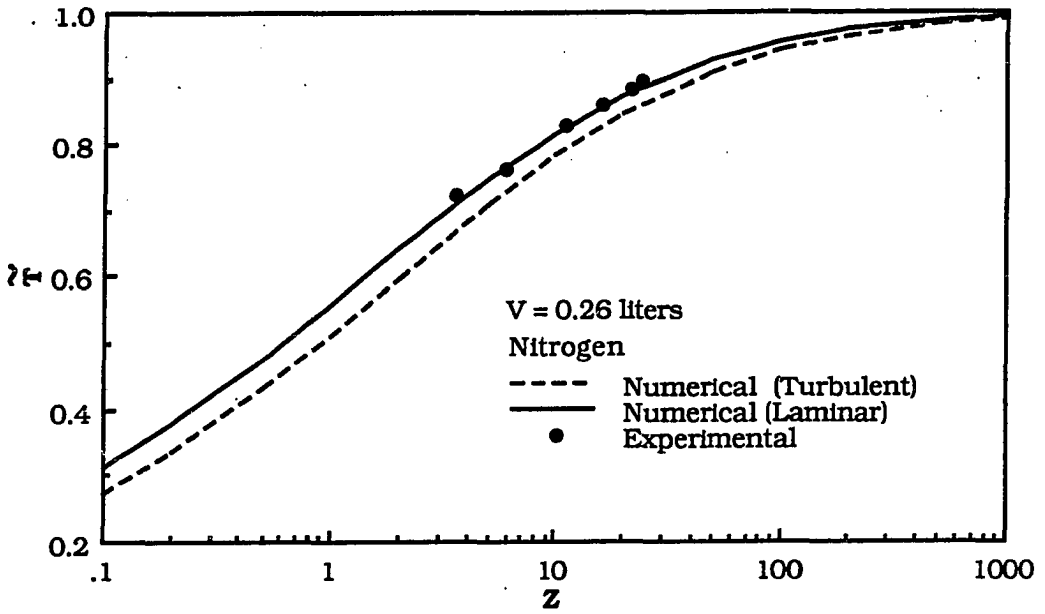

Figure 4-7 Dimensionless minimum temperature as a function of Z number in the case of laminar natural convection

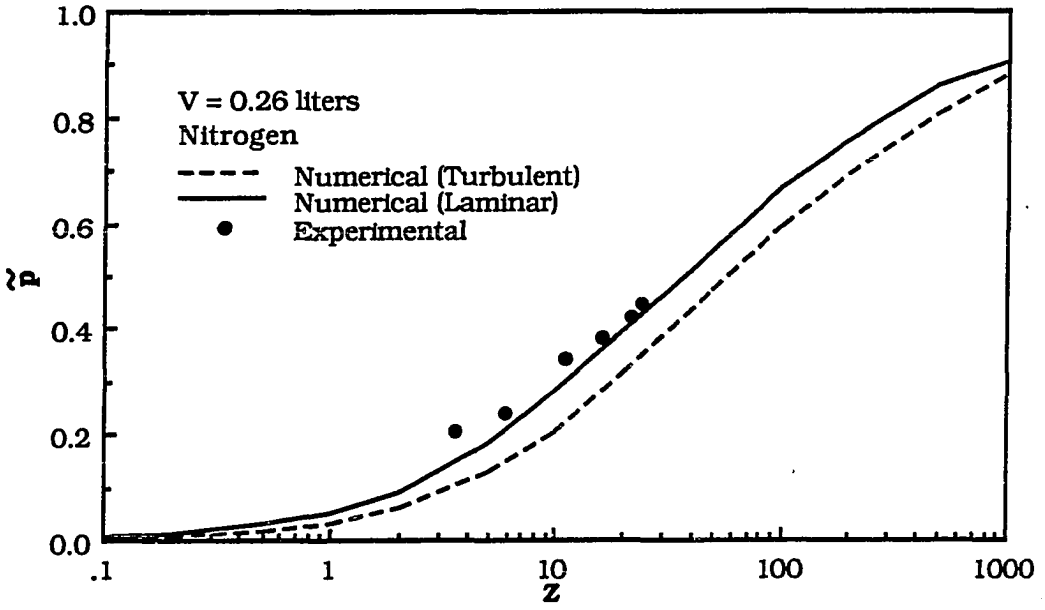

Figure 4-8 Dimensionless pressure at which the minimum temperature occurs as a function of Z number in the case of laminar natural convection

Since the turbulent natural convection coefficient h_T is independent of V and Γ, it is really convenient to use. What if we use h_T instead of h_L for the small chamber? The answer is that the temperature drop will be overestimated (see Fig.4-7). The reason is that in a laminar situation ($GrPr < 3.3 \times 10^7$), $h_L > h_T$. For nitrogen with $T_o = 298$ K and $p_o = 760$ Torr, numerical calculation shows that h_L/h_T at the point of $(\tilde{T}, \tilde{p})$ can be well approximated by

$$\frac{h_L}{h_T} = \left(\frac{V}{V_c}\right)^{-1/12} \qquad (V < V_c = 15 \text{ liters}) \qquad (4.32)$$

V is in units of liters. For V = 0.26 liters, this ratio equals 1.40.

4.6 CONCLUSIONS

A generalized theory has been developed to describe the paths along which the gas thermodynamic state changes during a pump-down in the continuum regime. Important discoveries are summarized below.

1) TSP represents the similarity solution to gas thermodynamic state (pressure and temperature). Under the condition that turbulent natural convection prevails and pumping rate is constant, the TSP is specified by a pair of dimensionless numbers Z and γ. Z, given by Eq.(4.17), is a measure of degree of adiabaticity of pump-down. Pump-down is adiabatic when Z equals zero. Pump-down is isothermal when Z equals infinity.

2) The independent variable for a TSP is gas pressure which can be obtained when the pumping time constant τ is given. τ is the ratio of the chamber volume to the effective pumping speed. Small τ means fast pumping or a small chamber.

3) The minimum temperature and associated pressure have been related with the Z number. For all the cases, numerical simulation agrees with the measured data. This indicates that Z and its constituents (τ, ξ, ω) have been properly scaled for chamber geometry, effective pumping speed, and gas thermophysical properties.

4) An equivalent spherical diameter, shape factor, and critical chamber volume for turbulent natural convection have been introduced in the heat transfer analysis. These notions are useful in characterizing the conditions of pump-down processes.

CHAPTER 5

CRITICAL PUMP-DOWN CONDITIONS FOR VAPOR CONDENSATION OR NUCLEATION

ABSTRACT

In this chapter, a theory is developed for finding the critical pump-down condition that initiates vapor condensation or nucleation. Numerical simulation and an experimental study using water vapor is carried out to verify the theory. It is found that the critical condition for water vapor condensation or nucleation depends on the combination of dimensionless Z number and initial relative humidity. Based upon the theory, a quantitative criterion is proposed for the design of clean vacuum systems.

5.1 INTRODUCTION

Vapor is often present with the carrier gas inside a vacuum system. In contrast to the carrier gas, such as nitrogen, argon, or helium, the vapor may change its phase under the range of pressure and temperature during pump-down.

The origin of the phase change can be seen from Fig.5-1. Pure matter has three phases: vapor, liquid, and solid. In the pressure-temperature diagram (p-T diagram), the phase domains are divided by three equilibrium curves. On the condensation curve (*ax*), vapor and liquid phases are in thermodynamic equilibrium, so are the liquid and solid phase on the freezing curve (*bx*), and vapor and solid phase on the sublimation curve (*cx*). The cross-point x of the three curves is called the triple point.

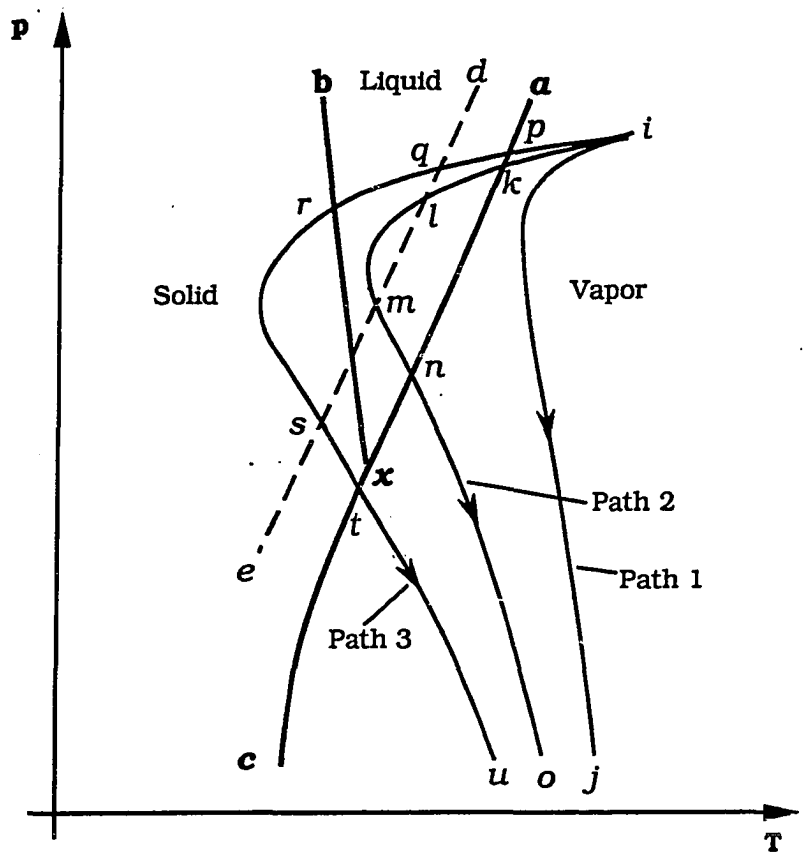

Figure 5-1 Pressure-temperature diagram of phases and vapor thermodynamic state pathes during pump-down

The vapor saturation ratio, S, is the principal variable in governing vapor behavior.

$$S = \frac{p_v}{p_s} \tag{5.1}$$

p_v is the actual vapor pressure. p_s is the saturation vapor pressure (the curve *ac*) which is described by the Clausis-Clapeyon equation

$$\log(p_s) = A + \frac{B}{T_v} \tag{5.2}$$

T_v is vapor temperature. A and B are vapor constants.

In the p-T diagram, the vapor state is represented by a point (T_v, p_v). At each point, the vapor saturation ratio S can be calculated. Vapor is said saturated when S = 1, unsaturated when S < 1, and supersaturated when S > 1. The initial vapor state (T_o, p_{vo}) is unsaturated.

Pump-down is a nonequilibrium thermodynamic process which involves the change of vapor state. In the T-p diagram, the loci of the change in vapor state during pump-down describes a path. Depending on the conditions of pump-down, three situations may arise, which are represented by three paths 1, 2, and 3 (see Fig.5-1).

Path 1: The vapor remains unsaturated, and its behavior is similar to the carrier gas. No phase change occurs.

Path 2: Along this path, the vapor state passes the vapor pressure curve at point *k*; the vapor becomes supersaturated. Further, the path intersects the critical saturation curve (*de*) at point *l*. This signifies the phase change from vapor to liquid, i.e., the vapor may either condense on existing particles or be converted to new liquid droplets. Upon temperature recovery,

the condensation or nucleation stops at point *m*, and the evaporation of formed liquid droplets may begin. After point *n*, the vapor will be at the unsaturated state again.

Path 3: This represents an extreme cooling situation when the vapor path even circumvents the triple point. Compared to Path 2, two more phenomena may occur: (i) at point *r*, the liquid droplets, which are formed along the segment (*qr*), may start to freeze to become solid crystals; vapor may directly condense to the crystals; (ii) upon temperature recovery, sublimation or melting of solid crystals may start after point *t*.

Therefore, all types of phase change: vapor to liquid, liquid to solid, solid to vapor, or the reverse, may occur during pump-down. It should be pointed out here that these paths are sketched in neglecting any disturbance from phase changes. In the actual process, these phase changes, for example vapor to liquid, will not only disturb the homogeneity of the vapor system (by adding liquid droplets), but may also release the latent heat to disturb the vapor state. Due to these disturbances, the actual paths may not be as smooth as those drawn in Fig.5-1. However, the essential physical phenomena remain.

It is difficult to completely understand the phase change phenomena just described. This study is limited to the change from vapor to liquid -- condensation and nucleation -- during pump-down. In this chapter, the critical saturation ratio S_c for condensation and nucleation is first described. Next a model is developed to predict the potential vapor saturation ratio S for given pump-down conditions including the quantities and properties of vapors, properties of carrier gas, homogeneities of the mixture, chamber geometry, and pumping rate. By comparing S and S_c, we can find the critical condition for condensation or nucleation.

5.2 CRITICAL SATURATION RATIO

Phase change from vapor to liquid can take place in two situations: (i) Condensation on existing particles. As the result of condensation, the particles grow in size, but particle number remains the same. (ii) Nucleation (vapor condensing onto molecule clusters or ions) to form stable liquid particles. As the result of nucleation, new particles are generated.

From the view of macroscopic thermodynamics, the driving force for phase transformation is the difference of the chemical potential

$$\Delta\mu = \mu_L - \mu_v \tag{5.3}$$

where μ_L and μ_v are the chemical potential of a molecule in liquid phase and vapor phase respectively. If a vapor is regarded as an ideal gas and its phase transformation takes place at a constant pressure and temperature, Gibb's relation shows

$$\Delta\mu = -\kappa T \ln(S) \tag{5.4}$$

where κ is Boltzmann constant.

A necessary condition for vapor to change to liquid is that $\Delta\mu < 0$ (i.e. when $\mu_l < \mu_v$: liquid is a stable phase). Consequently, S must be greater than 1, which indicates that the vapor must be, at least, at a supersaturated state.

However, supersaturated vapor cannot change to a liquid state until an energy barrier is overcome. The energy barrier is the energy required to create a new liquid surface through either creation of new stable nuclei or growth on an existing nucleus. Depending on the characteristics of the vapor system, the energy barrier and the critical

saturation ration S_c may differ significantly in both nature and magnitude. The complete physical picture of nucleation and condensation, especially in the presence of more than one vapor species and foreign nuclei, is not clear. Some cases that are best understood and relevant to pump-down are described below. Nuclei of a spherical shape are considered.

5.2.1 Homogeneous Condensation

This refers to condensation on a stable particle that contain the same type of molecule as the vapor. Let the particle diameter be d_o. If condensation occurs and the particle growth to a new size d, the change in Gibb's free energy is

$$\Delta G = \frac{-1}{6v_l} \pi (d^3 - d_o^3) k \ln(S) + \pi (d^2 - d_o^2) \sigma \qquad (5.5)$$

where v_l is the molecule volume in liquid phase and σ is the surface tension of the flat liquid surface. The first term in the RHS represents the decrease in chemical potential when vapor molecules change to a bulk liquid. The second term represents the increase in surface energy.

The condition for the particle to survive and continue to grow (i.e. for condensation to proceed) is

$$\frac{d(\Delta G)}{d(d)} \Big|_{d=do} \leq 0 \qquad (5.6)$$

i.e.,

$$\kappa T \ln(S) \geq \frac{4 \sigma v_l}{d_o} \qquad (5.7)$$

The term on the right side is the energy barrier for condensation on the particle of size d_o. The critical saturation ratio for the onset of condensation, S_c, is obtained when two sides in Eq.(5.7) are equal, i.e.

$$\ln(S_c) = \frac{4\sigma v_l}{\kappa T d_o} \qquad (5.8)$$

This is the well known Kelvin equation. The special case is $d_o = \infty$ (flat surface), where the energy barrier is zero, and $S_c = 1$. Figure 5-2 shows S_c for water vapor condensation as a function of particle diameter. For particles with diameter larger than 0.1μm, S_c is very close to 1.

Strictly speaking, the Kelvin equation is only applicable to homogeneous condensation. In the presence of foreign nuclei, condensation is heterogeneous. However, if the foreign nuclei are chemically and electrically neutral with respect to the vapor molecules, the Kelvin equation can still be used.

5.2.2 Homogeneous Nucleation

If particles are absent in the mixture, phase change from vapor to liquid must start with the creation of new nuclei. This is called a nucleation process. If a single vapor is involved, the nucleation process is homogeneous.

It is necessary to describe the terminology for nucleation processes before further discussion. According to Springer (1978), characteristics of a pure vapor system are described by single molecules, aggregates, embryos, critical nuclei, and stable nuclei (or particles). An aggregate contains from 2 to (g_o-1) molecules, where g_o is small enough such that the aggregate can disintegrate spontaneously into molecules. Aggregates are treated as gas like. An embryo contains enough molecules such that its properties can be described by the bulk liquid properties and surface tension of a flat surface. A single embryo of a certain size is physically unstable (if one observes a single embryo, one may find the embryo undergoes size change its size

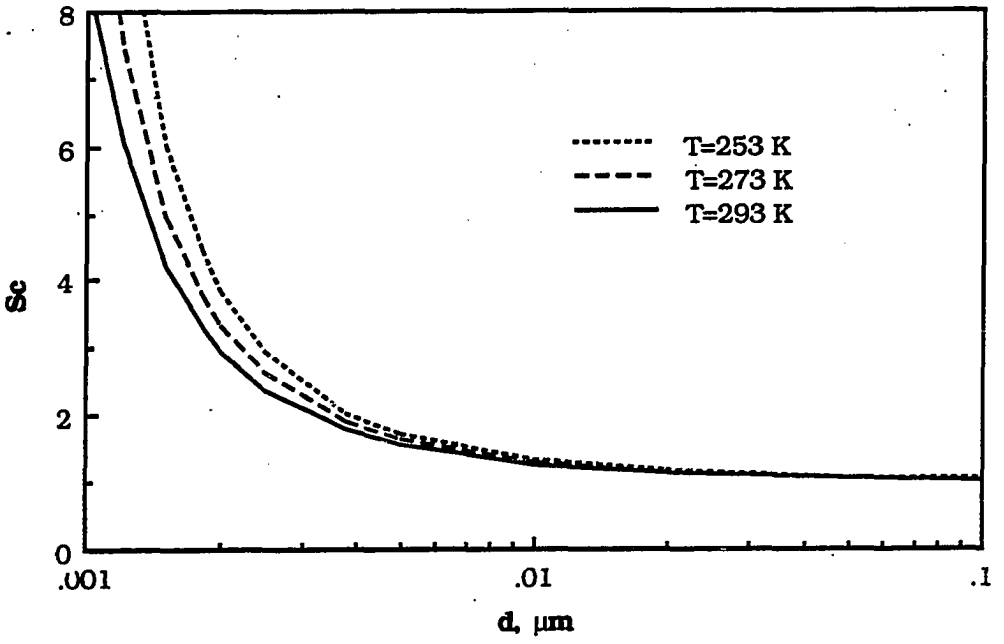

Figure 5-2 Critical saturation ratio of water vapor condensation as a function of nuclei diameter

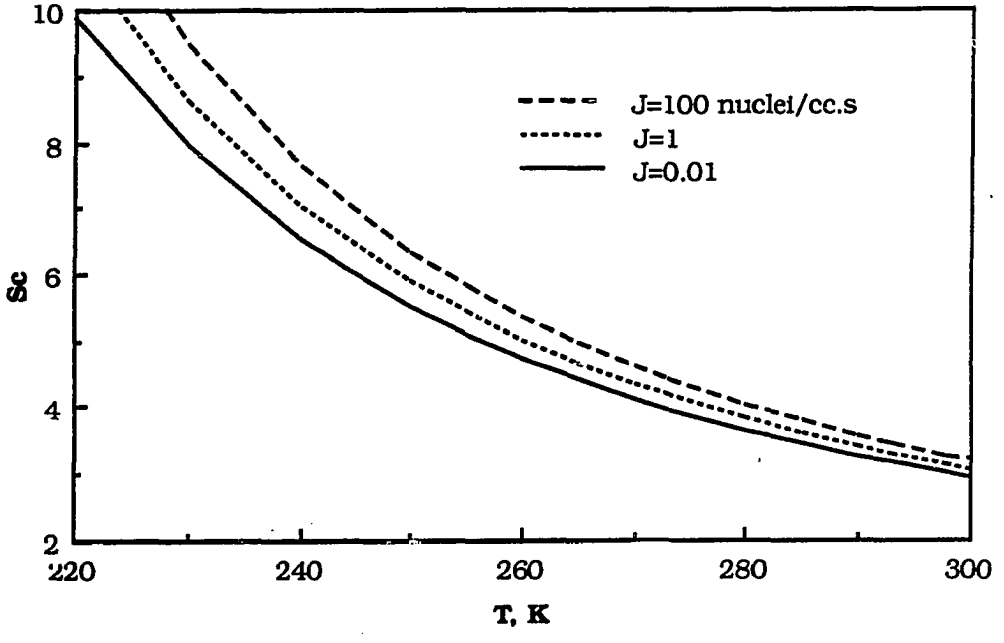

Figure 5-3 Water vapor homogeneous nucleation: Critical saturation ratio as a function of temperature

randomly or even disappear because of microscopic thermal and density fluctuation in the vapor system). Statistically, however, there is a stable population distribution of embryos. A critical nucleus contains g^* molecules; g^* is the smallest number that makes the nucleus physically stable. The value of g^* depends on the vapor state. Nuclei are those particles containing molecules greater than g^*. Nuclei are physically stable; their size may still change, but this change is not random and can be determined from the macroscopic thermodynamic state of the vapor system.

One may suspect that a vapor molecule (d_o = 3.85 Å) may serve as a nucleus. If this were the case, S_c must be 268 for water vapor, calculated by the Kelvin equation (assuming that surface tension and bulk density still have meaning). The cloud chamber experiments show $S_c < 8$ (When T = 268K). Therefore, the nucleus in this case cannot be single molecule. According to nucleation theory, an embryo distribution exists:

$$\frac{n_d}{n_1} = \exp\left(\frac{-\Delta G_d}{\kappa T}\right) \tag{5.9}$$

where n_d is the concentration of embryo of diameter d, n_1 is the concentration of vapor molecules, and ΔG_d is the free energy associated with the formation of embryos of diameter d. The expression ΔG_d is the same as Eq.(5.5) except that $d_o = 0$ (actually d_o should be equal to the vapor molecule diameter)

For S > 1, the vapor is at a metastable state, ΔG_d is a maximum at

$$d^* = \frac{4\sigma v_1}{\kappa T \ln(S)} \tag{5.10}$$

where d^* is called the critical nuclei diameter.

According to classical nucleation theory, the nucleation rate (the rate for generating stable nuclei) can be expressed as

$$J = C^* Ze\, n_{d^*} \tag{5.11}$$

where C^* is the collision frequency between vapor molecules and the critical nuclei; Ze, the Zeldovich nonequilibrium factor; and n_{d^*}, the critical nuclei concentration. Expressions for C^*, Ze, and n_{d^*} have been summarized by Springer (1978).

The classical theory remains the best for explaining most available experimental data, especially for water vapor. An expression for S_c, derived from the Beker-Doering-Zeldovich theory (one of the classical theories), is given by Katz and Ostermier (1967) as:

$$\left(\frac{p_s}{T}\right)^2 \frac{\sqrt{\sigma M}}{\rho'} S_c^2 \exp\left\{-17.56 \left(\frac{M}{\rho'}\right)^2 \left(\frac{\sigma}{T}\right)^3 \left[\ln(S_c)\right]^{-2}\right\} = 1.05 \times 10^{-26} \tag{5.12}$$

where p_s is the vapor saturation ratio in Torr; σ, the surface tension in dyne/cm; ρ', the liquid density in g/cc; T, the absolute temperature in K; and M, the molecular weight in g/mole. This criterion is based on the rate of formation of stable nuclei to be 1 drop/(cc.sec).

Figure 5-3 shows S_c for homogeneous nucleation of water vapor verses temperature. The classical theoretical prediction agrees with experimental data within 8% (Heist and Reiss, 1968). When temperature is reduced from 300 to 230 K, S_c for nucleation increases from 3.1 to 8.6 (corresponding to the size of stable nuclei of 20 to 10 Å).

5.2.3 Nucleation on Ions

Ions can become condensation sites when saturation is high enough (beyond 4 for water vapor). An ion provides a central electrical field. In this case, the free energy change associated with the condensation is

$$\Delta G = \frac{-1}{6v_1}\pi (d^3 - d_o^3)\, k \ln(S) + \pi (d^2 - d_o^2)\, \sigma + \frac{q^2}{2}\left(\frac{1}{\varepsilon_g} - \frac{1}{\varepsilon}\right)\left(\frac{1}{d} - \frac{1}{d_o}\right) \tag{5.13}$$

where ε is the liquid dielectric constant, ε_g is the dielectric constant surrounding the gas mixture, q is the ion charge, and d_o is the ion diameter. When comparing Eq.(5.13) with Eq.(5.5), the additional term (third term in the RHS) represents the change in ion electrical field energy due to the condensate.

The necessary condition for vapor to condense onto ions is

$$\frac{d(\Delta G_d)}{d(d)}\Big|_{d=do} \leq 0 \tag{5.14}$$

This condition is always satisfied for $S > 1$. However, if S is not large enough, the scale of condensation is very limited because of the local minimum present in ΔG_d (Fig.5-4). For a singly charged ion when $S = 3$, the minimum of ΔG_d for water vapor occurs at $d = 5$Å, beyond which condensation can not proceed because of the local increase in free energy. The size of $d = 5$Å is usually undetectable. In order for vapor to continuously condense onto ions, the local minimum in ΔG_d must be absent. This type of condensation is often referred to as a catastrophic condensation. Mathematically, it requires that

$$\frac{d^2(\Delta G_d)}{d^2(d)} \leq 0 \tag{5.15}$$

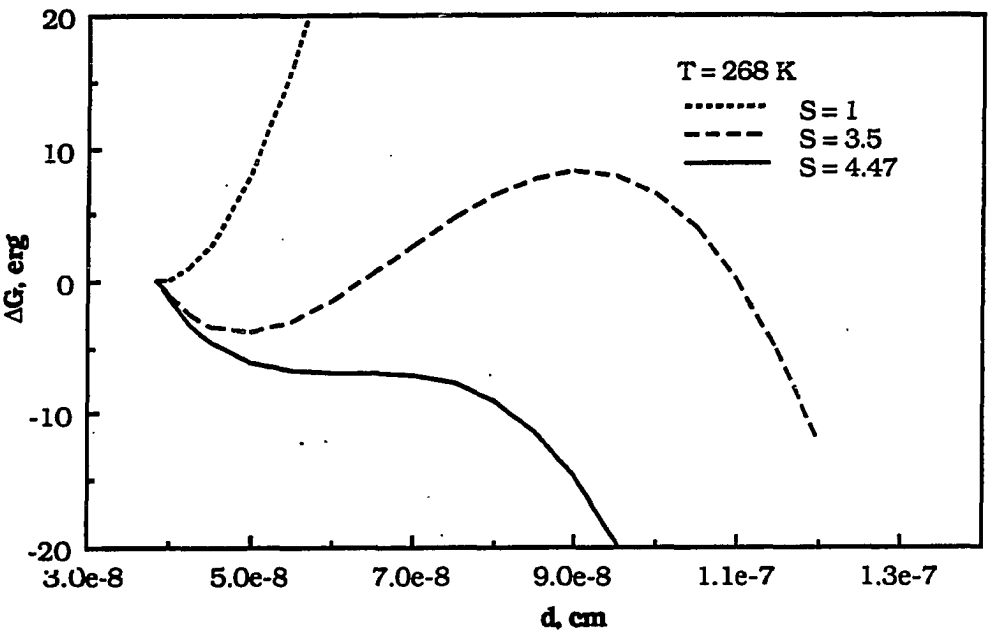

Figure 5-4 Water vapor condensation on ions: Free energy change vs. drop diameter at different saturation ratios

When Eq.(5.15) equals zero, S_c for the catastrophic condensation on ions is obtained:

$$\ln(S_c) = \frac{3.874\,\sigma^{4/3} v_l}{\kappa T q^{2/3} \left(1/\varepsilon_g - 1/\varepsilon\right)^{1/3}} \qquad (5.16)$$

For water vapor condensation onto a singly charged ion at T = 268 K, $\varepsilon_g = 1$, $\varepsilon = 80$ (water), and $q = 4.8 \times 10^{-10}$ esu, S_c is evaluated to be 4.26 which agrees with experimental value ($S_c = 4.2$ for negative ion in Wilson's cloud chamber experiment).

It is noted that the polarity of ions has not been taken into account in Eq.(5.16). Actually, higher saturation is needed for condensation onto positive ions. Experimental results summarized by Mason (1972) shows that S_c is close to 6 for a singly charged positive ion. White and Kassner (1971) have modified the theory to include the effect of polarity to make the theoretical prediction consistent with experimental observation.

5.3 POTENTIAL VAPOR SATURATION RATIO

With an understanding of the critical saturation ratio for condensation or nucleation, we now proceed to find the actual vapor saturation during pump-down. For this purpose, the following assumptions are made:

1) Vapor and gas exhibit ideal gas behavior and are uniformly distributed inside the vacuum chamber.
2) Vapor and gas are always in thermal equilibrium.
3) Vapor and gas are pumped out at the same speed.
4) No vapor condensation or nucleation is allowed.
5) Turbulent natural convection prevails inside the chamber.

6) Pumping rate remains constant.
7) Wall temperature remains constant.

Before finding an expression for the actual saturation ratio S, we first develop an ordinary differential equation (ODE) that describes the mixture and the vapor state during pump-down. In a dimensionless form, the thermodynamic state is specified by (p*,T*), where

$$p^* = \frac{p}{p_o} \quad \text{and} \quad T^* = \frac{T}{T_o} \tag{5.17}$$

p is the mixture (total) pressure with initial value p_o; T is the mixture temperature with initial value T_o. In terms of T* and p*, the ODE is written as (see Chapter 4 for details)

$$\frac{dT^*}{dp^*} = \left\{ \frac{-0.13\,Z\left(\frac{1-T^*}{T^*}\right)^{4/3} T^{*1/2} p^{*-1/3} + (\gamma - 1)}{-0.13\,Z\left(\frac{1-T^*}{T^*}\right)^{4/3} T^{*1/2} p^{*-1/3} + \gamma} \right\} \frac{T^*}{p^*} \tag{5.18}$$

with the initial condition T* = 1 at p* = 1.

Originally, this equation was developed for the mixture temperature and pressure. However, based on the assumption that the mixture and vapor are always in thermal equilibrium and the vapor pressure is proportional to the total pressure, we have

$$\frac{p_v}{p_{vo}} = p^* \quad \text{and} \quad \frac{T_v}{T_o} = T^* \tag{5.19}$$

Therefore, ODE (5.18) also describes the vapor state.

The ODE (5.18) can be solved by numerical integration for a given Z and γ. The solution can be expressed in a functional form as

$$T^* = f_1(Z, \gamma, p^*) \tag{5.20}$$

On the on T*-p* plane, this function describes a curve which will be referred to as thermodynamic-state-path (TSP) of the mixture or the vapor.

At each point of TSP, (p^*, T^*), the vapor saturation ratio can be calculated as:

$$S = p_{vo} \frac{p^*}{10^{(A + \frac{1}{T^*}\frac{B}{T_o})}} \tag{5.21}$$

Since of $T^* = f_1(Z, \gamma, p^*)$, the saturation ratio can be expressed in a functional form as

$$S = f_2(Z, \gamma, A, B, p_o, T_o, p_{vo}, p^*) \tag{5.22}$$

This specifies a curve (S versus p*) for the pump-down process. We will refer to this curve as a saturation curve (S-Curve).

A very important point on the S-Curve is the point where the maximum saturation ratio occurs. Let us denote the maximum saturation ratio as S_{max} and the associated dimensionless pressure as $\hat{p}$ and temperature as $\hat{T}$. It is found that $\hat{p}$ and $\hat{T}$ must satisfy the following constraint (derived from the condition of $dS/dp^* = 0$).

$$\hat{p}^{-1/3}\left(\frac{1 - \hat{T}}{\hat{T}}\right)^{4/3}\hat{T}^{1/2} = \frac{\left\{(\gamma - 1) + \frac{1}{(1 + \frac{1}{\hat{T}}\frac{B}{T_o})}\right\}}{0.13\,Z} \tag{5.23}$$

Since $\hat{p}$ and $\hat{T}$ must also satisfy Eq.(5.21), they must have a solution of the form

$$\hat{p} = f_1(Z, \gamma, T_o, B) \quad \text{and} \quad \hat{T} = f_2(Z, \gamma, T_o, B) \tag{5.24}$$

Substituting $\hat{p}$ and $\hat{T}$ to Eq.(5.21), one can find that S_{max} can be expressed as

$$S_{max} = f(Z, \gamma, A, B, p_o, T_o, p_{vo}) \tag{5.25}$$

where p_o is included into the function because it is needed to define the dimensionless pressure.

The above formulation enables us not only to find the TSP and S-Curve during pump-down but also to specify the pump-down parametrically. However, it is necessary to stress once more that Eqs.(5.18) and (5.21) do not consider any disturbance due to the phase change. The phase change (condensation or nucleation), consumes the extra vapor (in addition to that being pumped out). It also releases latent heat which will significantly warm up the mixture. Therefore, the saturation calculated by Eq.(5.21) may be referred to as a potential vapor saturation ratio (PVSR) because it is a maximum attainable value at a given p^* and T^* during pump-down. Through the calculation of PVSR, the critical condition of pump-down can be determined by comparing PVSR with the critical saturation ratio S_c.

5.4 CRITICAL CONDITION OF PUMP-DOWN

The general thermodynamic criterion for vapor condensation or nucleation is that the actual vapor saturation ratio S must exceed the critical saturation ratio S_c, i.e.,

$$S > S_c \tag{5.26}$$

From the discussion in Section 5.3, it is known that S_c depends on the type of process involved (condensation or nucleation; homogeneous or heterogeneous). S_c also varies with vapor temperature. Since it has been proven that $T_v/T_o = f(Z, \gamma, p^*)$, S_c during pump-down may be expressed in the functional form

$$S_c = f(\Psi, Z, \gamma, T_o, p^*) \tag{5.27}$$

where Ψ represents the type of process and associated parameters.

From the formulations in Section 5.3, we find that actual saturation ratio (in the absence of any disturbance) can be expressed as

$$S = f(\Omega, p^*) \tag{5.28}$$

where $\Omega = (Z, \gamma, A, B, p_o, T_o, p_{vo})$ is a group of constants representing characteristics of a pump-down. This includes the properties of vapor and carrier gas, initial conditions, and dimensionless Z number. We will refer to Ω as the condition of pump-down. The critical condition of pump-down, denoted as Ω_c, is the Ω that will just initiate a condensation or nucleation process.

Ω_c can be studied conveniently with the help of S-p* diagram (Fig.5-5). For a given Ω, Eq.(5.28) specifies a curve, which is a S-Curve. When the type of condensation process is determined (Ψ is given), Eq.(5.27) also specifies a curve, which is called a S_c-Curve. The critical Ω_c is the condition such that the S-Curve is tangent to the S_c-Curve. If S_c is a constant, Ω_c can be found when

$$S_{max} = f(\Omega_c) = S_c \tag{5.29}$$

If S_c is a variable, Ω_c can be found from the following two conditions:

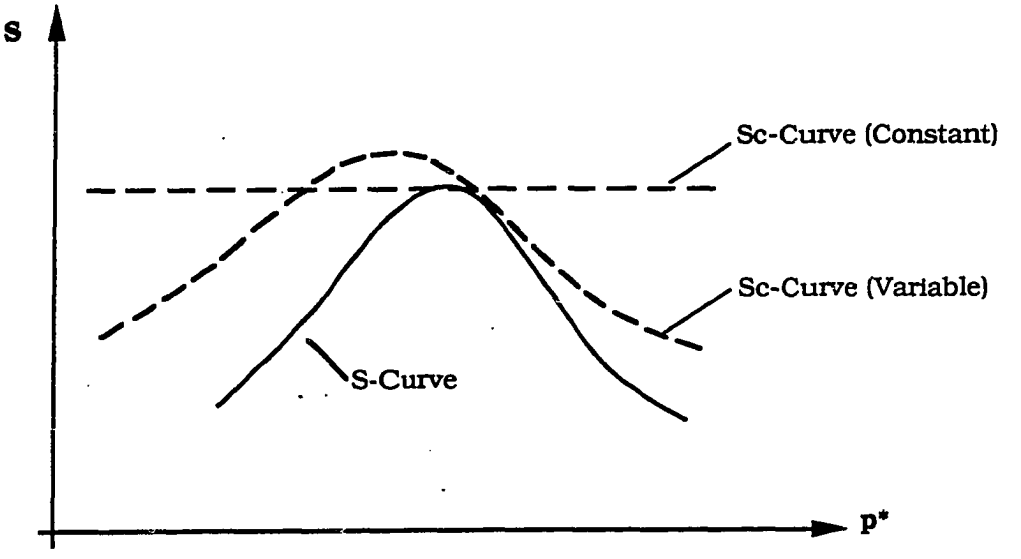

Figure 5-5 Saturation ratio vs. pressure during pump-down: Critical condition of pump-down is found when the S-Curve inscribes the Sc-Curve

$$\frac{dS}{dp^*} = \frac{dS_c}{dp^*} \quad \text{and} \quad S = S_c \tag{5.30}$$

5.5 NUMERICAL SIMULATION FOR WATER VAPOR

Water vapor is the most common condensable species in vacuum systems. As an application of the theory developed above, water vapor is investigated under the following conditions:

Vapor Constants: A = 9.183837, B = -2403.3699
Carrier Gas: Nitrogen or Air (γ = 1.4)
p_o = 760 Torr, T_o = 298 K

Variables in the investigation are Z number and relative humidity RH. Note that the initial water vapor pressure is related to RH by

$$p_{vo} = p_{so}\, RH \tag{5.31}$$

When γ, A, B, p_o, and T_o in Ω are given, Z and RH are sufficient to specify a pump-down process. In the following study, numerical simulation techniques are used to find the critical value for Z and RH that initiates water vapor condensation or nucleation. At the same time, the features such as TSP, S-Curve, and S_c-Curve will be illustrated.

5.5.1 TSP of Water Vapor

For a given Z, ODE (5.18) can be integrated to yield a TSP for water vapor, which can be expressed as

$$T^* = f_1(Z,\ p^*) \tag{5.32}$$

Figure 5-6 shows TSP for Z = 16. A valley in the temperature has been found because of competition of expansion cooling and wall heating (Chapter 4 has explained this phenomena in detail).

5.5.2 Potential Saturation Curve

For a given RH, PVSR can be calculated by Eq.(5.21) at each point (T^*, p^*) of TSP. The solution is of the form

$$S = f_2(Z, RH, p^*) \tag{5.33}$$

Fig.5-6 shows PVSR for Z = 16 and RH = 40%. A peak is found in PVSR during pump-down. As pressure is reduced, the saturation ratio starts to increase until it reaches a maximum, then decreases. The peak in the saturation ratio mainly results from the valley in the temperature. In the definition of $S = p_v/p_s$, the numerator p_v continually decreases during the entire period of pump-down. However, in the initial period when the temperature decreases, the denominator p_s decreases faster than p_v. As a result, S increases. In later period when the temperature recovers, p_s recovers while p_v continuously decreases which causes S to decrease.

Although the saturation curve is almost opposite of the temperature curve, the maximum saturation ratio occurs before the temperature reaches the minimum for a given Z. For Z = 16, S_{max} occurs at 257 Torr ($\hat{p}$ = 0.338). The minimum temperature occurs at 200 Torr ($\hat{p}$ = 0.263). This phenomena can be proved analytically. It can be shown that at S_{max}:

$$\frac{dT}{dt} = -\frac{T}{\rho}\left(\frac{1}{1+\frac{B}{T}}\right)\frac{d\rho}{dt} \tag{5.34}$$

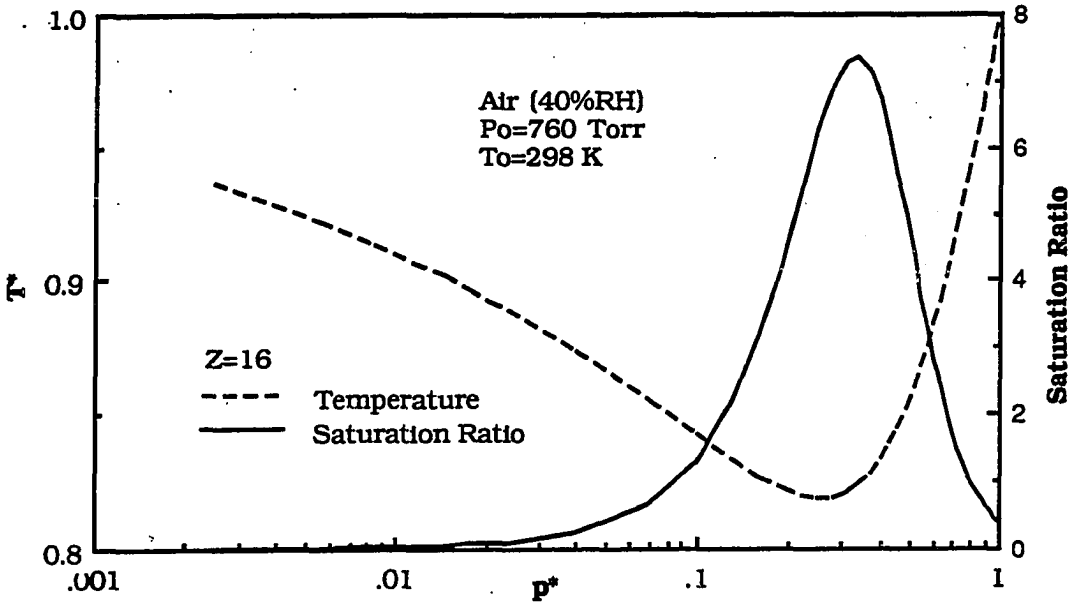

Figure 5-6 Water vapor saturation ratio and air temperature during pump-down: Maximum saturation ratio occurs before the minimum temperature

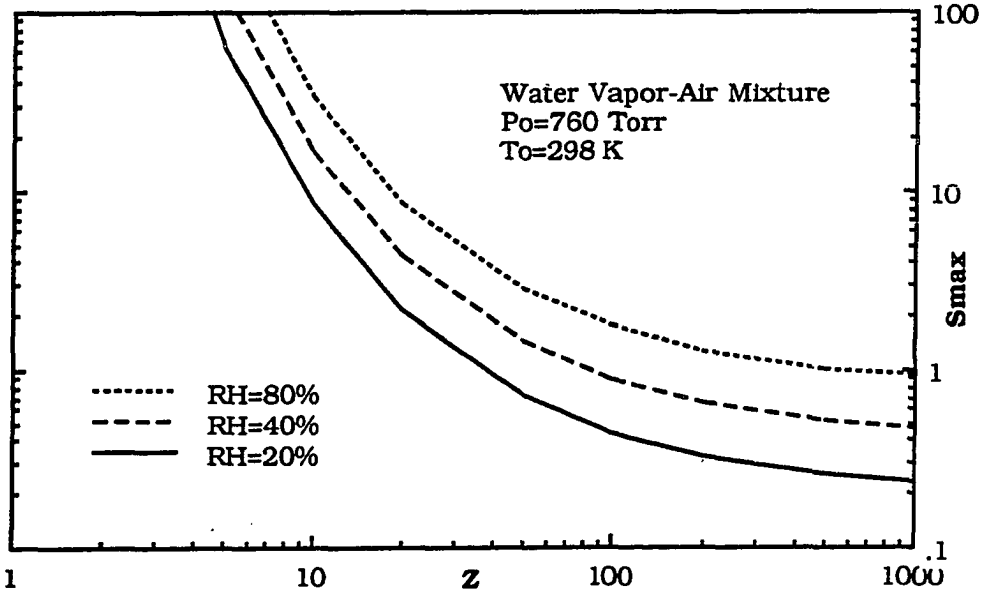

Figure 5-7 Maximum water vapor saturation ratio as a function of Z number and initial RH

Since $(1 + B/T) < 0$ for water vapor and $d\rho/dt < 0$ during pump-down, $dT/dt < 0$ at S_{max} indicates that the gas temperature at S_{max} still decreases (has not reached the minimum yet).

It is noted that S_{max} here is only a function of Z and RH.

$$S_{max} = f(Z, RH) \tag{5.35}$$

The numerical results for S_{max} are plotted in Fig. 5-7. It needs to be reemphasized that S_{max} is obtained by neglecting condensation. It shows the maximum potential of pump-down to saturate a vapor.

Figure 5-8 shows the numerical results of $\hat{p}$ and $\hat{T}$ for different Z. Since $\hat{p} = f(Z)$ and $\hat{T} = g(Z)$, correlation between $\hat{p}$ and $\hat{T}$ must exist. When $p_o = 760$ Torr, $T_o = 298$ K, and $\gamma = 1.4$, it is found that

$$\hat{p} = 0.98\,\hat{T}^{5} \tag{5.36}$$

Shown in Fig.5-9, this equation fits the numerical data well.

With the help of Eq.(5.36), S_{max} can be found without need to solve differential equations (5.22). Substituting Eq.(5.36) into Eqs.(5.21) yields

$$Z = \frac{0.98\,\hat{T}^{5/3}\left\{0.4 + \dfrac{1}{\left(1 + \dfrac{1}{\hat{T}}\dfrac{B}{T_o}\right)}\right\}}{0.13\,(1 - \hat{T})^{4/3}\,\hat{T}^{1/2}} \tag{5.37}$$

Substituting Eq.(5.36) into Eq.(5.23) yields

$$S_{max} = p_{so}\,RH\,\frac{0.98\,\hat{T}^{5}}{10^{\left(A + \frac{1}{\hat{T}}\frac{B}{T_o}\right)}} \tag{5.38}$$

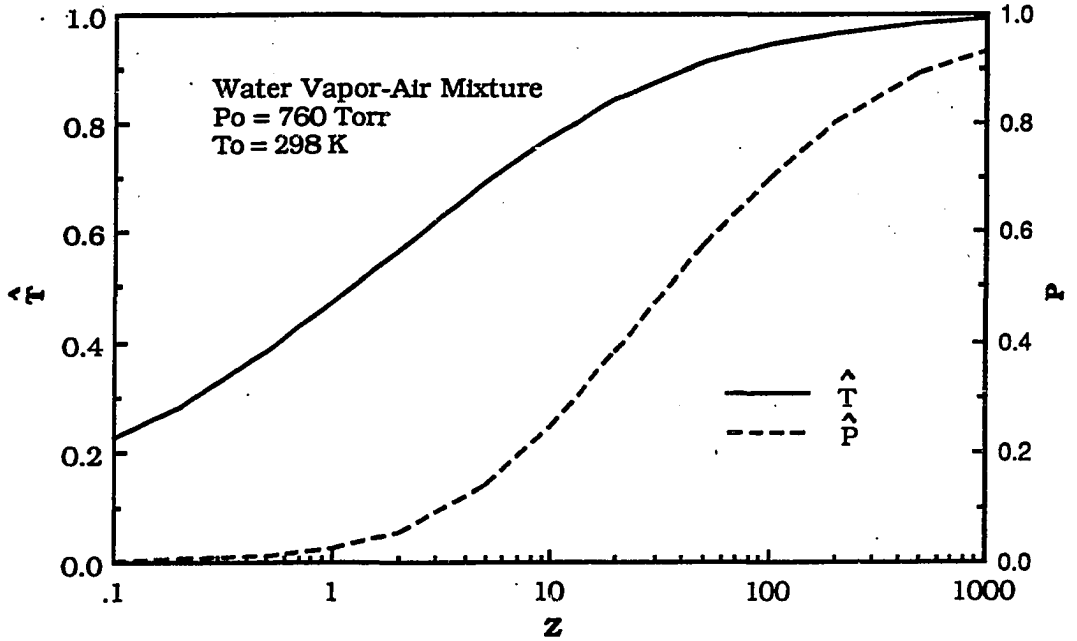

Figure 5-8 Dimensionless temperature and pressure at maximum water vapor saturation ratio as a function of Z

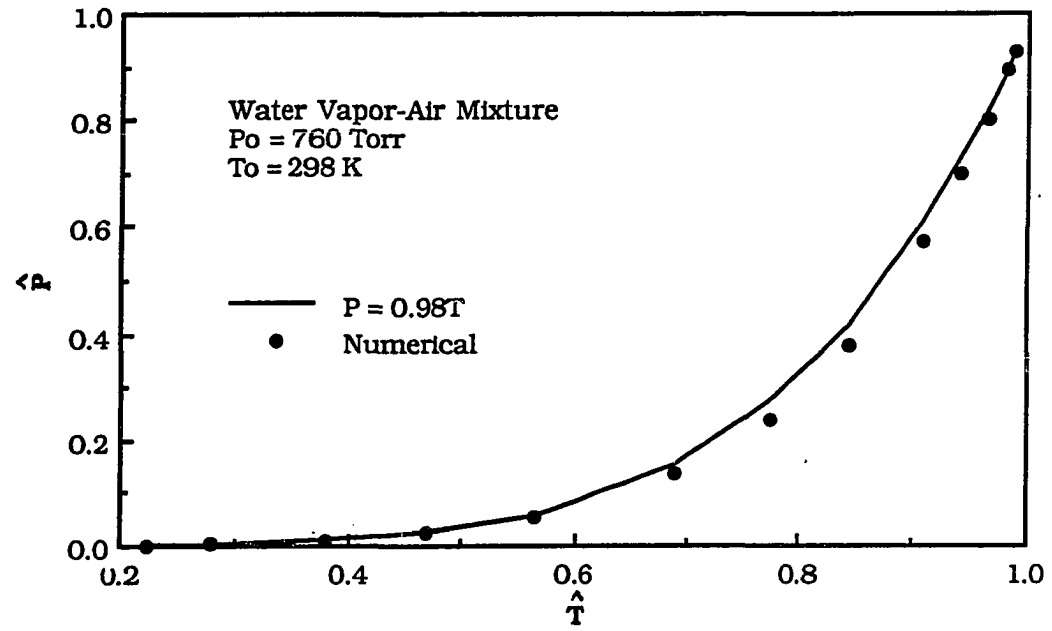

Figure 5-9 Relationship between dimensionless pressure and temperature at maximum water vapor saturation ratio

For a given Z, $\hat{T}$ can be solved in Eq.(5.37) by iteration. After $\hat{T}$ is found, S_{max} is then calculated by Eq.(5.38). The conditions for Eqs.(5.37) and (5.38) are p_o = 760 Torr, T_o = 298 K, and γ = 1.4.

5.5.3 Critical Saturation Curve

Two limiting cases will be studied here: heterogeneous condensation and homogeneous nucleation. The first case assumes that a great amount of foreign nuclei is present in the mixture, and the condensation process dominates. S_c for condensation depends very weakly on the mixture temperature, and is very close to 1. In this case, S_c-Curve is a horizontal line.

The second case assumes that no foreign nuclei are present. S_c for nucleation strongly depends on the mixture temperature, and varies during pump-down. Since T* now depends on Z and p*, S_c for nucleation can be expressed as

$$S_c = f_5(Z, p^*) \qquad (5.39)$$

Figure 5-10 shows the results of a simulation for which Z = 16. The S_c-Curve is exactly opposite to the temperature curve. At the initial temperature T = 298 K (T* =1), S_c = 3.12. At the minimum temperature T = 244 K (T* = 0.82), S_c = 6.65.

5.5.4 Critical Condition of Pump-Down

Since γ, A, B, p_o, and T_o have been fixed, the pump-down condition Ω is dependent upon only two variables Z and RH. The task now is to determine the combination of Z and RH such that the S_c-Curve is tangent to the S-Curve.

If Z is fixed, there is a critical relative humidity, denoted as RH_c, that makes the S-Curve tangent to the S_c-Curve (Fig.5-11); if RH >

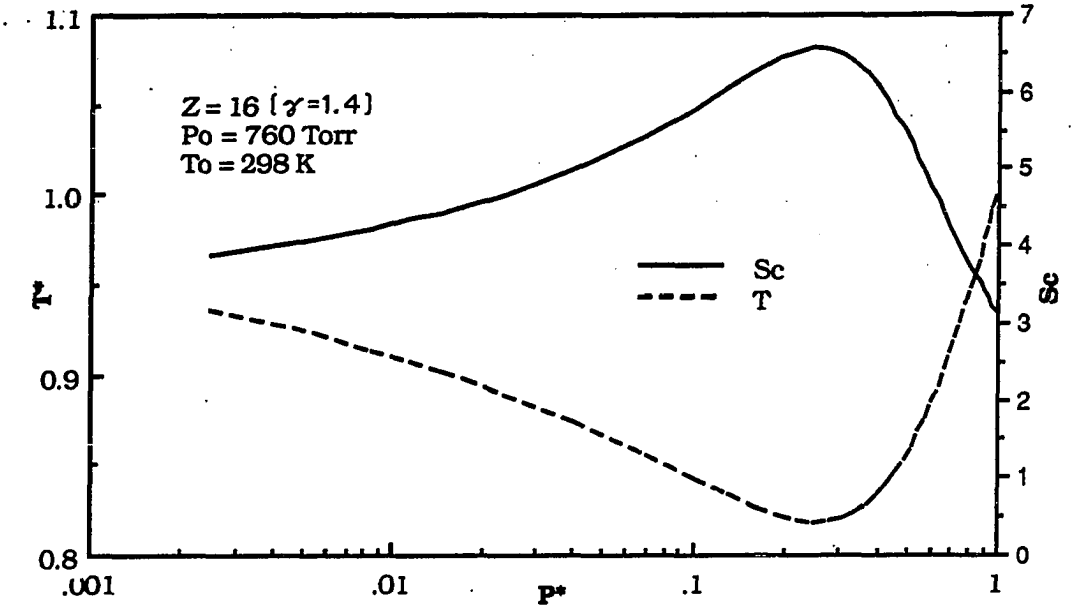

Figure 5-10 Critical saturation ratio of water vapor vs. pressure during pump-down

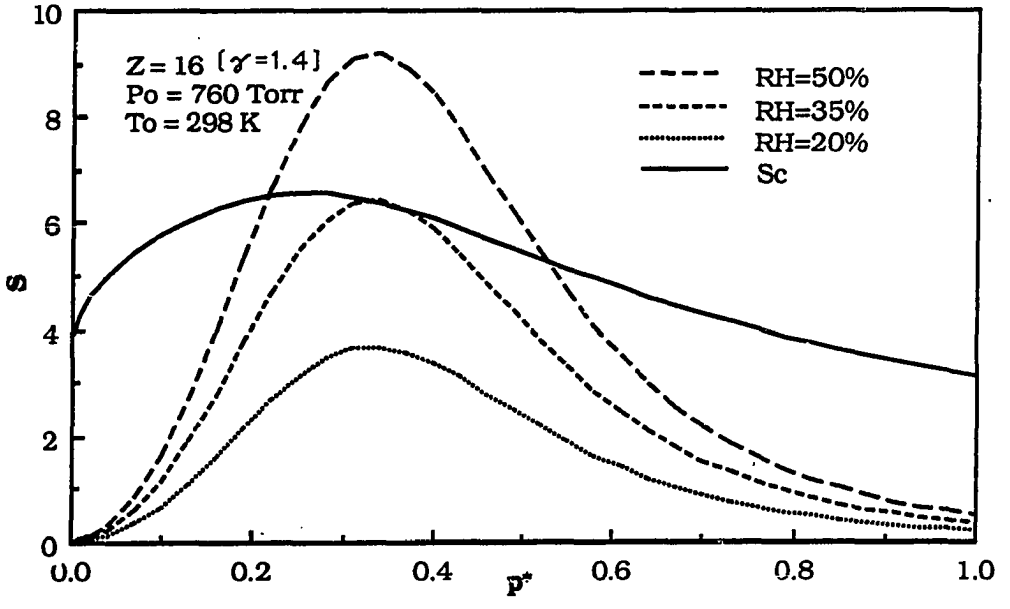

Figure 5-11 Saturation ratio of water vapor vs. pressure for different RH at fixed Z number

RH_c, the S-Curve crosses the S_c-Curve twice; if $RH < RH_c$, there is no contacting point. Similarly if the RH is fixed, there is a critical Z number, denoted as Z_c, that makes the S-Curve tangent to the S_c-Curve (Fig.5-12); if $Z < Z_c$, the S-Curve passes the S_c-Curve; if $Z > Z_c$, there is no contact point. By numerical calculation, the relationship between RH_c and Z_c is found, as shown in Fig.5-13. The data for the curve are listed in Table 5-1. It is found that when RH changes from 10 to 80%, S_c reduces from 10.0 to 4.80 (corresponding to temperature from 224 to 264 K).

Table 5-1 Critical conditions of water vapor homogeneous nucleation[a]

RH_c, %	Z_c	S	p/p_o	T/T_o
2.8	5	14.00	0.16	0.695
4.8	6	12.50	0.19	0.720
9.6	8	9.99	0.22	0.751
15.5	10	8.44	0.26	0.771
21.7	12	7.50	0.28	0.790
35.0	16	6.36	0.34	0.823
47.0	20	5.69	0.40	0.845
59.0	24	5.31	0.43	0.860
80.0	32	4.80	0.49	0.885
114.0	40	4.35	0.61	0.911

a. p_o=760 Torr, T_o=298 K.

When S_c is constant, the relationship between RH_c and Z_c can be determined by

$$S_{max} = f_3(Z_c, RH_c) = S_c \qquad (5.40)$$

This equation represents the contour of S_{max} in the Z and RH plane. Figure 5-14 shows the contours for S_{max} = 2, 4, 6 and 8. These

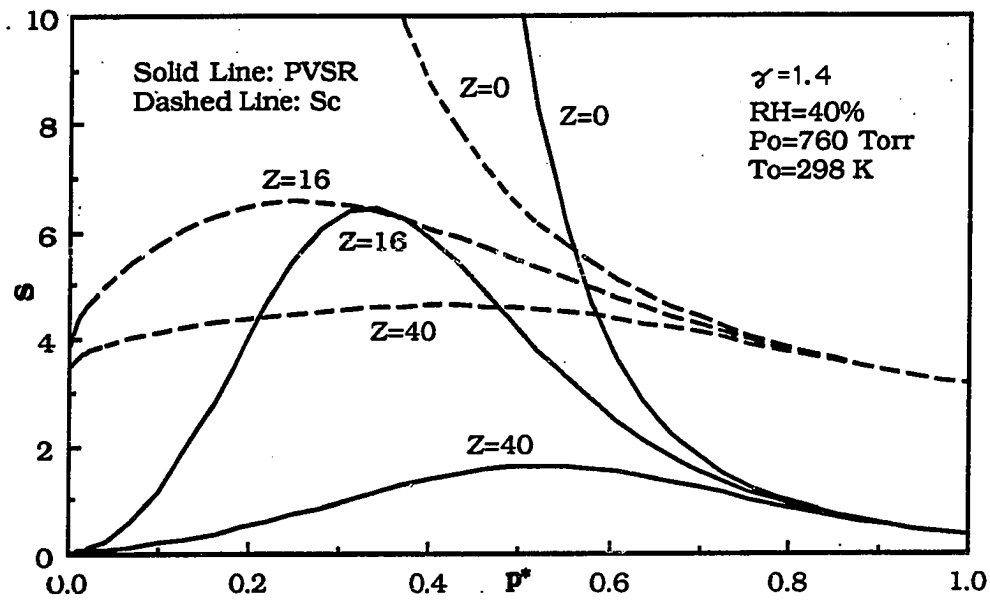

Figure 5-12 Saturation ratio of water vapor vs. pressure for different Z at fixed RH

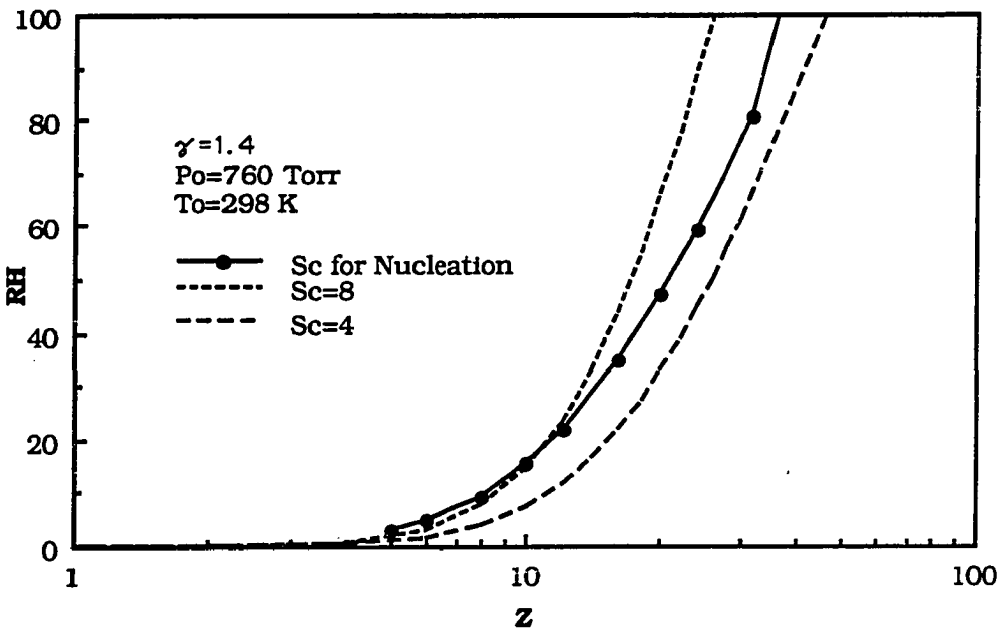

Figure 5-13 Critical Z and RH for water vapor nucleation

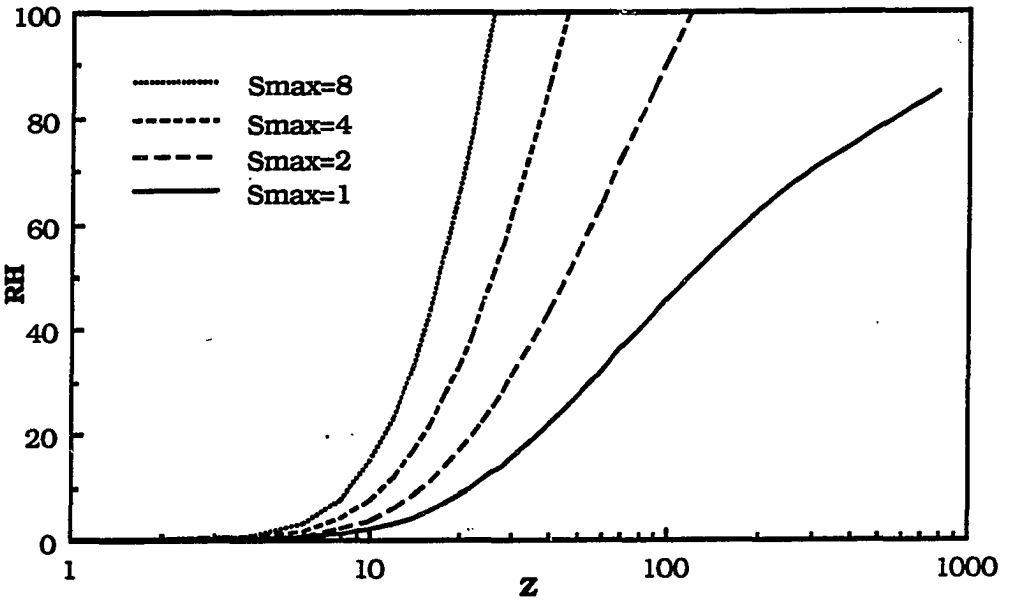

Figure 5-14 Contour of Smax in Z and RH plane

contours are very useful. If S_c varies from 4 to 8, the critical Z_c and RH_c must fall between the regions limited by $S_{max} = 4$ and $S_{max} = 8$.

5.6 DESIGN CRITERION FOR CLEAN PUMP-DOWN

The pump-down process is known to generate a large number of particles, which are the contamination sources to semiconductor manufacturing and other vacuum related processes.

When condensable species, especially water vapor, are present in a clean carrier gas, it is believed that liquid particles formed by vapor nucleation and condensation constitute the major portion, if not all, of the particles that occurs in pump-down. Nucleation is responsible for the formation of new particles. The number of particles generated by nucleation can be as high as 10^4/cc (see Chapter 6). The size of particles depends on condensation which is responsible for the growth existing particles (including those formed by nucleation). The liquid particles in pump-down can grow larger than 10 μm (Borden and Baron, 1987).

Although these liquid particles formed in pump-down are transient (some of them will be pumped out, or evaporated at low pressure), they will have a residence time inside the vacuum chamber and might deposit on the substrate. In the nucleation and condensation process, many impurities may be scavenged into these newly formed particles. Nucleation on ions generate charged particles which may be more easily deposited on the substrate. The growth of particle size increases the particle deposition velocity (or settling velocity).

In order to eliminate particle formation from vapor condensation or nucleation, the pump-down must be operated under this condition:

$$S(\Omega, p^*) < S_c(\Psi, \Omega, p^*) \qquad (5.41)$$

This gives a design criterion for clean pump-down (in the sense of no vapor condensation or nucleation).

Water vapor is the most common, usually the largest, condensable species in a vacuum system. Pump-down is usually started at near STP conditions. Therefore the results presented in Fig.5-13 and Fig.5-14 can be directly used in pump-down parameter design.

Two design examples are given below. Assume a cubic chamber with dimensions of 30 cm on each side; the volume is then 27 liters (1 cubic foot). Assuming the water vapor-air mixture is pumped out at T_o = 298 K and p_o = 760 Torr, there are two practical design problems:

1) Pumping Rate Design

In this case, the initial RH must be given. Assume RH = 40%. For the given chamber:

$$V = 27 \text{ liters}$$
$$\xi = \frac{a}{6} = 5 \text{ cm}$$

and at the STP condition

$$\omega = 6.74 \text{ cm/s}$$

From Fig.5-13, Z_c = 18 for nucleation. Then to avoid nucleation:

$$S_e < \frac{V\omega}{\xi Z_c} = 2 \text{ liter/s}$$

From Fig.5-14, $Z_c = 62$ for condensation ($S_c = 1$). Then to avoid condensation:

$$S_e < 0.587 \text{ liter/s}$$

2) Control of RH

If a pumping rate is given, the relative humidity must be controlled such that

$$RH < RH_c$$

For example, given $S_e = 6$ liter/s, and $\tau = \frac{V}{S_e} = 4.5$ s, then

$$Z_c = \frac{\omega \tau}{\xi} = 6.05$$

From Fig.5-13, to avoid nucleation,

$$RH < 5\%$$

To avoid condensation,

$$RH < 2\%$$

For a faster pumping rate, say $S_e > 10$ liter/s, water-vapor-free carrier gas is required. This means that the chamber must flushed with dry nitrogen in order to avoid any kind of condensation.

5.7 CONCLUSION

A theory has been developed to predict the critical condition of pump-down that initiates vapor condensation or nucleation. It is found that the conditions of a pump-down process can be specified parametrically in terms of Ω, from which the potential vapor saturation

can be determined. The critical saturation ratio, on the other hand, mainly depends on the type of condensation. This work has described homogeneous condensation, homogeneous nucleation, and nucleation on ions.

Water vapor-air mixture, initially at 760 Torr and 298K, have been investigated in detail by a numerical simulation technique. It is found that the critical condition is determined by a combination of the dimensionless Z number and the initial relative humidity. The numerical results presented in Fig.5-13 and Fig.5-14 can be used to specify and design clean vacuum pump-down processes.

CHAPTER 6

PARTICLE FORMATION IN THE PRESENCE OF WATER VAPOR DURING VACUUM PUMP-DOWN

ABSTRACT

Particle formation in the presence of water vapor during vacuum pump-down has been experimentally investigated in a cylindrical chamber of volume 260 cc filled with particle-free air with known relative humidity. It is found that the number of particles generated during pump-down depends on the pumping time constant, relative humidity, and terminal pressure. It is also found that these particles have residue sizes of 20 to 100 nm. Several hypotheses for particle generation have been tested. It is believed that particles generated during pump-down are water droplets containing impurities. The mechanism of droplet generation is through water vapor nucleation on water molecules (homogeneous nucleation) or on ions. These droplets grow in the initial period of pump-down due to water vapor condensation. The impurities scavenged by droplets may chemical react to form residue particles. The most likely reaction is that involving liquid phase oxidation of pollution species such as SO_2 and neutralization by NH_3 to form $(NH_4)_2SO_4$.

6.1 INTRODUCTION

It is well known that many aerosol particles may evolve in a vacuum chamber during pump-down. The presence of particles has been detected by the following three techniques.

1) Wafer Scanning

A bare silicon wafer is used as the particle detector. The wafer is first inspected by using a surface scanner to ensure that none or few

particles are present. After the inspection, the wafer is loaded into a vacuum chamber and the pump-down is then performed. After pump-down, the wafer is taken out and reinspected by the scanner. As observed by Hoh (1984), Bowling (1986), and others, many particles are detected on the wafer, indicating the presence and deposition of particles during pump-down.

This technique provides the most direct method for detecting the particle contamination on a wafer. Although expensive, modern surface scanners are fully automated and easy to use. However, this technique has the following limitations: (i) it is not real-time; (ii) the minimum detectable particle size is 0.15 μm; (iii) the relationship between particle concentration (suspended particle) and particles added to the wafer is difficult to find.

2) Light Scattering

A vacuum particle counter, model PM-100, recently developed by High Yield Technology (HYT), has been widely used to monitor the particles in vacuum processing tools. The PM-100 uses a laser net to detect particles that pass through the net covering an area of 9 cm^2. As the inventor of the counter, Borden and Baron (1988) first monitored particles in vacuum processing tools such as ion implanters or in the vacuum loadlock. They found pump-down produced a high peak in particle counting, exceeding 1000 particles/minutes and consisting of many particles larger than 10 μm. They also found that particle count quickly disappeared when the pressure dropped below 200 to 100 Torr. Recently, particle monitoring in pump-down using the PM-100 also has been carried out by Chen et al. (1989) and Wu et al. (1989).

The main advantages of the PM-100 are its real-time measurement capability and flexibility in installations. However, it is a monitoring device which is unable to measure particle concentration

accurately because of its low particle count efficiency (0.6% for 0.5 μm and 13% for 1μm), and the flow rate through the detecting area is uncertain under vacuum.

3) Vacuum Particle Sampler (VPS)

The concept of the VPS, schematically shown in Fig.6-1, is to use aerosol instruments that operate at atmosphere conditions to measure particles in vacuum systems (Szymanski, et al., 1987). Each measurement cycle includes four operations: (i) pump-down the sampling chamber from one atmosphere to a specific pressure, lower than that in the vacuum system; (ii) drawing particle samples from the vacuum system into the chamber; (iii) venting the chamber to atmosphere pressure again; (iv) measuring particles contained in the chamber using a CNC or other instruments that operate at atmospheric pressure. None of these four operations should produce particles. However, when fast pumping was performed, a large number of particles were found during pump-down. Consequently, this setup becomes a ready tool for investigating particle formation during pump-down. With this tool, much information about generated particles has been obtained such as concentration, charge, and volatility.

The characteristics of particle formation during pump-down will be investigated in this chapter. The following issues will be discussed.

1) Experimental technique.
2) Quantitative measurement of particle generation and determination of critical conditions.
3) Hypotheses of particle generation and testing.
4) Theoretical analysis of particle generation patterns.

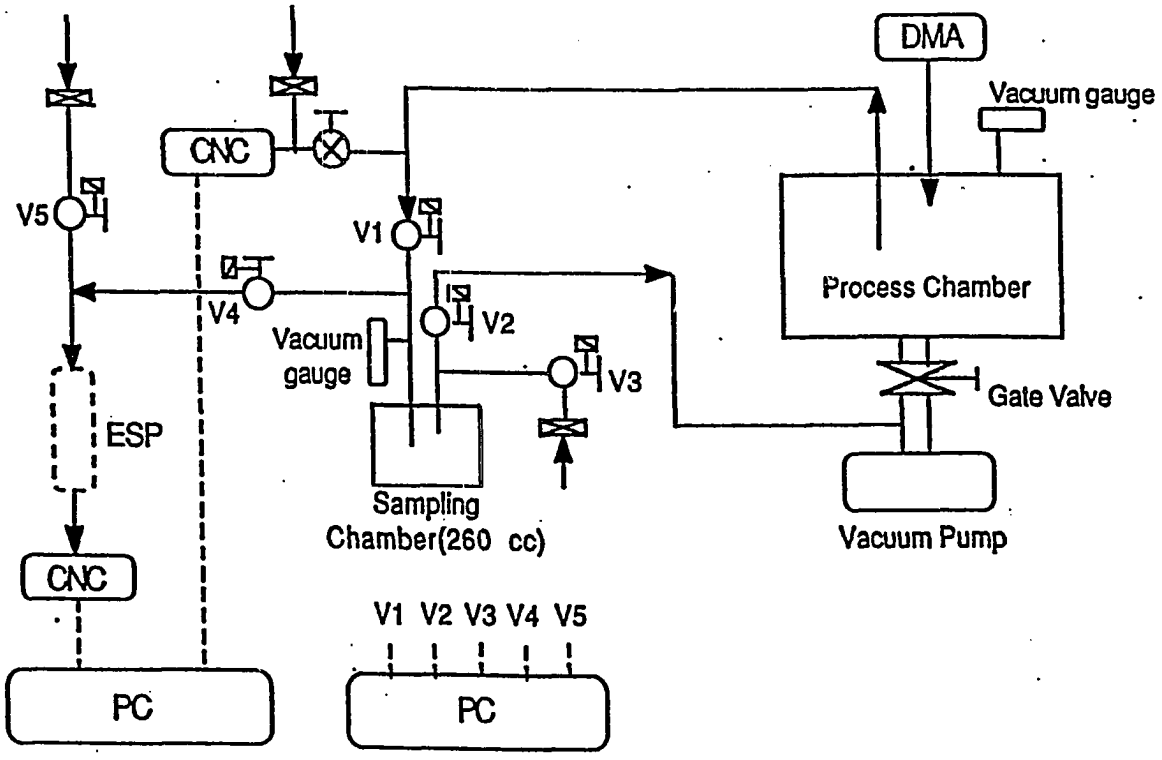

Figure 6-1 Vacuum particle sampler

6.2 EXPERIMENTAL INVESTIGATION

Particle formation in the presence of water vapor during pump-down depends on two major factor: (i) condition of pump-down including pumping rate, chamber geometry, initial quantities of water vapor, properties of carrier gas, and initial pressure and temperature; (ii) characteristics of nucleigenic agents including particle size and population, ion charge and population, type and amount of residue gases.

In the first case, we limit the study to three experimental parameters, namely,

Pumping time constant: $\tau = V/S_e$
Initial relative humidity: RH
Pump-down terminal pressure: p

Other conditions are fixed:

Cylindrical chamber: V=260 cc (D x H = 8 x 5.2 cm)
Carrier gas: air
Initial conditions: p_o= 1 atmosphere, T_o=298 K

In the second case, we limit our study to water vapor-air mixtures which are initially particle free but may contain ions or impurity gases such as SO_2 or NH_3.

6.2.1 Experimental Setup and Procedure

Figure 6-2 is a schematic diagram of the experimental apparatus for investigating particle formation during pump-down. The apparatus consists of an electropolished stainless steel chamber of 260 cc; a condensation nucleus counter (CNC) for particle number measurement; a convectron vacuum gauge (CVG) for pressure

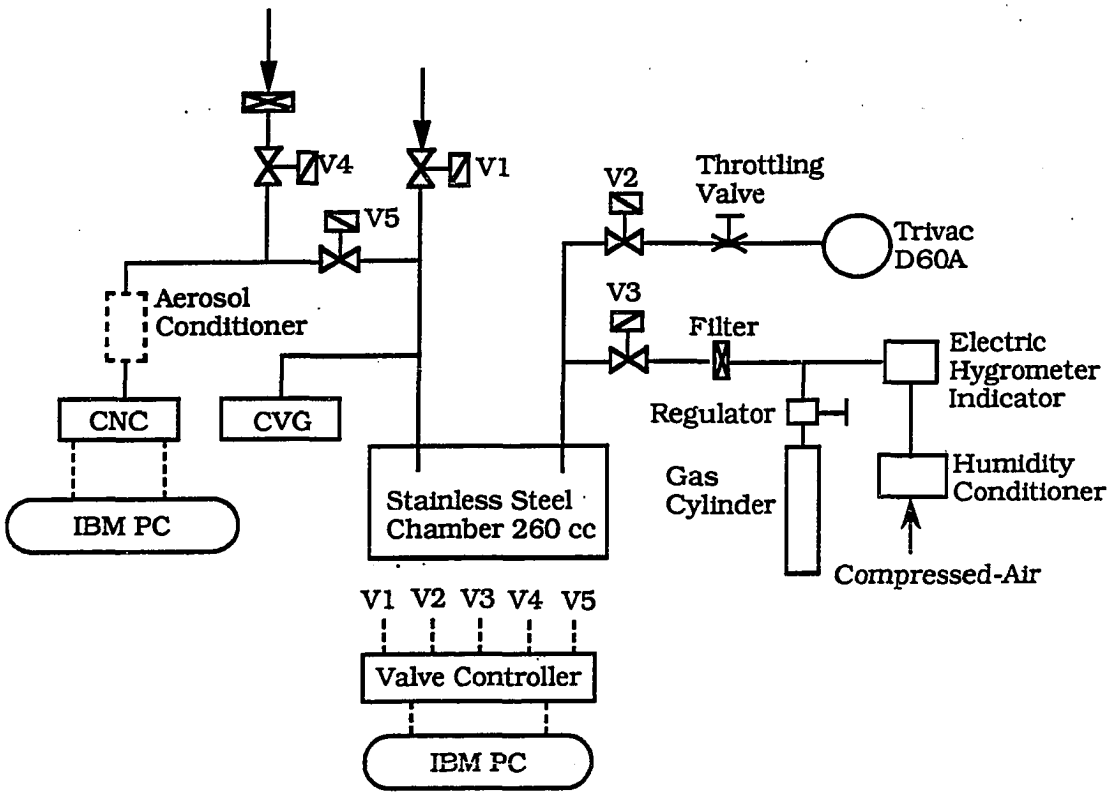

Major Conmponent Specifications

V1 to V5: NUPRO Air Activated Valve (SS-BNS4-C)
Filter: MILLIPORE Wafergard Gas Filter Cartrige (6-stack)
CNC: TSI 3720
Valve Controller: Special Made by TSI

Figure 6-2 Experimental apparatus for investigation of particle formation during pump-down

measurement; a humidity control and measurement system; a flow system consisting of a mechanical vacuum pump, a throttling valve, solenoid pneumatic valves, and Wafergard membrane filters; and a computer control system for valve control and data processing.

The experimental procedure is as follows:

1) Flushing the chamber with air of known RH.
2) Pump-down the chamber with a known pumping rate.
3) Venting the chamber with fixed venting rate.
4) Sampling particles contained in the chamber.

Fig.6-3 draws the valve configuration and the apparatus for each operation. Fig.6-4 defines the timing variables for each operation. These operations are automated using four solenoid valves (V2 to V5). The on/off timing (0.1 seconds accuracy) and sequence of these valves are controlled by a personal computer and a valve controller. Note that valve V1 was not used because drawing a sample from the vacuum system was not necessary. Details for each operation are discussed in the following section.

6.2.2 Experimental Considerations

The following requirements are proposed in this experiment:

1) Particles inside the chamber are only generated by pump-down.
2) The experimental parameters τ, RH, and p can be controlled accurately.
3) Timing of each operation should be optimized for the sake of saving time and minimizing any particle loss due to settling or diffusion.

Keeping these requirements in mind, we now proceed to describe the experimental details.

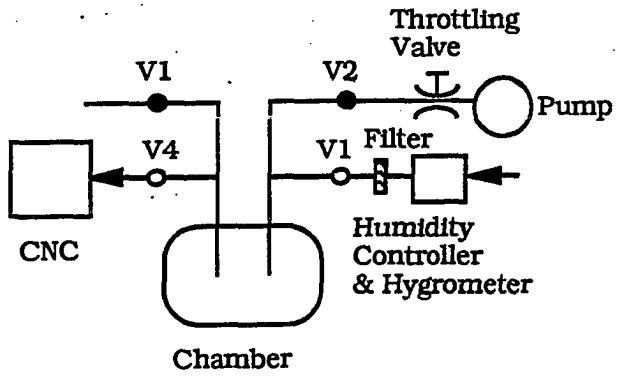

1. Flush chamber with humid air. V3 and V4 open. V1 and V2 closed. CNC pump is used to maintain air flow.

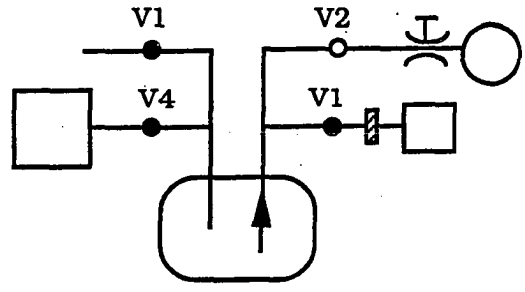

2. Pump-down the chamber. V2 open. V1, V3, and V4 closed. Pumping rate is controlled by a throttling valve. V2 open time is controlled by a PC.

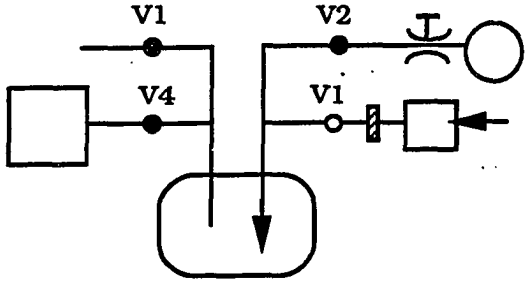

3. Venting chamber with the same humidified air. V3 open. V1, V2, and V4 closed.

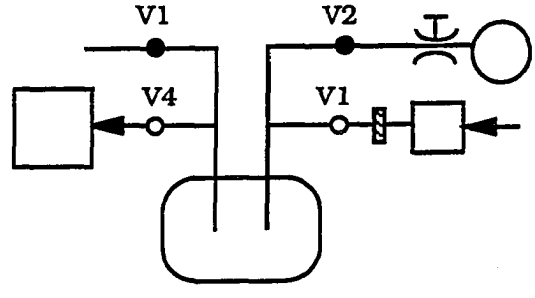

4. Sample the total particles generated during pump down by a CNC. V3 and V4 open. V1 and V2 closed.

Figure 6-3 Experimental procedure for measureing particle generation during pump-down.

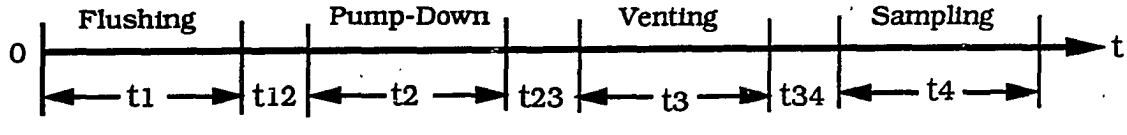

Figure 6-4 Timing of a experimental cycle

A. Cleaning the Chamber

For eliminating possible particle reentraiment from the chamber surface, the vacuum chamber was carefully cleaned. The chamber was first immersed into an ultrasonic bath (filled with 1% "Liqio-Nox" detergent) for 30 minutes, then thoroughly washed with pure DI water, and finally baked in an oven at 250°C for 30 minutes. Note that the chamber is made of eletropolished stainless steel, and thus is easily cleaned. After cleaning using the above mentioned procedure, the surface of the chamber is believed to contain few, or to be free of particles.

B. Flushing

In this operation, we need to control the RH and cleanliness of the air in the chamber. The method of RH control and measurement is described by Liu, et al. (1988). The RH is adjusted by mixing humidified air with dry air. The humid air is obtained by bubbling compressed air through water, and the dry air is obtained by passing compressed air through a chemical dryer. The maximum range of RH obtainable is from 10% to 80%. The RH is measured by a salt-film transducer and a electrical hygrometer indicator. The uncertainty of RH measurement is ±2.5%.

RH both the upstream and downstream of the chamber are measured. As expected, the downstream RH is a few percent lower because the pipe and filter in the line may absorb some water vapor. The RH in the chamber is taken as the average of the upstream and downstream values.

The air filling the chamber is filtered by a membrane filter (Millipore Wafergard 6-stack hydrophobic cartridge). The filter has a collection efficiency of nearly 100% for all particle sizes (at the most

penetrating size 0.05μm, the penetration is 10^{-9}). Downstream of the chamber, the CNC continuously monitors the air through the chamber, and nearly no CNC count appears. Therefore, the air inside the chamber is believed to be free of particles of any size. However, impurities in gaseous form, such as ions, organic vapor, SO_2 and NH_3, may exist since they cannot be filtered out.

The flushing time t_1 is the time required to establish a constant RH which takes about 3 minutes.

C. Pump-Down

In this operation, τ and p are controlled. Since V is given, τ varies with the pumping rate S_e. Pumping is performed by a mechanical vacuum pump and a throttling valve. Since the intrinsic pumping speed of the pump (705 lpm for air) is much greater than the conductance of the valve, gas flowing through the valve is always choked (sonic flow). At a given valve turn, the effective pumping speed S_e is nearly constant, and it is determined by the "constant volume" method (Levin, 1965):

$$S_e = \frac{V}{t_{v2}} \ln\left(\frac{p_o}{p_{tv2}}\right) \qquad (6.1)$$

where t_{v2} is the open time of valve V2, which is set by the computer; p_o, the initial pressure; p_{tv2}, the pressure at t_{v2}. Both pressures are measured by the CVG. After S_e is found, $\tau = V/S_e$ is calculated. In this work, τ ranges from 0.7 to 7 seconds corresponding to S_e from 22.3 to 2.3 lpm.

The terminal time of pump-down, t_2, depends on the terminal pressure p. For a given τ,

$$t_2 = \tau \ln\left(\frac{p_o}{p}\right) \qquad (6.2)$$

The pause time between pump-down and venting, t_{23}, is 2 seconds, which allows pressure and flow stabilization in the chamber after pump-down.

Depending on the RH and the τ used, particles may or may not be generated in pump-down. If τ is small (fast pumping) and the RH is high, particles will be generated. However, these particles are transient both in size and number (i.e. they are being generated and at same time are being pumped out). These particles may also grow, settle, diffuse, or evaporate. Therefore, the number of particles inside the chamber is a function of pressure (or time). What we can measure, using the VPS technique, is the number of particles remaining inside the chamber at the terminal pressure, designated as:

$$N = N(\tau, RH, p) \qquad (6.3)$$

and the corresponding particle concentration, defined using the chamber volume:

$$n = \frac{N}{V} = n(\tau, RH, p) \qquad (6.4)$$

The goal of the experimental measurement is to find N or n at different τ, RH, and p.

D. Venting

The venting speed S_v and the venting time t_3 must be considered. S_v is the volumetric flow rate upstream of the chamber which is at atmosphere condition. If S_v is a constant, the time required to vent the chamber from p to p_o is

$$t_3 = \frac{V}{S_v}\left(1 - \frac{p}{p_o}\right) \qquad (6.5)$$

In this experiment, t_3 is about 1 second when the chamber is vented from 1 to 760 Torr, the average venting speed is then calculated to 15.6 slpm. The pause time t_{34} is 1 second for pressure stabilization and flow inside the chamber after venting.

We must be sure that venting does not generate or bring any particles into the chamber. This may occur when the venting rate is too high and the chamber or other elements such as pipes, valves, or filters are dirty. To check the cleanness of venting, slow pumping and venting at a rate of 15.6 slpm is performed. Air with the same RH as that in pump-down is vented. The same venting test has also been carried out with dry nitrogen. In either case, the CNC counts nearly no particles, which indicates that the venting operation is clean.

It should be pointed out that venting is a compression precess, which heats up the mixture inside the chamber. As a result, water vapor condensation or nucleation will not occur during venting. Just the opposite, if liquid particles are present in the chamber, venting may enhance particle evaporation.

E. Sampling

After venting, particles in the chamber are sampled by the CNC. If the venting has not caused any particle loss, the number of particles after venting, N_0, is equal to that when pump-down stops, i.e.,

$$N_0 = N(\tau, RH, p) \qquad (6.6)$$

During sampling, the CNC pump continuously draws particles, if any, out of the chamber at a fixed flow rate Q_{cnc} = 23.6 cc/s. At the same time, filtered air (particle free) enters the chamber with the

same flow rate. Particle concentration in the chamber is thus continuously diluted. If we assume that the particle concentration in the chamber remains uniform and there is no sampling loss anywhere, we can find the cumulative CNC count N_{cnc} from

$$\frac{N_{cnc}}{N_o} = 1 - \exp\left(-\frac{V}{Q_{cnc}}t\right) \tag{6.7}$$

where t is the time elapsed. The second term on the right hand side of the equation represents the fraction of particles left in the chamber at time t.

The rate of the CNC count (the signals that are plotted on the PC monitor) is

$$\frac{dN_{cnc}}{dt} = N_o \frac{Q_{cnc}}{V} \exp\left(-\frac{V}{Q_{cnc}}t\right) \tag{6.8}$$

which decays exponentially (this has been observed in the actual measurement).

Two methods can be used to determine N_o. The first method uses the cumulative count. This is the method used in this work. It is accurate but may take a longer sampling period. Theoretically, the cumulative count N_{cnc} equals N_o only when $t = \infty$. However, if more than 99.9% of the particles ($N_{cnc}/N_o > 99.9\%$) are needed to be sampled, it requires

$$t > \ln(10^3)\frac{V}{Q_{cnc}} = 76 \text{ seconds} \tag{6.9}$$

In the actual measurements, the sampling time t_4 ranges from 90 to 180 seconds. The sampling interval of the CNC is set at 3 seconds.

The second method uses the decay rate of the count. By

Eq.(6.7),

$$N_0 = \frac{\frac{V}{Q_{cnc}}\left(\frac{dN_{cnc}}{dt}\right)}{\exp\left(-\frac{V}{Q_{cnc}}t\right)} = \text{constant} \qquad (6.10)$$

Theoretically, N_0 can be determined from the first count rate at t = 0:

$$N_0 = \frac{V}{Q_{cnc}}\left(\frac{dN_{cnc}}{dt}\right)_{t=0} \qquad (6.11)$$

A value of N_0 determined in this manner may not be very accurate. To improve the accuracy, one may use the average value of N_0 calculated at several time instances. For example, if five count rates are used with the sampling interval of CNC at 1 second, the total sampling time t_4 can be as short as 5 seconds. This method may be preferable if fast sampling cycles are required (the situation may arise when the VPS is used to sample particles from actual vacuum systems).

F. Measurement of Other Particle Properties

In addition to particle number, other properties about generated particles can also be measured by using an aerosol conditioner, shown in Fig.6-2. The conditioner can be a diffusion battery to measure size, a heating tube to measure particle volatility, or an electrostatic precipitator to detect charged particles. Preliminary measurements of these properties have been made by Szymanski et al.(1988) and Ahn et al.(1988).

6.2.3 Experimental Results and Discussion

Measurement results of particles generated during pump-down are presented in Figs. 6-5 to 6-8. This section first discusses the

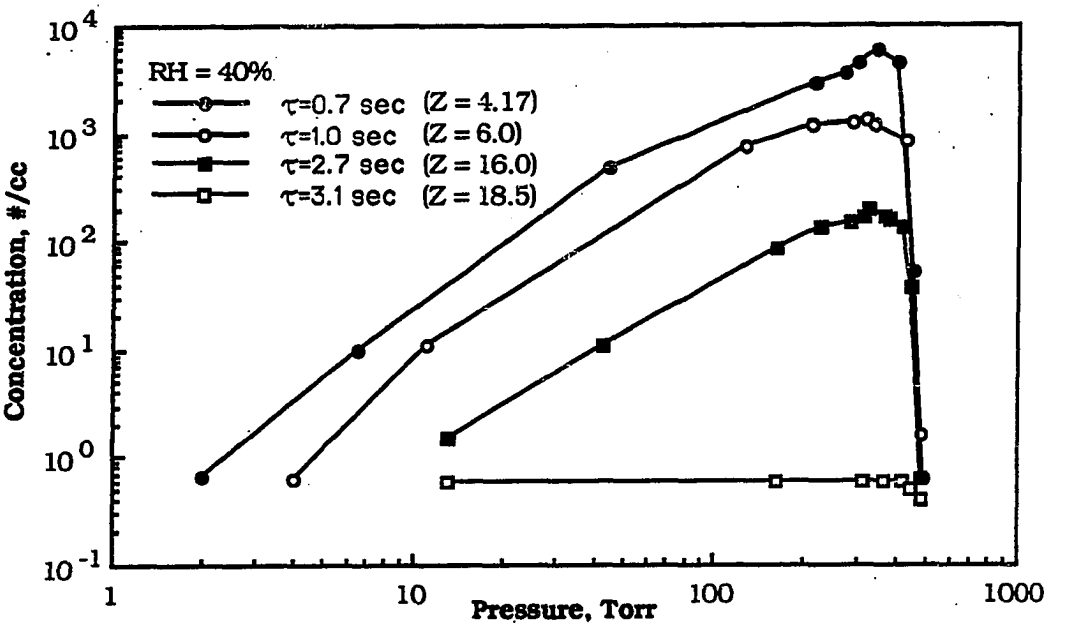

Figure 6-5 Particle concentration for RH = 40% as a function of pressure with different pumping time constants

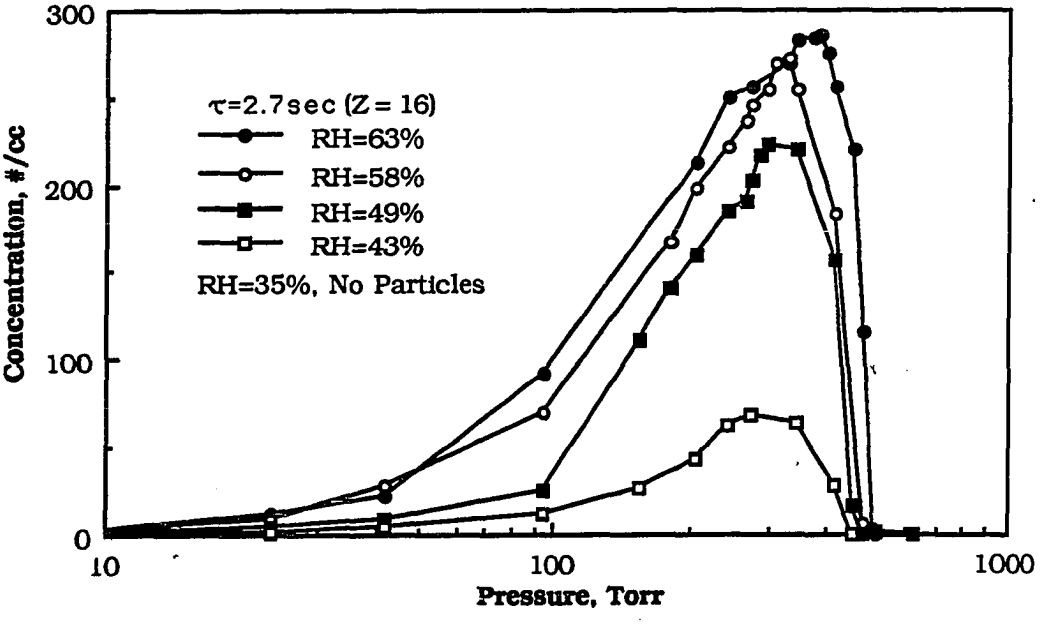

Figure 6-6 Particle aoncentration for a fixed τ = 2.7 sec. as a function of pressure with different initial relative humidities

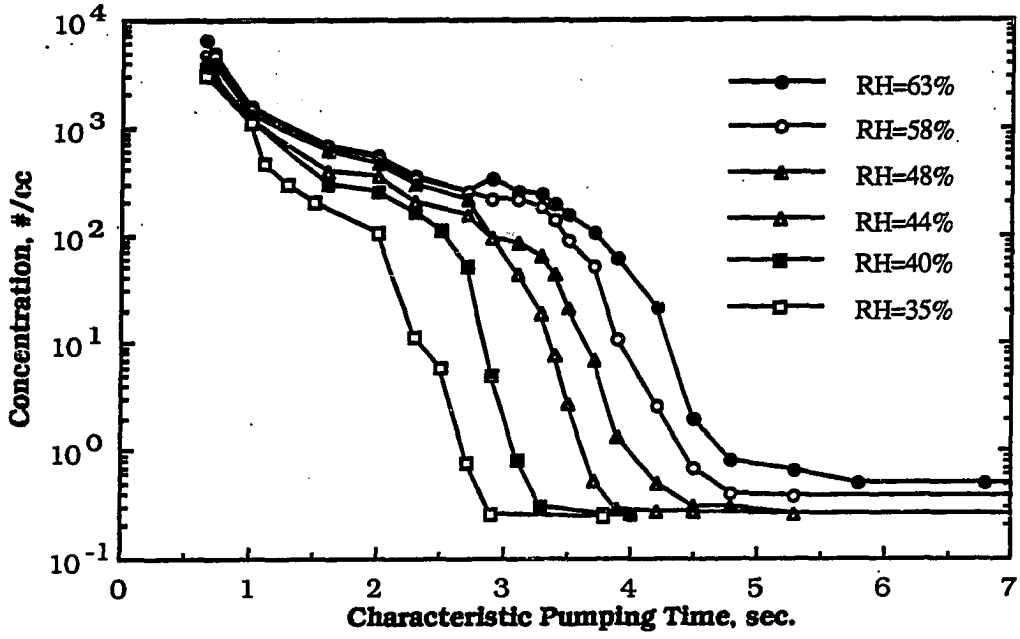

Figure 6-7 Particle concentration at a fixed p = 277 Torr as a function of pumping time constant and initial relative humidity

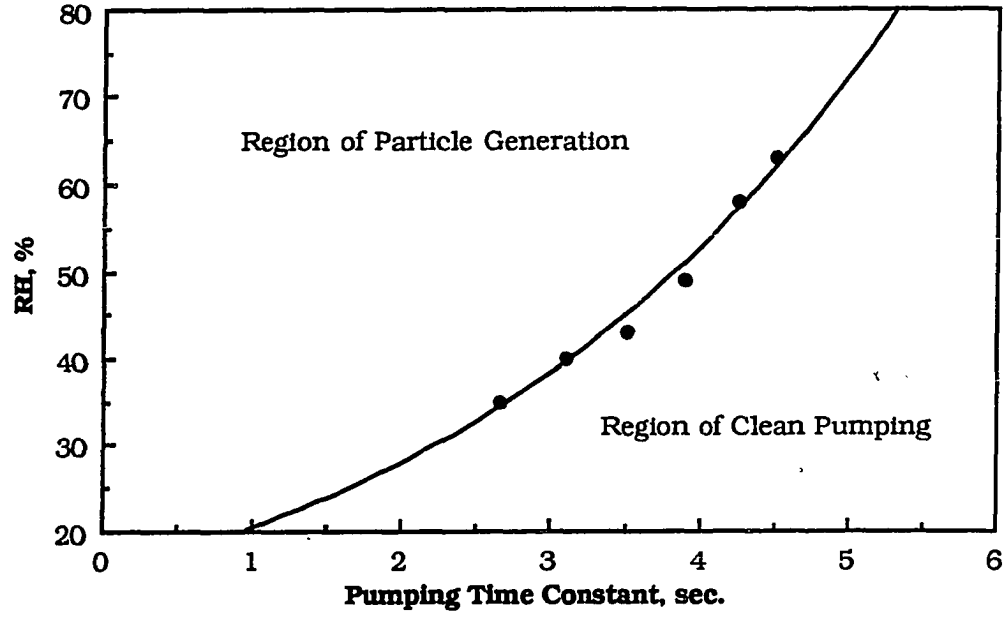

Figure 6-8 Critical conditions for particle generation

characteristics of particle formation and the effects of experimental parameters. In order to access the accuracy of the measurement, the particle deposition loss will be also estimated.

A. Effect of Terminal Pressure

If τ is short and RH is high, a pump-down has a potential to generate particles. However, the particle formation does not start at the initial pressure, and it only occurs until a certain terminal pressure (onset pressure) is reached. The onset pressure depends on the combination of τ and RH. When τ = 2.7 seconds and RH = 49%, the onset pressure is about 450 Torr (see Fig.6-6).

After the onset pressure is reached, particle concentration first increases and then decreases as the terminal pressure decreases. This peak is caused by the competition of particle generation and pumping loss. Initially, the generation dominates the pumping loss and the particle concentration increases. At lower pressure, the generation stops and only the pumping loss exists. Here the particle concentration is reduced. At the pressure where the peak concentration occurs, the generation equals the pumping loss.

B. Effect of τ

Fig.6-5 shows the particle concentrations versus terminal pressure at fixed RH for different pumping time constants. When RH is fixed, small τ, representing fast pumping, generates more particles. Concentrations as high as 10^4 particles/cc were detected for τ = 0.7 seconds and very few (almost no) particles were detected for τ > 3.7 seconds. At the given initial relative humidity, RH = 40%, the peak concentration almost always occurs at a fixed pressure of about 300 Torr.

C. Effect of RH

Figure 6-6 shows the particle concentration for fixed τ = 2.7 seconds as a function of pressure with different relative initial humidities. Higher initial RH causes more particles to be generated and shifts the peak in concentration to higher pressures. The maximum concentration for 63% RH (300 particles/cc) occurs at about 450 torr while the maximum concentration for 40% RH (60 particles/cc) occurs at 270 Torr. No particles were detected for RH $\leq$ 35%.

D. Maximum Particle Concentration

Figure 6-7 shows the particle concentration at a fixed pressure of 277 Torr as a function of pumping time constant and initial relative humidity. The concentrations shown in this figure are equal or close to the maximum concentration for the given τ and RH. It is found that (i) for a given RH, there is a critical τ below which particles will be generated, and (ii) for a given τ, there is a critical RH above which particle generation will occur. The condition of onset for particle generation depends on the particular combination of τ and RH. Taking 1 particle/cc as defining the critical condition, the relationship between the characteristic pumping time in seconds and relative humidity is shown in Figure 6-8.

E. Critical Pump-Down Condition for Particle Generation

Figure 6-8 shows the critical conditions for pump-down to initiate particle generation. The curve defines the conditions for generating 1 particle/cc. More particles would be generated when RH is higher or characteristic pumping time is shorter than that given by the curve. To avoid particle generation, a vacuum system must be operated in the region below the curve.

F. Particle Deposition Loss

Particles may be lost due to wall deposition both during pump-down and during the sampling period. As a result, the particles detected are fewer than those being generated. The estimation of particle loss under the experimental conditions of this work is carried out next.

During pump-down, some of the particles generated will be lost to the chamber wall because of turbulent and Brownian diffusion as well as gravitational sedimentation. Using the theoretical expression of Crump and Seinfeld (1981), Szymanski et al. (1988) estimated these losses under different vacuum conditions. Consider a closed chamber that contains particles of certain size, d, with initial concentration n_o. The chamber pressure is fixed. Assume turbulent mixing prevails inside the chamber, i.e., particle concentration is kept uniform all the time and turbulent wall deposition is dominant. In this situation, the particle concentration decays exponentially, i.e.,

$$\frac{n(d, t)}{n_o} = \exp\left(-\frac{t}{\tau_d}\right) \tag{6.12}$$

where t is the elapsed time and τ_d is decay constant which depends on particle diameter

$$\frac{1}{\tau_d} = \frac{6\sqrt{k_e D_d}}{\pi D_{ch}} \left(2\frac{1}{x}\int_0^x \frac{s\,ds}{e^s - 1} + \frac{1}{2}x \right) \tag{6.13}$$

where x is a dimensionless parameter

$$x = \frac{\pi V_s}{2\sqrt{k_e D_d}} \tag{6.14}$$

where D_d is the Brownian diffusion coefficient of particle; D_{ch}, the diameter of a sphere with volume equal to the volume of the chamber; k_e, the eddy diffusivity; and V_s, the particle settling velocity. V_s depends on particle diameter and pressure:

$$V_s = \frac{\rho_p d^2 C_c g}{18 \mu} \qquad (6.15)$$

where ρ_p is particle density; g, the gravitational constant; μ, the carrier gas viscosity; and C_c, the Cunningham slip correction factor:

$$C_c = 1 + \frac{2}{p d}\left[6.32 + 2.01 \exp(-0.1095\, p\, d)\right] \qquad (6.16)$$

where p is in Torr, and d in μm.

Fig.6-9 shows the percentage of particles left in the chamber at different vacuum conditions for a time period of 10 seconds. In these calculations, $k_e = 1$, $\rho_p = 1$ g/cc, $D_{ch} = 7.92$ cm (for the chamber used), and air properties at 300 K are used. Note that the wall deposition depends on particle diameter with a minimum occurring at a certain size. Large particles sediment faster while smaller particles diffuse quickly. Both processes become more pronounced at low pressures.

Since the particles in these experiments are mostly generated at pressures above 200 Torr. The time to reach this pressure plus venting time is about, or less than, 10 seconds. Therefore, the wall deposition loss is less than 10%. The particle loss during the sampling period is also negligible. Note that sampling is carried out in atmospheric conditions, particle deposition on chamber walls and in sampling pipes is not important.

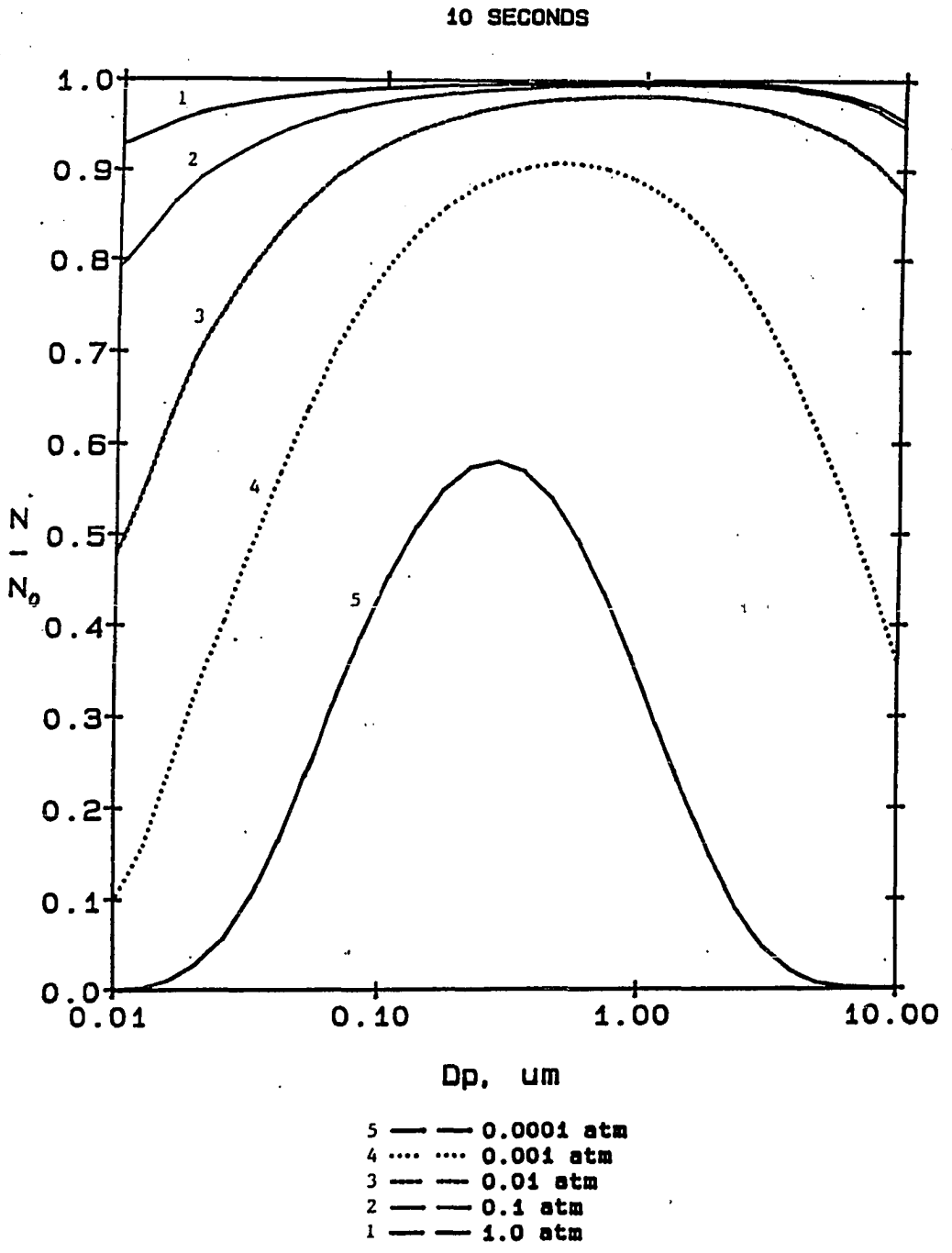

Figure 6-9 Particle deposition loss to chamber wall as a function of particle size for a elaped time of 10 secoends

6.3 MECHANISMS OF PARTICLE GENERATION IN PUMP-DOWN

A very fundamental question remains: where do these particles during pump-down come from? Three mechanisms may be hypothesized: particles detached chamber surface, particles brought in from outside, and particles generated due to gas-to-particle conversion. All three hypotheses will be tested by comparing the experimental observations with the consequences of each hypothesis.

6.3.1 Surface Particle Reentrainment

Some investigators (for example, O'Hanlon, 1987; Chen et al., 1989) hypothesized that particles appearing in the chamber mainly come from the chamber wall -- particles previously accumulated on the surface are detached and stirred up by the gas flow during pump-down. Consequently, they suggested that the number of particles is a function of gas Reynolds number. The conditions for this hypothesis are that particles must first exist, and these particles must be detachable by the gas flow. Both conditions will be tested below.

1) Particle Surface Concentration

Denote particle surface concentration as n_S. Assume that all particles on the surface are instantaneously detached and yield a volume concentration n_V. From the balance of particle numbers, $n_S A_S = n_V V$:

$$n_S = \frac{V}{A_S} n_V \qquad (6.17)$$

For the chamber used, the volume-to-surface area ratio V/A_S is 1.13 cm. Measured n_V is as high as 10^4/cc. If the particles came from the chamber surface, n_S should have been approximately $10^4/cm^2$. Since the chamber wall has been carefully cleaned, this can not occur.

2) Air Velocity for Particle Detachment

A particle can be detached from a surface only when the removal force overcomes the adhesive force. Forces on particles adhesive to a surface are complicated and have not been fully understood. Here, a spherical particle with diameter d sitting on a smooth surface is considered. Assume that the removal force only comes from air drag, and there is no boundary layer, i.e., the air velocity at surface equals the main stream velocity u. The question arises, what is the value of u that can detach the particle from the surface?

The drag force on the particle, F_d, is found from Newton's resistance law

$$F_d = C_d \left(\frac{1}{2} \rho_g u^2\right)\left(\frac{\pi}{4} d_p^2\right) \qquad (6.18)$$

where C_d is the dimensionless drag coefficient which is a function of particle Reynolds number,

$$Re_d = \frac{\rho_g u d}{\mu} \qquad (6.19)$$

$C_d = 0.44$ when $Re_d > 1000$; $C_d = \frac{24(1 + Re_d^{2/3}/6)}{Re_d}$ when $1000 > Re_d > 3$; and $C_d = \frac{24}{Re_d}$ when $Re_d < 3$.

The adhesive force F_a may come from a van der Walls force -- the long-range attractive force between the molecules of the particles and those of the surface, an electrostatic force if the particles contain charge, or a capillary force if a liquid film exists between the particles and the surface. All of these adhesive forces are proportional to

particle diameter. Experimental results for F_a on a smooth surface at 25°C (Hinds,1982)

$$F_a = 150\ d\ [1 + 0.0045\ (\%RH)] \tag{6.20}$$

where d is in cm and F_a is in dyne.

The velocity for particle detachment is obtained when $F_d \geq F_a$,

$$u \geq \sqrt{\frac{1200\ [1 + 0.0045\ (\%RH)]}{\pi\, C_d\, d\, \rho_g}} \tag{6.21}$$

For d = 10μm and RH = 50%, it is found that u ≥ 62 m/s. For smaller d and higher RH, higher u is required. If the boundary layer is considered, the actual u should be even higher than the value given by Eq.(6.21). This calculation indicates that a very high air velocity is required to detach particles of d < 10 μm.

According to Cleaver and Yates (1982), in addition to drag force, a turbulent burst -- the sudden random eruptions of gas near the surface, can produce a lift force to detach particles when

$$\tau_w\ d^{4/3} > \beta \tag{6.22}$$

where β is a constant depending on particle shape and type of adhesive force and τ_w is the wall shear stress which depends on boundary layer structure. This criterion is difficult to be quantitatively applied to the pump-down process because values for β are unavailable and τ_w for the gas flow inside the vacuum chamber is difficult to determine. Here, τ_w for pipe flow is used as an approximation: τ_w is proportional to $\mu \frac{u}{D} Re^{\eta}$, where u is the mean main stream velocity, D is the chamber diameter, u is the gas velocity, η is the boundary layer coefficient (η = 1/2 for laminar flow and η = 1/7 for turbulent flow),

and Re is the gas Reynolds number

$$Re = \frac{\rho_g u D}{\mu} \qquad (6.23)$$

In a given chamber and constant pumping rate (u is constant), the criterion (6.22) becomes

$$Re^{\eta} d^{4/3} > \text{constant} \qquad (6.24)$$

3) Experimental Observation

Now, let us examine the flow situation in our pump-down experiment. Consider the maximum pumping rate S_e = 250 lpm. The mean air velocity that occurs in the chamber, calculated using the chamber diameter, is 20 cm/cc. This is much too small for particle detachment. The gas Reynolds number at p_o = 760 Torr is calculated to be 1300, which corresponds to laminar flow. This shows that the particles in our pump-down experiments are not from the chamber surface.

Contradiction tests show that particles are not from surface reentrainment.

a) According to Eq.(6.21), increasing RH increases the adhesive force and thus reduce the particle reentraiment. Experiments show the opposite -- when RH increases, the number of particles increases.

b) According to Eq.(6.24), the particles, if they can be detached, should appear immediately at the start of pump-down when the Re is maximum. Note that for a constant pumping rate (u is constant) in a given chamber, $Re \approx Re_o \frac{p}{p_o}$ where Re_o is the Reynolds number at p_o which is maximum. However, experiments show that

particles do not appear until p < 500 Torr. The experimental measurements using the PM-100 also support the above observations.

4) Conclusion

The particles generated in our pump-down experiment are not from the surfaces of the chamber. In the case of clean surface, the model relating the particle generation during pump-down to the gas Reynolds number makes little sense.

Surface particle reentrainment needs to be considered when the chamber walls are dirty and the pumping rate is extremely high. These situations may arise when a chamber has been exposed for a long time to ambient air (which contains approximate 10^4/cc particles larger than 0.5 μm), or the chamber has accumulated many particles generated by a vacuum process, such as an etching process in semiconductor manufacturing.

6.3.2 Condensation on Fine Particles

As mentioned in Section 6.1, particles in pump-down have been detected by a laser counter (PM-100). Borden and Baron (1987) hypothesized that the particles detected were the results of heterogeneous condensation (water vapor condensation on fine particles originally contained in the carrier gas). They stated that these particles were initially too small to be detected, and they later grew to become detectable because of condensation. Heterogeneous condensation was also suggested by other works (Chen et al., 1989; Wu et al.,1989).

A key assumption of this hypothesis is that many particles exist in filtered air. Note that cleanroom air is filtered by HEPA or ULPA filters. The air used in this experiment is filtered by a membrane

filter. To test this assumption, two parameter must be known: natural aerosol particle concentration (unfiltered) and filter efficiency.

1) Natural Aerosol Particle Concentration

The air before filtration contains neutral aerosol particles which may be classified (Mason, 1971):

Fine Particles: $0.001\ \mu m < d < 0.2\ \mu m$
Giant Particles: $0.2 < d < 2\ \mu m$
Large Particles: $d > 2\ \mu m$

Room air usually contains 10^3 to 10^4/cc giant and large particles, and 10^4 to 10^6/cc fine particles (Junge, 1955; Mason, 1971; Clark and Whiteby, 1967). If unfiltered room air is used as the carrier gas, it is certain that heterogeneous condensation will occur during pump-down.

2) Filter Efficiency

The population and size distribution of particles in the filtered air depend on filter efficiency. It has been proved, both theoretically and experimentally (for example, Lee and Liu, 1980; Liu and Lee, 1976), that filter efficiency has a minimum which corresponds to the most penetrating particle size (MPPS). The actual filter efficiency for particles of sizes other than MPPS, larger or smaller, would be higher. Fig.6-10 shows the measured particle penetration curve for a membrane filter.

The reason for MPPS is explained by filtration mechanisms. In the absence of electrostatic deposition, airborne particles passing through a filter are captured by diffusion, interception, impaction, and gravitational settling. The giant particles are effectively collected by impaction and gravitational settling. Extremely small particles are

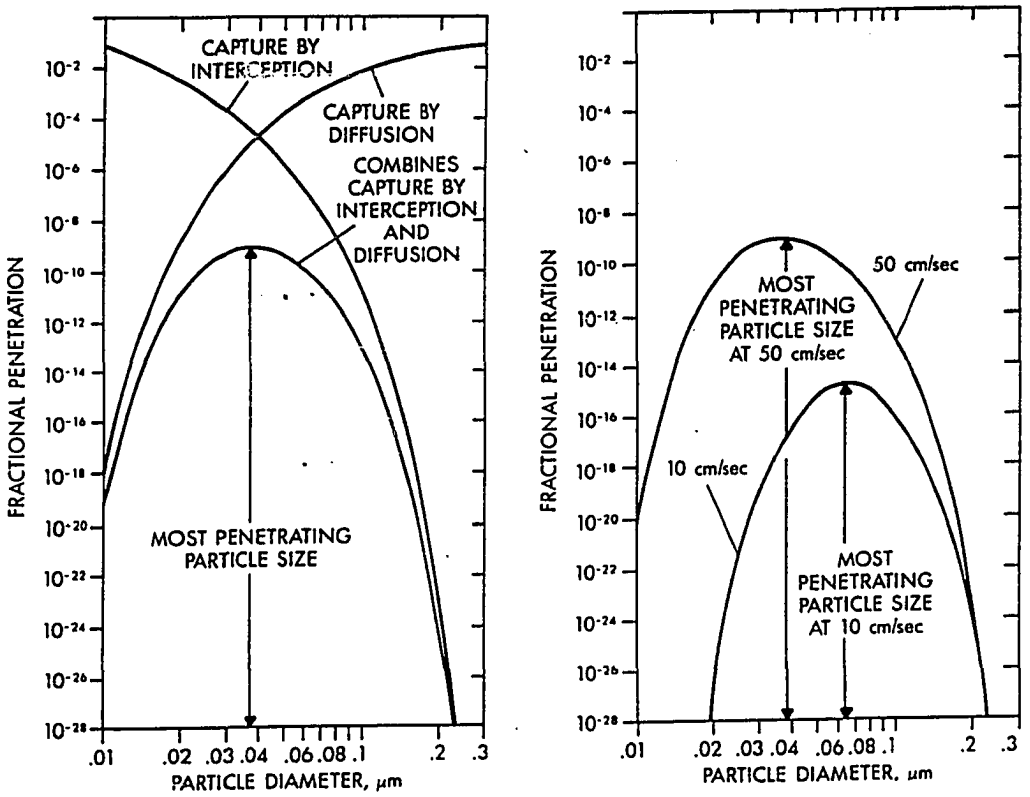

Figure 6-10 Schematic diagram showing characteristics of a membrane filter: (a) Mechanism for most penetrating particle size. (b) Filter efficiency as a function of particle size

effectively collected by diffusion. In the intermediate particle size near MPPS, neither diffusion, interception nor impaction is particularly effective.

Table 6-1 summarizes the experimentally measured MPPS and filter efficiency of HEPA, ULPA, and membrane filters. It shows that these filters have very high efficiencies even at MPPS. Therefore, it is believed that cleanroom air contains very few fine particles provided that the filters have no leaks, and that the air has not been contaminated by a internal fine particle source. The air used in this work was filtered by a Wafergard gas filter (a type of membrane filter) and can be regarded as particle-free.

Table 6-1 Particle concentration and filter efficiency at the most penetrating particle size[a]

Filter	[b]Efficiency	Particle Concentration #/cc
no filter		10^4
HEPA	99.97% at 0.3 μm	3
ULPA	99.999% at 0.12μm	0.1
Membrane	99.9999999 at 0.05μm	10^{-5}

a. See Accomazzo et al. (1985) for details

b. The efficiency at any other size (small or large) is higher

3) Conclusion

If the carrier gas is air filtered by HEPA, ULPA, or membrane filters, few fine particles are present. In this situation, heterogeneous condensation is not the major mechanism for particle formation in pump-down.

Experimental tests support this conclusion. The experimental results presented in Section 6.2.3 show that the particle

concentration can be as high as 10^4/cc. Assume that these particles come from fine particles which have a penetration efficiency of 10^{-9} (same as MPPS). This means that room air contains 10^{13}/cc fine particles, which is impossible because of the limit of coagulation (natural aerosol has maximum concentration of 10^6/cc).

6.3.3 Water Vapor Nucleation

Particles in pump-down are neither detached from the chamber surface nor brought in from the outside. They must, therefore, be generated in the gas. We hypothesize that particle generation during pump-down results from water vapor nucleation. Table 6-2 lists the saturation ratios and nuclei sources for these nucleation processes.

Table 6-2 Condensation processes, critical saturation ratio, and nuclei.

Process	**Saturation Ratio**	**Nuclei**
Heterogeneous Condensation	1 to 3	0.002 to 0.1 μm
Condensation on ions (singly charged)	4 6	negative ions positive ions
Homogeneous Nucleation	3 to 8	Molecule Clusters

Ions are normally singly charged containing about 30 air molecules (Hinds, 1982). Negative ions can become nuclei for water vapor nucleation when S exceeds about 4, and positive ions when S exceeds about 6. In a normal atmosphere, the equilibrium ion concentration of each sign is about 1000/cc. These ions are created by the reaction of cosmic radiation and radioactive gases that emanate from the ground. This indicates that if these ions all become particles, 2000 particles/cc would be generated.

Experimental observation suggests that as high as 10^4/cc particles are generated. This indicates that homogeneous nucleation (water molecule cluster as condensation nuclei) may also occur in pump-down. As shown in Chapter 5, the critical saturation of homogeneous nucleation ranges from 3 to 8 when gas temperature reduces from 300 to 250 K.

The best proof of this hypothesis is the Wilson cloud chamber experiments. As will be discussed latter, many aspects of particle generation patterns, such as the onset of pressure and critical condition, match predicted water vapor nucleation during pump-down.

6.4 MECHANISMS OF RESIDUE PARTICLE FORMATION

It must be pointed out that the particles in our experiment are measured after the pump-down process. Szymanski et al. (1988) passed these particles through a heated tube of 300°C, and still found numerous CNC counts, indicating that these particles are very persistent. Using a diffusion battery, Szymanski et al. measured the size of these particles which were found to have a median diameter of 50 nm and a geometric mean of 1.2. We will refer to these particles detected after pump-down as residue particles. Where do these residue particles come from? Before answering this question, we need to point out the following facts.

1) Residue particles cannot be pure water droplets.

If these particles were pure water droplets, they would have evaporated completely in a very short time once pump-down stops. As a result, no CNC counts should have occurred. The life time of a water droplet, LT, of diameter d can be estimated by the following formula

$$LT = \frac{R \rho_p d^2}{8 D_v M_v (p_d/T_d - p_v/T_v)} \qquad (6.25)$$

where R is the universal gas constant; M_v, vapor molecular weight; D_v, vapor diffusion coefficient; ρ, the density of water; p_v and T_v, vapor pressure and temperature in the gas; p_d and T_d, vapor pressure and temperature at the droplet surface. If the droplet is small, the Kelvin effect must be considered. The life time of a water droplet of 10μm at RH = 50% is only 0.15 seconds.

2) Residue particles are not likely to be organic oil droplets

It will be shown that the residue particles can not be, at least not pure, organic droplets because the life times of droplets are still too short to be detectable. Mechanical pump fluids have vapor pressures on the order of 10^{-5} to 10^{-8} Torr (O'Hanlon, 1980, Section 7.1). These vapors are likely to be present in a vacuum chamber. Consider pump fluid Convil (a type of hydrocarbon) which has a saturation vapor pressure 3.8×10^{-7} Torr at 25°C. Assume this vapor is saturated in the chamber and is converted to oil droplets with uniform size and concentration 10^3/cc (the order of the residue particle concentration measured in this work). With this assumption, one can find that the these droplets have a size of about 50 nm, which will have a estimated life time on the order of 10 seconds when ambient temperature is 25°C. If these droplets pass through a heating tube of 200°C, their life time is only on the order of 10^{-6} seconds.

The estimation is carried out with the following data at 25°C: $T_v = T_d = 298$ K, $p_v = 3.8 \times 10^{-7}$ Torr, $M_v = 400$ g/mole, $D_v = 0.1$ cm^2/s, $\sigma = 35$ dyne/cm (surface tension of organic oils usually range from 30 to 40 dyne/cm), and $\rho_p = 1$ g/cc. Since the droplet is small, the Kelvin effect must be considered: $p_d = p_s \exp\left(\frac{4 \sigma M}{\rho_p T d}\right)$, where

saturation pressure $p_s = 3.8 \times 10^{-7}$ Torr. With these data, the life time can be estimated by Eq.(6.25). At 200°C, all the data keep the same except that $T_v = T_d = 473$ K and $p_s = 1$ Torr. The M_v and p_s for Convil are found from O'Hanlon (1980). The other data have been assumed.

6.4.1 Hypotheses

We hypothesize that residue particles are formed by gas impurities that are captured by water droplets which are generated by water vapor nucleation and condensation during pump-down. These residue particles may be formed in a manner shown schematically in Fig.6-11.

1) Initially, the carrier gas is free of particles, but it contains water vapor and gaseous impurities such as SO_2 and NH_3, ions, organic vapors such as pump oil or grease, and others. These impurities can neither be filtered out by the filter nor detected by a CNC.

2) During pump-down, when water vapor is below the critical saturation, S* (curve *ab*), water molecules and impurities would stay in a gaseous form. They may form clusters because of the van der Walls force, but these clusters are physically unstable.

3) Once the critical saturation ratio for water vapor nucleation is reached (S = S*), stable droplets of size d* are generated.

4) These generated droplets grow because of water vapor condensation when water vapor remains supersaturated (curve *bc*: S > 1). At the same time, impurities are scavenged and absorbed by these droplets.

5) After pump-down or at any time during pump-down that the supersaturation is released (curve *cd*: S < 1), water molecules in

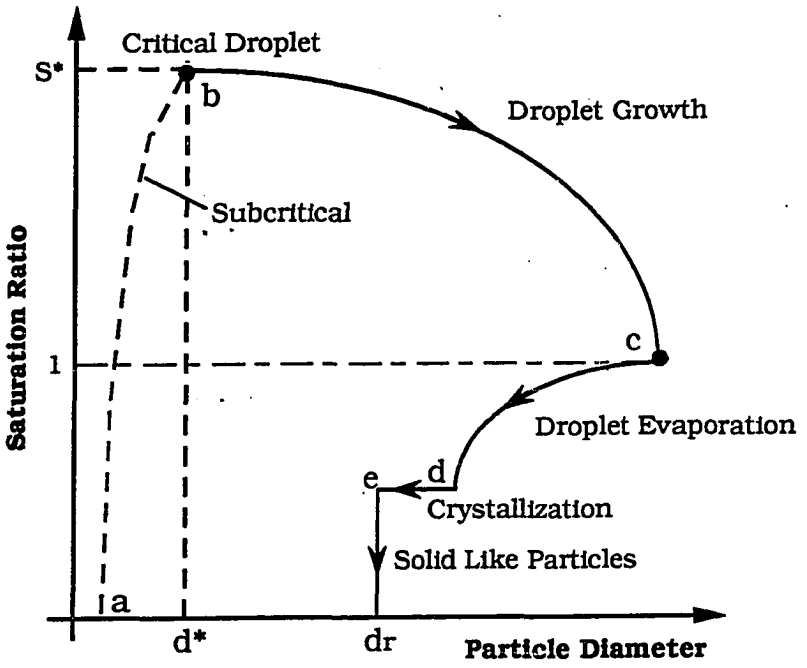

Figure 6-11 Schematic diagram showing the mechanism of residue particle formation

these droplets evaporate but the impurities may stay.

6) When water molecules are completely evaporated, impurities left form residue particles. If these impurities are salt-like, the crystallization my occur (curve *de*). These residue particles are physically stable and their sizes are in the detectable range of the CNC.

The following remarks can be made on the hypothesis. First, the impurities alone, in the absence of water vapor, cannot self-nucleate to form stable particles. These impurities can only be captured in the process of water vapor nucleation and condensation.

Secondly, once these impurities are captured in a droplet, they will not evaporate, at least not as easily as water molecules. This suggests that the impurities may chemically react with each other in liquid droplets to form stable product. For example, if SO_2 and NH_3 have been captured in a water droplet, they may react to form ammonium sulfate $(NH_4)_2SO_4$ -- a salt which will become a solid crystal after the droplet has dried.

Third, the total number of residue particles equals the number of droplets formed by the nucleation. Note that condensation only affects particle size.

Fourth, the presence of impurity molecules does not affect the critical saturation and the rate of water vapor nucleation. Note that the ratio of impurity molecules to water molecules in a gas is on the order of 10^{-7} (equal the ratio of their partial pressures). Consider $S_c = 5$. The critical nuclei predicted by the Kelvin equation is 1.30 nm which contains about 26 molecules. If the probability that all the molecules get into the critical nuclei is equal, the nuclei will contain nearly all water molecules. Thus the nucleation rate and S_c will not be disturbed by impurities. However, the impurities scavenged by the latter

condensation is not negligible. Consider the d = 5 μm which contains 2.2×10^{12} water molecules. By the same argument, the droplet will contain 2.2×10^{5} impurity molecules which corresponds to 60 nm residue particle.

6.4.2 Estimation of Residue Particle Size

As a test of the hypothesis, the size of residue particles is estimated. The size of water droplets during pump-down is first estimated. Assume that the total number of droplets in a unit volume (particles remaining in the chamber plus those have been pumped out) is n_d and all the droplets have equal size d_d. From mass balance between the liquid droplets and the vapor in conversion,

$$\rho_w n_d \left(\frac{\pi}{6} d_d^3\right) = \rho_w \, n_w \left(\frac{\pi}{6} \delta_w^3\right) F_c \qquad (6.26)$$

where δ_w is the water molecule diameter (3.85 Å), n_w is the initial water vapor molecule concentration, and F_c is the fraction of the vapor molecules in conversion. Note that $n_w = \frac{p_w}{\kappa T}$, where p_w and T are the initial vapor pressure and temperature respectively, and κ is the Boltzmann constant. Then

$$d_d = \left(\frac{F_c}{n_d} \frac{p_w}{\kappa T}\right)^{1/3} \delta_w \qquad (6.27)$$

For air of 50% RH at T = 298 K, p_w = 11.73 dyne/cm^2 (8.8 Torr). If F_c = 0.1 and $n_d = 10^3$/cc (as shown later, $n_d \approx n_{max}$, the maximum concentration measured), d_d is found to be 12 μm. In Border's real-time measurement, many droplets larger than 5μm have indeed been observed. It is interesting to take a look at a limiting situation -- all the vapors are converted to a single droplet (F_c = 1 and N_d = 1/cc), the single droplet would have a size of d_d = 261 μm.

The residue particle size can be estimated in a similar manner. Assume the impurities are equally distributed among the droplets formed, also assume that impurity is gas like with mean molecule or atom diameter δ_i and initial partial pressure p_i. Then one may estimate the residue particle diameter d_r by

$$d_r = \left(\frac{F_c'}{n_d}\frac{p_i}{\kappa T}\right)^{1/3}\delta_i \qquad (6.28)$$

where F_c' is the conversion factor for impurities. Assume $F_c' = F_c$ (the impurities and the water molecules have equal chance to form droplets) and $\delta_i = \delta_1$, Eq.(6.28) may also be written as

$$d_r = \left(\frac{p_i}{p_w}\right)^{1/3} d_d \qquad (6.29)$$

The SO_2 and NH_3 in the clean air is on the order of 10 $\mu g/m^3$ ($p_i \approx 10^{-6}$ Torr, then $p_i/p_w \approx 10^{-7}$). Assume that $p_i/p_w = 10^{-7}$, $F_c = 0.1$, and $n_d = 10^3/cc$, one can find that $d_r = 56$ nm, which is in good agreement with measured residue particle size.

6.5 THEORETICAL ANALYSIS

Experimental evidence shows that particle generation and water vapor nucleation are related during pump-down. The pattern of particle generation is represented by the curve of number of particles versus pressure, which will be referred to as the n-p curve. The pattern of nucleation is represented by the curve of saturation ration versus pressure, which will be referred to as the S-p curve. Here, we will theoretically investigate the characteristics of each curve and the mapping between them.

6.5.1 Characteristics of the n-p Curve

In order to analyze the n-p curve, we write the balance equation for particle concentration:

$$\frac{dn}{dt} = I - \frac{n}{\tau} + L_D + L_E \tag{6.30}$$

where I is the rate of particle generation, the term $-n/\tau$ is the rate of particles being pumped out, L_D is the wall deposition loss, and L_E is the particle evaporation loss.

From the hypothesis, the particles can not be completely evaporated because of the residue present. Then

$$L_E = 0 \tag{6.31}$$

It has been shown that the wall deposition loss is not significant (at least at pressure greater than 100 Torr). Here assume

$$L_D = 0 \tag{6.32}$$

Eq.(6.30) now becomes

$$\frac{dn}{dt} = I - \frac{n}{\tau} \tag{6.33}$$

As it has been shown in previous chapters,

$$\frac{dp}{dt} = -\frac{p}{\tau} \tag{6.34}$$

Then

$$\frac{dn}{dp} = \frac{n - \tau I}{p} \tag{6.35}$$

or

$$\frac{d\ln(n)}{d\ln(p)} = 1 - \frac{\tau I}{n} \qquad (6.36)$$

Fig.6-12 shows a sketch of a typical measured n-p curve on a log-log scale. Important pressures are identified:

p_o = initial pressure
p_1 = onset pressure for particle generation
p_2 = onset pressure for near steady particle concentration
p_3 = cease pressure for particle generation
p_{max} = the pressure at which the maximum particle concentration n_{max} occurs

with these pressures, the n-p curve can be divided into four regions:

(i) $p_o > p > p_1$

In this region, no particle generation. i.e.,

$$I = 0, \quad n = 0, \quad \text{and} \quad dn/dp = 0 \qquad (6.37)$$

This region is referred to as the no particle generation region.

(ii) $p_1 > p > p_2$

In this region, particle generation is dominant and thus n increases. It is assumed that the rate of particle generation is (k+1) times that of particle pumped out:

$$I = \frac{(k+1)\,n}{\tau} \qquad (6.38)$$

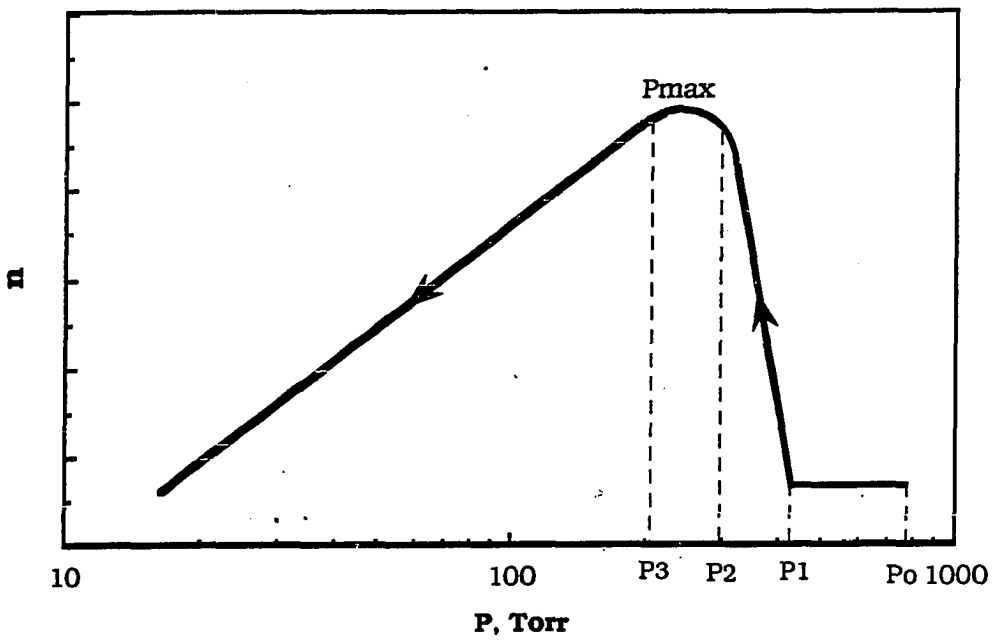

Figure 6-12 Schematic diagram showing the characteristics of particle formation as a function of pressure

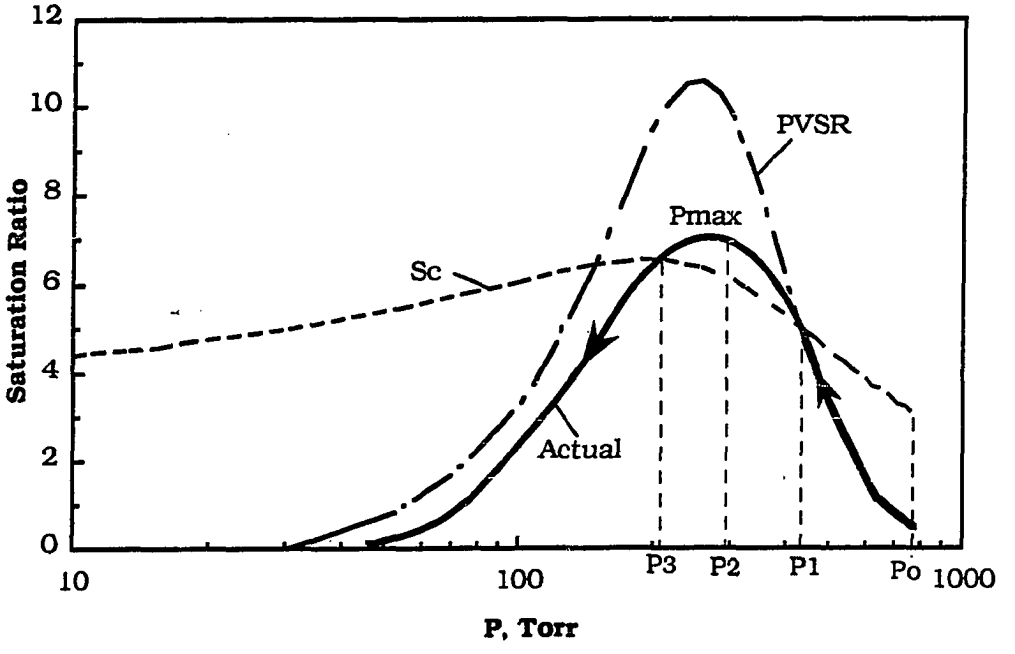

Figure 6-13 Schematic diagram showning the saturation ratio as a function of pressure and mapping between particle formation and water vapor nucleation

Substituting Eq.(6.38) to Eq.(6.36) yields

$$\frac{d\ ln(n)}{d\ ln(p)} = - k \qquad (6.39)$$

This equation indicates that ln(n) versus ln(p) is a straight line in the region of particle generation dominance which agrees with the measured results (see Fig.6-5). The solution to this equation is

$$\frac{n}{n_1} = \left(\frac{p}{p_1}\right)^{-k} \qquad (6.40)$$

where $n_1 = 1$ may be used. Substituting this equation to Eq.(6.38), one finds that

$$I = \frac{k+1}{\tau}\left(\frac{p}{p_1}\right)^{-k} \qquad (6.41)$$

(iii) $p_2 > p > p_3$

In this region, the particle concentration approaches a maximum and remains nearly constant (nearly stationary region). The characteristics are

$$\frac{dn}{dp} = 0,\ n \approx n_{max},\ \text{and}\ I = \frac{n_{max}}{\tau} \qquad (6.42)$$

(iv) $p > p_3$

In this region, the particle generation ends or at is at least negligible. The generated particles are simply pumped out. We consider this region as pumping loss dominant.

$$I = 0\ \text{and}\ \frac{d\ ln(n)}{d\ ln(p)} = 1 \qquad (6.43)$$

which has the solution of

$$\frac{n}{n_3} = \frac{p}{p_3} \tag{6.44}$$

This equation fits the experimental measured n-p curve in the pumping loss dominant region.

Another important issue is the total number of particles generated during pump-down, n_t, which can be written as

$$n_t = \int_{t_1}^{t_3} I \, dt \tag{6.45}$$

since $dt = -\tau \frac{dp}{p}$, then

$$n_t = \int_{p_3}^{p_1} \tau I \frac{dp}{p} = \int_{p_3}^{p_2} \tau I \frac{dp}{p} + \int_{p_2}^{p_1} \tau I \frac{dp}{p} \tag{6.46}$$

Substituting Eqs.(6.41) and (6.42) into Eq.(6.46) and noting $n_1 = 1$, one can show that

$$n_t = \frac{k+1}{k}(n_2 - 1) + n_{max} \ln(p_2/p_3) \tag{6.34}$$

Since $n_2 \approx n_{max}$ and $k >> 1$, n_t has the same order of magnitude of n_{max}.

6.5.2 Mapping Between the S-p Curve and the n-p Curve

Water vapor saturation patterns in pump-down (the S-p curves) have been investigated in Chapter 5. These patterns are schematically

shown in Fig.6-13, where PVSR stands for the potential vapor saturation ratio, S_c stands for the critical saturation ratio for nucleation, and both are theoretically predicted by the neglecting of any disturbance of condensation and associated latent heat. Fig.6-13 also shows the guessed actual saturation S which includes the disturbance of condensation. To support the hypothesis that particle generation is the result of water nucleation, the mapping between the n-p curve and the S-p curve are investigated below.

1) Overall Mapping

The particle generation pattern, shown in Fig.6-12, has been divided four regions by pressure p_o, p_1, p_2, and p_3. The counterparts of these regions and associated pressures are also found in the S-p curve, and the detailed explanations are summarized in Table 6-3.

Table 6-3 Overall mapping between water vapor saturation and particle generation

Pressure	**S-p curve**	**n-p curve**
$p_o > p > p_1$	$S < S_c$: no nucleation	No particle generation
$p_1 > p > p_2$	$S > S_c$: nucleation occurs Difference $(S-S_c)$ increases	Particle generation dominates pumping loss
$p_2 > p > p_3$	$S > Sc$: nucleation continues But difference $(S-S_c)$ reduces	Stationary: particle generation equals pumping loss
$p_3 > p$	$S < S_c$: nucleation stops	Particle generation stops, pumping loss is dominant

2) Prediction of Onset Pressure of Particle Generation

The no-particle-generation region in the n-p curve, from p_0 to p_1, corresponds to no-nucleation region in the S-p curve where PVSR and actual saturation is identical. According to this mapping, the onset pressure of particle generation, p_1, is the onset pressure for nucleation, which is at the intersection of PVSR and S_c. This intersection can be predicted by the theory developed in Chapter 5.

According to the theory, S_c depends on Z only and PVSR depends on both Z and RH for moist air at fixed initial temperature and pressure. For the experiment, p_0 =760 Torr, T_0 = 298 K, and $Z = 5.96\tau$ (note $Z = \frac{\tau \omega}{\xi}$, where ξ = 1.13 cm for the chamber and ω = 6.74 cm/s for the air).

Fig.6-14 shows the calculated S_c and PVSR for different RH at a fixed Z = 16, which corresponds to a fixed τ = 2.7 seconds in Fig.6-6. When RH = 58%, the intersection in Fig.6-15 is at 430 Torr while observed p_1 in Fig.6-6 is about 450 Torr. As RH increases, the intersection is shifted to higher pressure, which is also supported by experimental observation.

Fig.6-15 shows calculated S_c and PVSR at a fixed RH = 40% for Z = 6 and Z = 16, which corresponds to the situations of τ = 1.0 seconds and τ = 2.7 seconds in Fig.6-5 respectively. The limiting case Z = 0 (adiabatic expansion) is also shown in the figure. For smaller Z number (RH is fixed), the intersection of PVSR and S_c usually occurs at higher pressure. However, when Z < 6, the intersection does not change much, which indicates that the nucleation (particle formation) corresponding to these Z numbers starts more or less at the same pressure. This prediction agrees with our experimental observation.

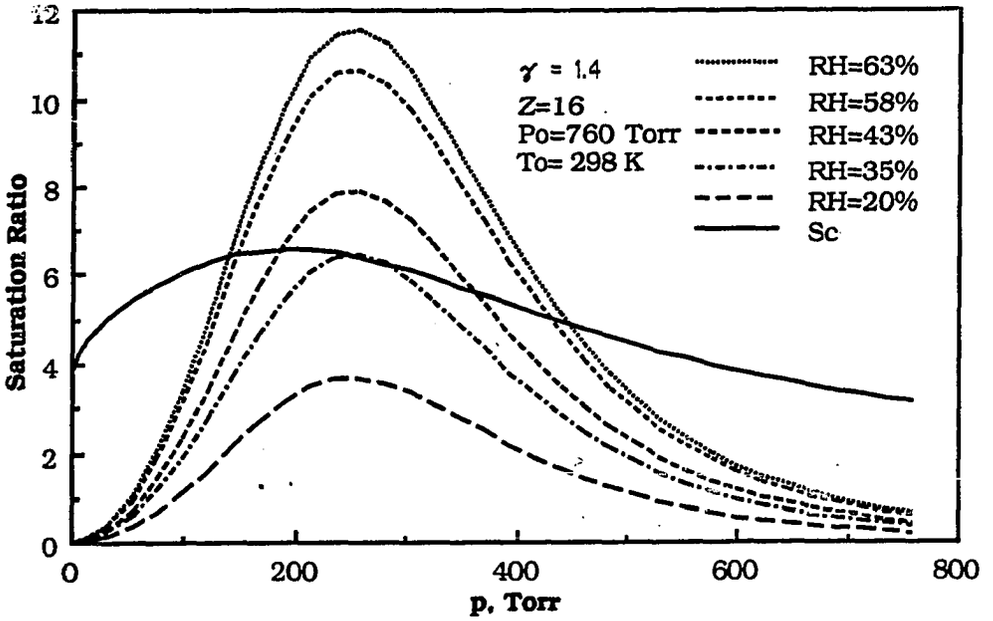

Figure 6-14 Onset pressure of particle formation at a fixed Z = 16 with different relative humidity

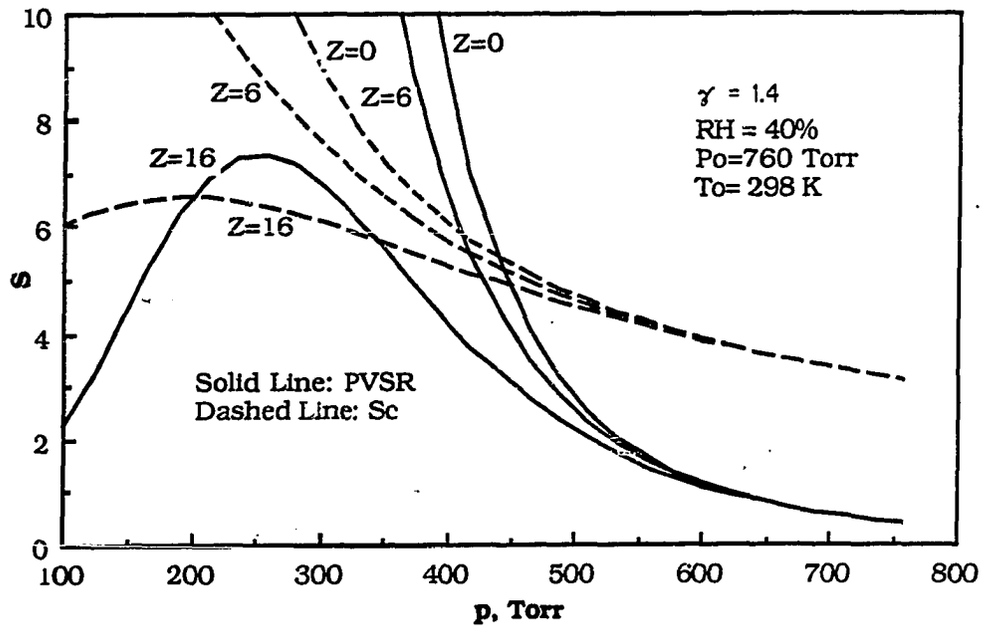

Figure 6-15 Onset pressure of particle formation at a fixed RH = 40% with different Z numbers

3) Predication of Critical Condition of Particle Generation

Fig. 5-13 in Chapter 5 shows theoretical prediction of critical conditions of water vapor nucleation, which depends on the combination of Z and RH. The curve represents the nucleation rate of 1 nucleus/s.cc. Higher RH and smaller Z mean higher nucleation rate. Fig. 6-8 shows the experimental observed critical condition for particle formation, which depends on the combination of τ and RH. The data points represents that 1 particle/cc will be generated. Higher RH and small τ mean more particle generation.

Comparison between Fig.5-13 and Fig.6-8 is made in Fig.6-16, where the data points (τ,RH) in Fig. 6-8 are converted to (Z,RH) according to $Z = 5.96\tau$ for the experimental condition. It is found that these data points fall in the region limited by $S_c = 4$ (the value for water vapor nucleation on ions) and S_c for water vapor homogeneous nucleation. This comparison verifies the hypothesis that particle formation in this experiment is the result of water vapor nucleation.

6.6 CONCLUSIONS

Particle generation during pump-down, in the presence of water vapor, has been quantitatively measureed and theoretically investigated. The discoveries are summarized as follows:

1) The number of particles generated is a function of pumping time constant, initial relative humidity, and terminal pressure of pump-down. The particle generation is the result of water vapor nucleation: homogeneous nucleation, nucleation on ions, or both. In the experimental conditions, the types of nucleation are not distinguishable.

2) Residue particles are formed during pump-down. They are persistent and will not completely evaporate after pump-down.

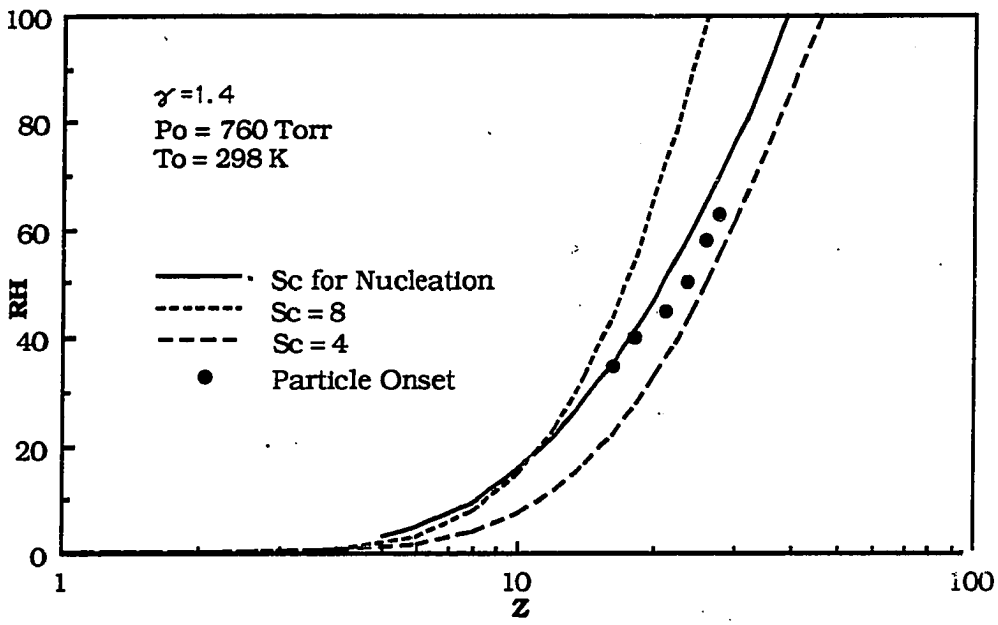

Figure 6-16 Critical Z and RH: Comparison of onset of measured particle formation and predicted water vapor nucleation

These residue particles are likely to contain $(NH_4)_2SO_4$ (a reaction product of SO_2 and NH_3), which may be scavenged and absorbed by the droplets during the water vapor nucleation and condensation.

3) It is found that the critical condition of particle generation depends on the combination of Z and RH for a given vapor-gas mixture. The critical condition predicted theoretically agrees with that determined experimentally .

4) The experimental observations and analyses show that the particle generation is not caused by the surface particle reentraiment or the heterogeneous condensation on fine particles.

CHAPTER 7

CONCLUSIONS

A vacuum pump-down process has been studied experimentally and theoretically from two points of view: thermodynamics and particle formation. The important contributions of this thesis are as follows:

1) The first and the most complete transient temperature measurement during pump-down has been provided.

2) A thermodynamic theory has been developed for the continuum regime, which has been ignored before, and thus made the pump-down theory more complete. Moreover, a similarity solution to pump-down has been found, and a dimensionless Z number has been introduced to measure the adiabaticity of pump-down.

3) A theory has been developed for vapor condensation and nucleation during pump-down, on the bases of which design criterion for clean vacuum pump-down is found.

4) Particle formation has been quantitatively investigated which shows that the particles are mainly water droplets and formed by water vapor homogeneous nucleation, or nucleation on ions, or both. The impurities scavenged by droplets may be chemical reactions to form residue particles. The most likely reaction is that $SO_2 + NH_3 \rightarrow (NH_4)_2SO_4$.

In Chapter 2, transient temperature of gas during vacuum pump-down has been systematically measured with a modern data acquisition system. A substantial drop in gas temperature is observed. In a 47.3 liter chamber, when the effective pumping speed is 705 lpm

and the initial temperature is 25°C, the maximum temperature drop is 70 °C for 50%RH room air, 95°C for dry nitrogen, 105°C for high purity argon. It is found that the following factors have significant effects on gas temperature history: effective pumping speed, chamber geometry, gas medium, initial pressure, water vapor, and measurement location.

In Chapter 3, a mathematical model for the process of vacuum pump-down, based on fundamental thermodynamics and processes of heat and mass transfer in the continuum regime, has been developed to predict the temperature and pressure of gas, and the saturation ratio of condensable species. The input to the model is the physical properties of gas and vapor, their initial states, the chamber geometry, and the pumping conditions. Numerical calculations based on the model are carried out for various pump-down conditions. The predictions are in good agreement with the experimental data. Along with the development of the model, order-of-magnitude analysis in this chapter lead to the following conclusions regarding to the pump-down process: (i) natural convection is the predominant process affecting heat transfer to and from the chamber walls; (ii) the chamber wall temperature remains nearly constant during pump down; (iii) the latent heat released from water vapor condensation or ice formation may be a significant heat source affecting the gas temperature.

In Chapter 4, a generalized theory based on the model in Chapter 3 is developed to describe the thermodynamic path of pump-down which is the form of $T^* = f(Z, \gamma, p^*)$. This is the similarity solution to pump-down which can be applied to all chambers, pumping conditions, and carrier gases. Z is a dimensionless number which is determined for a given gas, chamber, pumping rate, and initial pressure and temperature. The physical significance of Z is a measure of the degree of adiabaticity of pump-down process. When $Z = 0$, pump-down is adiabatic, and when $Z = \infty$, it is isothermal. Some parameters are also introduced in this chapter, such as equivalent

spherical diameter, shape factor, and critical volume for turbulent natural convection in the analysis. These parameters are very useful in characterizing the conditions of pump-down processes.

In Chapter 5, a general theory is developed for a critical pump-down condition that initiates vapor condensation or nucleation. Potential vapor saturation ratio is used to measure the ability of pump-down saturating a vapor. The critical saturations for homogeneous nucleation, homogeneous condensation, and condensation to ions are described. Numerical simulation of the theory shows that the critical conditions for water vapor nucleation, or condensation depend on the combination of Z number and initial RH. Based on the developed theory, a quantitative criterion is proposed for the design of clean vacuum systems.

In Chapter 6, particle generation in pump-down, with the presence of water vapor, has been quantitatively measured and theoretically investigated. The contributions are summarized as follows:

1) The number of particles generated is a function of pumping time constant, initial relative humidity, and terminal pressure. The particle generation is a result of water vapor nucleation (homogeneous nucleation), or nucleation on ions, or both. In the experimental condition, the types of nucleation mentioned are not distinguishable.

2) Residue particles are formed in pump-down, they are persistent and will not completely evaporate after pump-down. These residue particles are likely to contain $(NH_4)_2SO_4$ which are the reaction product of SO_2 and NH_3, and are scavenged and absorbed by the droplets during water vapor nucleation and condensation.

3) The critical condition for particle generation depends on the combination of Z and RH for a given vapor-gas mixture. The critical

condition theoretically predicted agrees with that experimentally determined.

4) Hypothesis test shows that the particle generation is not caused by the surface particle reentrainment in clean chamber, or the heterogeneous condensation on fine particles in filtered air.

REFERENCES

Accomazzo, M. A., K. L. Rubow, and B. Y. H. Liu, (1984). "Ultrahigh Efficiency Membrane Filters for Semiconductor Process Gases," Solid State Tchnol. 27(3): 141-146.

Ahn, K. H., B. Y. H. Liu and Z. Xu, (1988). "Further Development of Vacuum particle measurement system," presented at the 7th Review Meeting of Particulate Contamination Control Research Consortium, Willoughby, Ohio

Allard, E. F. and J. L. Kassner, Jr., (1965). "New Cloud-Chamber Method for the Determination of Homogeneous Nucleation Rates," The Journal of Chemical Physics, Vol. 42, No. 4, pp. 1401-1405.

Bird, G. A., (1976). Molecular Gas Dynamics, Clarendon Press, Oxford, Chap. 1, p. 18.

Borden. P. G. and Y. Baron (1987). "Water Aerosol Formation During Pump-Down in State-of-the-Art Process Equipment", High Yield Technology, Mountain View, CA

Bowling, A. R. and G. Larrabee, (1986). "Particle Control for Semiconductor Processing in Vacuum Systems," Microcontamination Conference Proceedings, Canon Communications, Inc., Santa Monica, CA, pp. 161-168.

Chen, Degang, T. Seidel, S. Belindki, and S. Hackwood, (1989). "Dynamic particulate characterization of a vacuum load-lock system," J. Vac. Sci. Technol. A7 (5). p.3105

Clark, W. E. and K. T. Whitby, (1967). "Concentration and Size Distribution Measurements of Atmospheric Aerosols and a Test of the Theory of Self-Preserving Size Distributions," Journal of the Atmospheric Sciences, Vol. 24, pp. 677-687.

Cleaver, J. W. and B. Yates, (1973). "Mechanism of Detachment of Colloidal Particles from a Flat Substrate in a Turbulent Flow," Journal of Colloid and Interface Science, Vol. 44, No. 3, pp. 464-474.

Crump, J. C. and J.H. Seinfeld, (1981). J. Aerosol Sci., 5: 405-415

Dushman, S., 1962, Scientific Foundations of Vacuum Technique, 2nd Ed., John Wiley & Sons, New York

Evans, L.B. and N.E. Stefany, (1965). "An Experimental Study of Heat Transfer to Liquid in Cylindrical Enclosures," Chemical Engineering Process Symposium Series, No. 64, Vol. 62, p. 209.

Friekander, J. K., Smoke, (1977). Dust, and Haze: Fundamentals of Aerosol Beheavior, Wiley-Interscience, New York

Garanville-Phillips Co., Instruction Manual for Series 316 Vacuum Gauge Controller, Boulder, Colorado.

Heist, R. H. and H. Reiss, (1973). "Investigation of the Homogeneous Nucleation of Water Vapor Using a Diffusion Cloud," The Journal of Chemical Physics, Vol. 59, No. 2, pp. 665-671.

Hoh, Peter D., (1984). "Summary Abstract: Quantitative Particle Contamination Studies Utilizing Reduced Turbulence Pumping and Venting," J. Vac. Sci. Technol. A5(4): 2067-2072.

Holman, J. P., (1986). Heat Transfer, McGraw-Hill, New York, Chap.7

Horowitz, P. and Winfield Hill, (1980). The Art of Electronics, Cambridge University Press, Cambridge, pp. 594-595.

Junge, C., (1955). "The Size Distribution and Aging of Natural Aerosols as Determined From Electrical and Optical Data on the Atmosphere," Journal of Meteorology, Vol. 12, pp. 13-25.

Kanazawa, K., (1989). "Analysis of pumping down process," J. Vac. Sci. Technol. A 7(6). pp.3361-3370

Kuehn, T. H., B. Y. H. Liu, and J. Zhao, (1987). "Thermodynamic Model of Vacuum Pump Down Processes," presented at the 5th Review Meeting of Particulate Contamination Control Research Consortium, IBM, Essex Junction, Vermont

Lee, K. W. and B. Y. H. Liu, (1980). "On the Minimum Efficiency and Most Penetration Particle Size for Fibrous Filters," J. Air Poll. Control Assoc. 30: 377-381

Lewin, Gerhard, (1965). Fundamentals of Vaccum Science and Technology, McGraw-Hill, New York

Liepmann, H. W., (1961). "Gaskinetics and Gasdynamics of Orifice Flow," J. Fluid Mech., Pt. 1, vol. 10, pp. 65-79.

Liu, B. Y. H and K. W. Lee, (1976). "Efficiency of Membrane and Nuclepore Filters for Submicrometer Aerosols," Env. Sci. Tech., 10: 345-350

Liu, B. Y. H, J. C. Wilson, and D. Y. H. Pui, (1990). Laboratory Manual for Basic Instrumentation, University of Minnesota, Minneapolis, Minnesota

Liu, B. Y. H., K. L. Rubow, and D. Y. H. Pui, (1985). "Performance of HEPA and ULPA Filters," Proceedings of the 31st Annual Meeting of the Institute for Environmental Sciences, pp. 25-28.

Liu, B.Y. H, T. H. Kuehn and J. Zhao, (1989). "Nucleation, Condensation, and Particle Growth during Vacuum Pump-Down," presented at 8th Review Meeting of Particulate Contamination Control Research Consortium, Applied Materials, Santa Clara, CA

Mason, J., (1971). The Physics of Clouds, 2nd Ed., Clarendon Press, Oxford.

Miller, R. W., (1983). Flow Measurement Engineering Handbook, McGraw-Hill, New York, Chap.10.

O'Hanlon, J. F., (1980). A User's Guide to Vacuum Technology, John Wiley & Sons, New York.

O'Hanlon, J. F., (1987). "Advances in Vacuum Contamination Control for Electronic Materials Processing," J. Vac. Sci. Technol. A5, No. 4, p. 2067

O'Hanlon, J. F., (1989). "Contamination Reduction in Vacuum Processing Systems," J. Vac. Sci. Technol. A7, No. 3 p. 2500

Smith, T. C., (1989). "Detection and Control of Particles in Vacuum Environments for Semicondutor Manufacturing," 20th Annual Meeting of the Fine Particles Society, Boston, MA.

Springer, G. S., (1978). "Homogeneous Nucleation," Advances in Heat Transfer, Vol. 14, p. 281.

Szymanski, W. W., B. Y. H. Liu and K. H. Ahn,(1987). "Particle Measurement in Vacuum Systems," presented at the 5th Review Meeting of Particulate Contamination Control Research Consortium, IBM, Essex Junction, Vermont

Szymanski, W. W., B. Y. H. Liu and Z. Xu,(1988). "Particle Measurement in Vacuum Systems," presented at the 6th Review Meeting of Particulate Contamination Control Research Consortium, University of Minnesota, Minneapolis, Minnesota

Ulrich, R. D., D. P. Wirtz, and R. H. Nunn, (1964). "Transient Heat Transfer in Closed Containers After Injection," J. of Heat Transfer, p. 461.

Van Atta, C.V., (1968). Vacuum Science and Engineering, McGraw-Hill, New York, Chap. 2.

Wagner, P. P. (1969). "Gasdynamics of expansion flows with condensation, and homogeneous nucleation of water vapor," Nonequilibrium Flows, (Ed. P. P. Wegner). Vol. 1, Part 1, p. 163, Marcel Dekker, New York

White, D. R. and J. L. Kaaner, (1971). "Experimental and Theoretical Study of the Sign Preference in the Nucleation of Water Vapor," J. Aerosol Sci, Vol. 2, p. 201.

Wu. J. J., D.W. Copper and R. J. Miller, (1989). "Aerosol Model of Particle Generation During Pressure Reduction," 1989 Annual Meeting of the American Association of Aerosol Research, Reno, Neveda.

Zhao, J., T. H. Kuehn and B. Y. H. Liu, (1988). "Temperature and Pressure Measurement during Vacuum Pump-Down" presented at the 6th Review Meeting of Particulate Contamination Control Research Consortium, University of Minnesota, Minneapolis, Minnesota

Zhao, J., T. Kuehn, and B. Y. H. Liu, (1987). "Thermodynamic Model and Particle Formation in Evacuation Processes in Vacuum System, Part 1: basic theory used in simulation & Part 2: computational model and simulation results," Particle Technology Laboratory, Department of Mechanical Engineering, University of Minnesota.

APPENDIX A

THERMOPHYSICAL PROPERTIES USED IN THE CALCULATIONS

Table A-1 Physical properties of E-type thermocouples

Type	Composition	ρ, g/cc	c_p, erg/g.°C	κ, erg/cm.s.°C
Chromel (+)	10%Cr - 90%Ni	8.666	0.444×10^7	17.0×10^5
Constantan (-)	60%Cu - 40%Ni	8.922	0.410×10^7	22.7×10^5

$d_j = 0.0055$ cm (2 times TC wire diameter)
$\rho_j = 8.80$ g/cc
$c_{pj} = 0.425 \times 10^7$ erg/g.°C

Table A-2 Coefficient to convert emf to temperature (°C) for E-type thermocouples

Range	$a_1 \times 10^{-1}$	$a_2 \times 10^1$	$a_3 \times 10^3$	$a_4 \times 10^5$
0 to 400°C	1.7022525	-2.209724	5.4809314	-5.7669892
0 to -100°C	1.7372525	"	"	"

Table A-3 Air properties at 1 Atm and 300 K[a]

ρ	=	1.1774×10^{-3}	g/cc
c_p	=	1.0057×10^7	erg/g.°C
μ	=	1.8462×10^{-4}	g/cm.s
κ	=	0.02227×10^5	erg/cm.s.°C
Pr	=	0.772	
M	=	28.9	g/mole

a: The data are from Holman (1986, p643)

Table A-4 Properties of water vapor[a]

Lv	=	2.84×10^{10}	erg/g
D_v	=	0.24	cm^2/s
σ	=	72	dyne/cm
A	=	9.183837	
B	=	- 2403.3689	

a: From Handbook of Chemistry and Physics, 53rd Ed. CRL Press.

Table A-5 Physical constants

R	=	8.31×10^{7}	erg/K.mole
σ'	=	5.669	$erg/cm^2.K^4$
No	=	6.02×10^{23}	molecules/mole
k	=	1.38×10^{-16}	dyne.cm/K

APPENDIX B

TRANSIENT PRESSURE MEASUREMENT WITH A CONVECTRON VACUUM GAUGE

The Convectron Vacuum Gauge (CVG), a type of Pirani gauge made by Granvill-Phillips Co., measures pressure by measuring heat loss from a heated wire. Unlike other thermal gauges which usually measure pressure from 10 to 10^{-2} Torr (O'Hanlon,1980), the CVG can measure pressure over six decades from 10^{3} to 10^{-3} Torr. The gauge has been calibrated under steady pressure by the manufacturer. Using it to measure transient pressure during pump-down, we find that without correction the CVG over-reads the pressure above 30 Torr. In this appendix, we will discuss the gauge operation principles, its calibration under steady pressure, and its response to transient pressure.

B.1 PRINCIPLE OF GAUGE OPERATION

As shown schematically in Fig.B-1(a), the CVG is placed in a Wheatstone-Bridge circuit with feedback control circuitry. Of the four resistors of the bridge, R_1 is a pressure sensing wire (a 0.0005" diameter tungsten wire with a 50 x 10^{-6} μm thick gold plate of length 3.8") enclosed inside the gauge tube envelope. R_2 is a resistor network for compensating the variation in ambient temperature. As shown in Fig.B-1(b), the wires within R_2, whose electrical resistance are temperature sensitive, are wrapped around a Kovar mandrel. If the mandrel temperature remains at 20°C, R_2 = 55 Ω. R_3 and R_4 are constant resistors of 261 Ω and 523 Ω respectively.

In pressure measurement, the feedback circuitry always balances the bridge when pressure changes. The operation is briefly described here. At a steady pressure, for example p = 1 atm, the bridge is

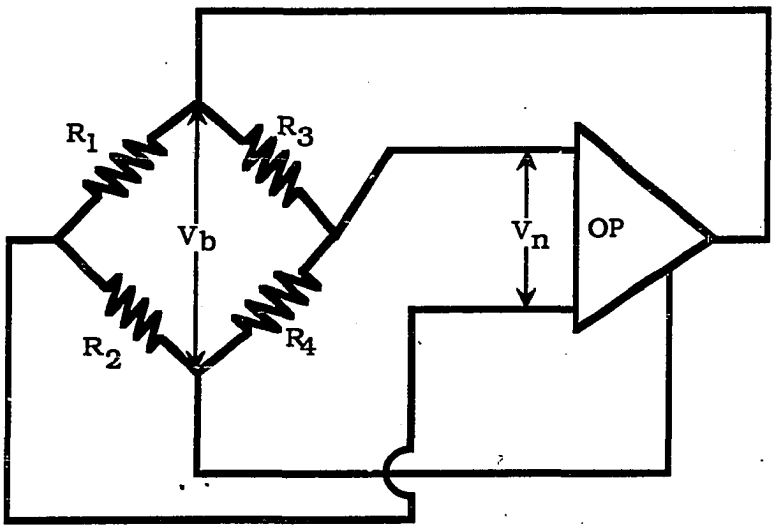

(a) The Wheatstone bridge with feed back control circuitry to maintain constant sensor wire temperature constant.

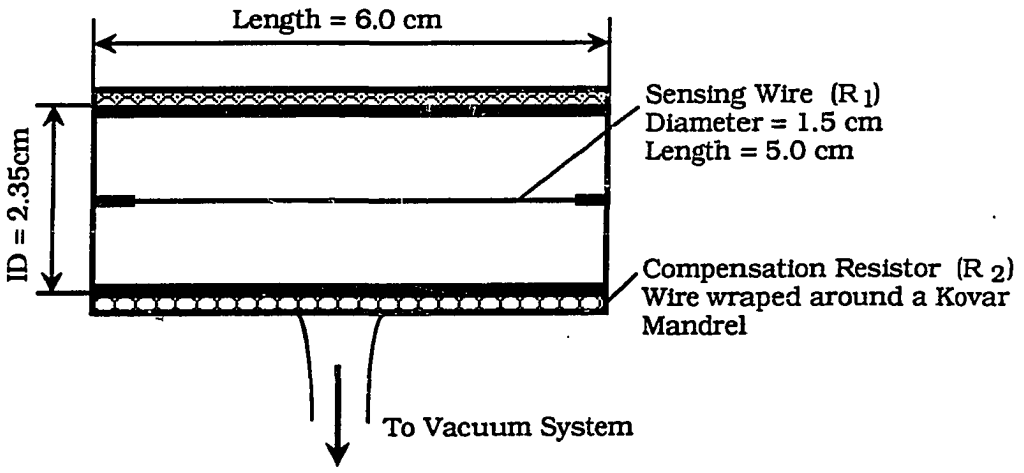

(b) Construction of the gauge

Figure B-1 Schematic of a convectron vacuum gauge

balanced and null voltage $V_n = 0$. If pressure is reduced to another steady pressure, the heat loss from the sensor wire will be reduced because less molecules carry the heat away. The decrease in heat loss increases T_s and thus R_1 which causes the bridge to unbalance($Vn \neq 0$). The feedback circuitry senses nonzero Vn and decreases V_b (the bridge supply voltage) until V_n is zero again.

It can be easily shown at the bridge voltage

$$V_b = G_c \sqrt{h + h_o} \tag{B.1}$$

where h is the pressure-dependent heat transfer coefficient for the sensor wire, h_o is the pressure-independent heat transfer coefficient, and G_c is the gauge constant

$$G_c = \sqrt{\frac{(R_3/R_4 + 1)^2}{R_3} R_2 (T_s - T) A_s} \tag{B.2}$$

where T_s is the sensor wire temperature, T is the gas temperature, and A_s is the surface area of the wire.

Equation (B.1) is derived from an energy balance for the sensor wire. The bridge balance requires that $R_1 = (R_2R_3)/R_4$ and thus T_s should be a constant. Constant T_s further requires

$$Q_e = Q_h \tag{B.3}$$

where Q_e is the electrical energy dissipated through the wire

$$Q_e = \frac{R_2R_3}{(R_3/R_4 + 1)^2} V_b^2 \tag{B.4}$$

and Q_h is the heat loss from the sensor wire

$$Q_h = h A_s(T_s-T) + A_s \sigma \varepsilon (T_s^4 - T_w^4) + \text{end loss} \tag{B.5}$$

The radiation and end loss are important at low pressure ($p < 10^{-4}$ Torr) which is a constant independent of pressure for a given gauge. For this reason, equation (B.3) can be rewritten as

$$Q_h = (h + h_o) A_s (T_s - T) \qquad (B.6)$$

where h_o is evaluated from the heat loss of the wire at zero pressure (actually at the lower limit of the gauge, 10^{-4} Torr). For the CVG 275, $h_o = 3.14$ Watt/m^2-°C for N_2 equivalent gas.

For the CVG 275, the gauge constant G_c may be evaluated at the nominal operation condition: $T_s = 120$°C, $T = 20$°C, and $R_2 = 55\ \Omega$, which yields $G_c = 0.212$ and thus

$$V_b = 0.212 \sqrt{h + 3.14} \qquad (B.7)$$

h is in Watts/m^2-°C and V_b is in Volts. This equation indicates that the voltage V_b at the bridge balance depends only on h which is a function of pressure as shown in Fig.B-2. Thus by measuring V_b, p is measured. This explains the gauge operation principle.

For accurate pressure measurement, G_c must be a constant independent of gas temperature (or ambient temperature), i.e.

$$R_2 (T_s - T) = \text{constant} \qquad (B.8)$$

Eq.(B.8) provides the base for the design of R_2. As shown in Fig.B-1, R_2 consists of the wires wrapped around the Kovar mandrel, and it changes only when the temperature of the mandrel changes. Thus in compensating the gas temperature change, the manufacturer assumes that the gas temperature is equal to the tube wall temperature, T_w, i.e., $T = T_w$ = ambient temperature. According to the manufacturer, R_2 is able to compensate for the changes of ambient temperature from +15 to +50°C.

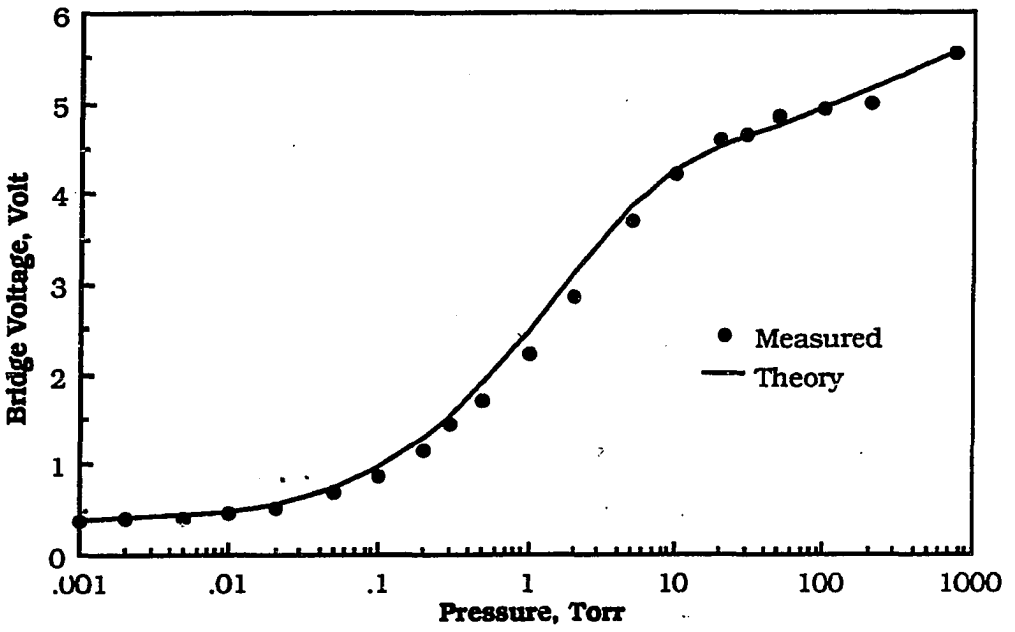

Figure B-2 Bridge voltage vs. pressure for CVG 275

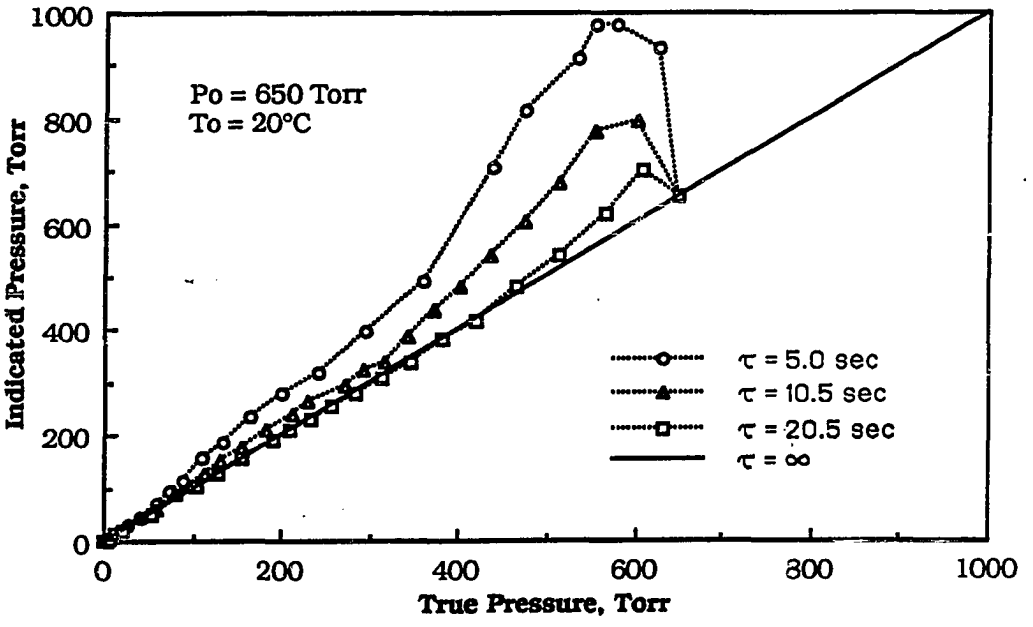

Figure B-3 Convectron Vaccum Gauge: Indicated pressure vs. true pressure for different pumping time constant

B.2 GAUGE CALIBRATION AND ITS THEORETICAL JUSTIFICATION

The bridge voltage V_b of the CVG has been calibrated against steady pressure for various gases by the manufacturer. Fig.B-2 is the calibration for air or N_2 equivalent gases. This calibration data can be theoretically justified. To do so, the dependence of h on steady pressure is investigated.

As pressure reduces from atmospheric pressure to high vacuum, the heat transfer coefficient, h, varies with the pressure, p, differently corresponding to the flow regimes classified by Knudsen number: Kn = λ/d_s, where λ is the gas mean free path and d_s is the diameter of the sensor wire. Table B-1 lists the general expression for h in the different regimes. It is noted that for air at 20°C $p\lambda$ = 4.6 Torr.cm. Thus, for the sensor wire ($d_s = 1.3 \times 10^{-3}$ cm), Kn can be expressed in terms of the pressure in Torr as Kn=3/p. Next, the specific expressions in all the regimes are derived for air at 20°C.

1) Continuum Regime (Kn < 0.1 or p < 30 Torr): The heat loss from the sensor wire is carried away by convection. If the pressure is steady, only natural convection takes place due to the temperature gradients near the sensor wire. Using air properties at a mean temperature 333 K and pressure 760 Torr: Pr = 0.697, ν = 0.188 cm^2/s, k_g = 0.02874 Watts/m.°C, one can find

$$h = 316\, p^{0.116} \qquad \text{(B.9)}$$

Note that in the continuum regime at high pressure the heat loss of the wire is proportional to $p^{0.116}$ and thus V_b is proportional to $p^{0.058}$, which is not sensitive to the pressure change. Since the orientation of the wire affects natural convection, the gauge has been calibrated for the gauge tube in the horizontal position.

Table B-1 Heat transfer of the sensor wire in different regimes

Regime	Steady Pressure	Transient Pressure
Continuum Kn < 0.1	Natural convection dominates $h = \frac{Nuk_g}{d_s}$ For a horizontally oriented wire(Holman) $Nu = 0.675(GrPr)^{0.058}$ $10^{-9} < GrPr < 10^{-2}$ $Pr = \frac{\mu c_v}{k_g}$: Prandtl number $Gr = \frac{g\beta\rho^2 d_s^3 (T_s - T_g)}{\mu 2}$: Grashof number c_v = gas specific heat μ = gas dynamic viscosity k_g = gas thermal conductivity β = thermal expansion coefficient g = gravitational constant ρ = gas density : function of pressure	In addition to natural convection, forced convection also occurs. King's Law for forced convection across the wire $Nu = 0.24 + 0.56Re_s^{0.45}$ $Re = \frac{\rho u d_s}{\mu}$: Reynolds number u = mean velocity over the sensor wire. d_s = wire diameter
Transition 0.1<Kn < 10	Conduction dominates. Temperature discontinuity near the wire is a function of pressure. $h = \frac{k_g}{0.5 d_s \ln(d/d_s) + \Theta(\Omega/p)(d_s/d + 1)}$ (Dushman,chap 1) $\Theta = \frac{(2-\alpha)}{\alpha}\frac{(9\gamma - 5)}{2(\gamma + 1)}$ d = gauge tube diameter Ω= a constant depends on unit and gas α = thermal accommodation coefficient γ = specific ratio λ = gas molecule mean free path	Same as that in steady pressure
Free molecule Kn > 10	Molecule collision with the wall dominates. Heat loss from the wire is linearly proportional to pressure. $h = \frac{3}{2}(2\pi mkT_s)^{1/2} k \frac{\alpha}{(1-\alpha)(d_s/d)} p$ (Dushman, chap 1) k = Boltzmann constant m = gas molecule mass	Same as that in steady pressure

2) Transition Regime (0.1 < Kn < 10 or 0.3 < p < 30 Torr): Conduction is the main heat transfer mechanism -- the heat from the wire is lost to its surrounding by the way of transferring kinetic energy from one molecule to another on a microscopic scale. For a thin wire, the discontinuity in temperature near the wire occurs because of the "slip" (Dushman, 1962), and it is a function of pressure. Using the expression in Table B-1 for the CVG, one can find that

$$h = \frac{2874}{5.593 + 16.44/p} \qquad (B.10)$$

In deriving this equation, the thermal accommodation coefficient becomes $\alpha = 0.646$, which is obtained by equating h in the transition regime to that in the continuum regime at 30 Torr.

3) Free Molecule Regime (Kn > 10 or p < 0.3 Torr): In this regime, the inner collision of molecules is negligible. The heat losses from the sensor wire occurs by the bombardment of air molecules on the wire and then on the tube wall.

$$h = 175p \qquad (B.11)$$

This equation is the limiting case of Eq.(B.10)

4) Radiation and End Loss Dominant Regime (p < 10^{-4} Torr): In this regime,

$$h = h_o \qquad (B.12)$$

Here the heat loss is independent of pressure and the CVG losses the sensitivity. Thus 10^{-4} Torr is the lower limit for the CVG. To be safe, the CVG sets its limit to 10^{-3} Torr.

The response of the gauge V_b to steady pressure can be

theoretically calculated by substituting Eqs. (B.9), (B.10) and (B.11) to Eq.(B.1). As shown in Fig.B-2, the theoretical V_b agrees well with the measured V_b.

V_b is a nonlinear function of pressure. In the actual measurement, V_b is conditioned by the Vacuum Gauge Controller (VGC) whose output V_p in Volt is a linear function of pressure in Torr in a log scale

$$V_p = \log(p) + 4 \qquad (B.13)$$

As the pressure varies from 10^{-3} to 10^3 Torr, the V_p varies from 1 to 7 Volt. If steady pressure is measured, the equation (B.13) is accurate in the entire measurement range.

B.3 GAUGE RESPONSE TO TRANSIENT PRESSURE

As shown in Chapter 3, the transient pressure from 760 to 0.1 Torr during pump-down can be predicted by

$$p/p_o = \exp(-t/\tau) \qquad (B.14)$$

where τ is the time constant of pressure decay and p_o is the initial pressure. Using the CVG to measure the transient pressure, we find that its response depends on not only the pressure but also τ and p_o.

Fig.B-3 plots the indicated pressure versus the true pressure for air under different τ. The indicated pressure is obtained by measuring V_p and then converting it to pressure using Eq.(B.13). The pressure predicted by Eq.(B.14) is regarded as the true pressure. It is found that below 30 Torr, the indicated pressure agrees with the true pressure; while above 30 Torr, the indicated pressure is higher. For example, when τ = 5.0 seconds, the true pressure is 512 Torr while the indicated pressure is 1000 Torr.

There two reasons which may cause the CVG to over-reads transient pressures above 30 Torr. (i) h changes because of the forced convection resulting from gas pumped out. (ii) T decreases because of the gas expansion cooling. As discussed in Section B.1, the pressure reading of the CVG depends on $\sqrt{R_2 (T_s-T) h}$; T_s is a constant because of the gauge is always balanced regardless of whether pressure is transient or steady; R_2 also remains constant because the Kovar mandrel temperature remains constant. Thus deviations in h and T from the calibration condition cause the gauge to misread the pressure.

Deviation in h due to Forced Convection

Under the transient pressure condition, the gas inside the gauge tube is continuously pumped out, and its flow is similar to a sink flow as shown in Fig.B-4. Forced convection takes place as the gas flows across the sensor wire. As shown in Table B-1, the effects of forced convection can be neglected at low pressure when conduction or molecule bombardment is the main heat transfer mechanism. However, the effects of forced convection may be significant in the continuum regime at high pressure (p > 30 Torr for air at 20°C). In addition to natural convection, forced convection also carries heat away from the sensor wire. In this mixed convection situation, the total heat transfer coefficient becomes

$$h = (h_F^n \pm h_N^n)^{1/n} \qquad (B.15)$$

where h_N is the natural convection heat transfer coefficient calculated by Eq.(B.9), and the h_F is the forced convection heat transfer coefficient which may be estimated using King's law

$$h_F = \frac{k_g}{d_s} (0.24 + 0.56 Re^{0.45}) \qquad (B.16)$$

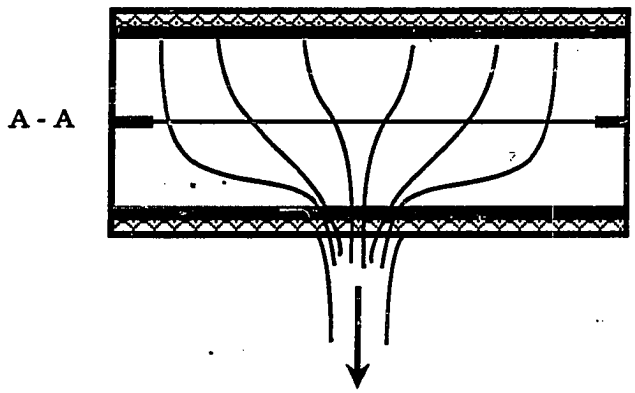

When gas is pumped out, the flow field is similar to sink flow. Gas velocity across the wire may be approximated by the gas velocity at A-A cross section.

Figure B-4 Gas flow pattern inside the gauge tube

where the Reynolds number

$$Re = \frac{\rho d_s u}{\mu} \qquad (B.17)$$

where u is the average gas velocity approaching the wire, which may be estimated by the gas velocity at the cross-section A-A in Fig.B-4. When the time constant τ is a constant, the total volumetric flow at the gauge outlet is a constant and equal to the volume of the gauge tube divided by τ, and the flow rate at the A-A cross-section is one half the total. Then

$$u = \frac{\pi}{8}\frac{D_T}{\tau} \qquad (B.18)$$

where D_T is the tube diameter which is equal to 2.35 cm.

The effect of forced convection on pressure can be estimated at 760 Torr and 300K. Air properties are used. Consider τ = 5 seconds. Calculation shows that u = 0.184 cm/s, Re = 1.8 x 10^{-3}, and h_F = 522 Watts/m.K. The natural convection heat transfer coefficient at 760 Torr is h_N = 682 Watts/m.K. This shows that h_F and h_N are on the same order of magnitude. Therefore, when p > 30 Torr, mixed convection indeed occurs during pressure change. Assuming n = 10 in Eq.(B.15), one can find that forced convection causes h to deviate from Eq.(B.7) by ±2% which will cause the CVG to misread the pressure by about ±18% (Note $p \propto h^{8.62}$).

Deviation in T due to Gas Expansion

With the theory developed in Chapter 4, the gas temperature inside the gauge tube is calculated when the pressure is reduced from 760 to 0.1 Torr. For air or nitrogen, T versus p under different time constants τ is plotted in Fig.B-5. The following features have been revealed by the simulation:

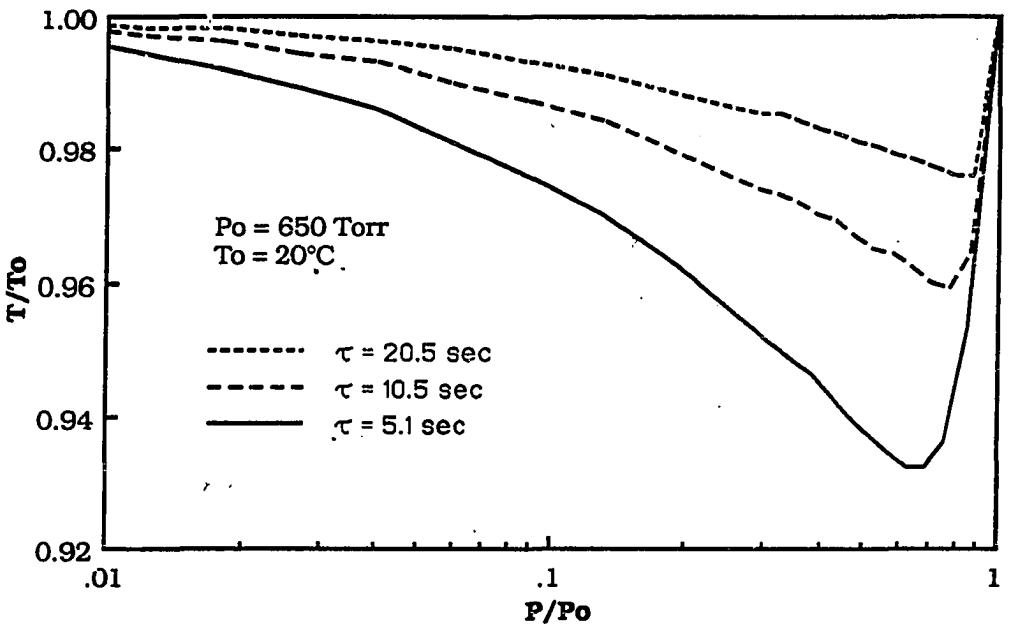

Figure B-5 Air or nitrogen temperature inside the gauge tube as a function of pressure for different pumping time constants

1) The tube wall temperature remains constant because of its large thermal capacity.

2) The temperature first decreases because of gas expansion cooling and later recovers because of heat transfer from the tube wall.

3) The faster the pressure decays (smaller τ), the more the gas has been cooled. For different τ, the maximum (T_w-T) and the pressure at which it occurs is listed in Table B-2.

4) The major changes in temperature occurs between 760 to 30 Torr. Below 30 Torr, the difference between T and T_w can be neglected.

The immediate consequence of decreasing the gas temperature is the increase in the heat loss from the sensor wire. More importantly, this temperature change can not be compensated by the compensation resistor R_2 inside the CVG because R_2 remains constant as the wall temperature (or Kovar mandrel temperature) remains constant.

Table B-2 Maximum gas temperature drops inside the CVG when gas pressure is reduced[a].

τ, s	$(T_w-T)_{min}$, °C	p_{min}, Torr
5	15	448
10	9	510
20	4	519

a. Data is obtained from the simulation with the following parameters: gauge tube diameter is 2.54 cm and length is 17.5 cm. p_0 = 650 Torr; T_w = 20°C. τ is the pumping time constant.

It is noted that as the pressure decreases, the indicated pressure first increases and then decreases which is just the opposite

to the gas temperature pattern. This gives a clue that the over-reading of the pressure is mainly associated with the decrease in the gas temperature. The magnitude of the over-reading can be estimated from the simulated temperature. As shown in Table B-2, when τ = 5 seconds, the maximum (T_w - T) is 15°C which is equivalent to increasing h by 15% (Note the original temperature difference between the wire and gas is about 100°C). This will cause the gauge to over-read the pressure by 300% which may saturate the gauge voltage -- this has been observed in the measurements. This estimation again shows that the expansion cooling is the major reason for the over-reading.

B.4 CONCLUSIONS

The response of the CVG to steady pressure and transient pressure has been investigated. It is found that

1) The gauge can measure steady pressure accurately from 10^{-3} to 10^{3} Torr.

2) Without correction, the gauge over-reads the transient pressure above 30 Torr for air or N_2. Below 30 Torr, the gauge reading of transient pressure is nearly the same as that for steady pressure.

3) The misreading of pressure above 30 Torr is caused by i) the deviation in heat transfer coefficient due to forced convection, and ii) the decrease in gas temperature due to the gas expansion cooling. The second factor is the major reason for pressure over-reading.

4) The gauge can not compensate for the expansion cooling because the temperature of the tube wall (mandrel) remains constant while the gas temperature changes.

APPENDIX C

TERMINOLOGY IN VACUUM TECHNOLOGY

The definitions of terminology in vacuum technology are explained in this appendix. Remarks on throughput continuity are made.

C.1 PUMPING LINE

The pumping line is the gas flow path form the exit of a chamber to the inlet of a pump.

C.2 VOLUMETRIC FLOW RATE, MASS FLOW RATE, PUMPING SPEED, AND EFFECTIVE PUMPING SPEED

Along the pumping line at any cross-section with an area of A, if the gas molecule mean drift velocity is u, the volumetric flow rate for this cross-section is

$$\dot{V} = u\,A$$

and the mass flow rate at any cross-section is

$$\dot{m} = \rho\,\dot{V}$$

where ρ is the gas density at the cross-section.

There are two special cross-sections in the pumping line: the inlet of the pump, and the outlet of the chamber. Two special names are given to the volumetric flow rate at these two cross-sections. The volumetric flow rate at the inlet of a pump is called intrinsic pumping speed of the pump device, i.e.,

$$S_p = \dot{V}_{\text{pump inlet}}$$

S_p is a function of pressure at the inlet of the pump, and this function is usually referred to as a pumping curve which is calibrated and published by the pump manufacturer. The volumetric flow rate at the outlet of the chamber is called effective pumping speed, i.e.,

$$S_e = \dot{V}_{\text{chamber exit}}$$

S_e is a function of S_p and conductance of the pumping line.

C.3 THROUGHPUT, Φ

The product of the inlet pressure and the pumping speed is defined as the throughput of the pump.

$$\Phi = p_{in} S_p$$

Note that the throughput has a unit of power. The throughput at any cross-section other than the pump inlet may be similarly defined

$$\Phi = p\dot{V}$$

where p is the pressure at the cross-section. From this definition, we can see that the throughput is the rate of expansion work at the cross-section.

It is commonly regarded in vacuum technology that the throughput through the pumping line is continuous (at a given moment, the throughput is equal at any cross-section). Since pressure changes along the pumping line, the volumetric flow rate is different at different cross-section by the requirement of throughput continuity.

C.4 COMMENTS ON THE THROUGHPUT CONTINUITY

The series law of conductance and the calculation of S_e are based on the requirement of throughput continuity through the pumping line. It is worthwhile to check the conditions for the continuity. For this purpose, we rewrite the definition of throughput by using the perfect gas law $p = R\rho T$ and $R = (\gamma-1)c_v$

$$\Phi = (\gamma-1)\, c_v T\, \rho\dot{V} = (\gamma-1)\, c_v T\, \dot{m}$$

where $\dot{m}$ is the mass flow rate, and $c_v T\, \dot{m}$ is the gas internal energy flow rate at a cross-section. Since c_v and γ are constant, the necessary and sufficient condition for throughput Φ to be continuous is that $T\, \dot{m}$ is continuous. This is satisfied only in one practical situation: steady state flow and isothermal process -- $\dot{m}$ is constant and T is uniform all over the vacuum system. Both conditions can not be exactly satisfied during pump-down. Two facts have been demonstrated in Chapter 2. The first is that the pump-down process is transient in nature and that steady state exists only when the ultimate pressure is reached, and the second fact is that the pump-down process is not isothermal at high pressure. Thus it is only an approximation to assume that the throughput is continuous during the pump-down processes.

Two other equivalent conditions for throughput continuity may also be stated as: (1) the mass capacitance of the pumping line is negligible, and (2) the heat transfer between gas and pipes or other devices in the pumping line is negligible. The first condition ensures that the mass flow rate is continuous, while the second condition ensures that the temperature (stagnation) is uniform.

In a pump-down, the effect of capacitance may be significant when large pipes are used or in the beginning of a pump down process when the pipes function as a gas reservoir. The effect of heat transfer may also be significant in the initial pump down when the temperature

difference between wall and gas is large or in the situation when a cold baffle is present. In these situations, the throughput is not continuous.

C.5 CONDUCTANCE OF A CONNECTING ELEMENT, C

If a constant throughput through a connecting element in the pumping line is Φ and the pressure drop across the element is Δp, the conductance is defined as

$$C = \frac{\Phi}{\Delta p} = \frac{p}{\Delta p}\dot{V}$$

Note that the conductance has a unit of volumetric flow rate, but it does not equal the volumetric flow rate at any cross-section of the element.

C.6 SERIES LAW AND PARALLEL LAW OF CONDUCTANCE

The series law states that if two elements with conductance C_1 and C_2 are connected in series, the equivalent conductance is C.

$$\frac{1}{C} = \frac{1}{C_1} + \frac{1}{C_2}$$

The parallel law states that if two elements with conductance C_1 and C_2 are connected in parallel, the equivalent conductance is C

$$C = C_1 + C_2$$

The series law is first proved. By definition

$$C_1 = \frac{\Phi_1}{\Delta p_1}; \quad C_2 = \frac{\Phi_2}{\Delta p_2}; \quad \text{and } C = \frac{\Phi}{\Delta p} \qquad \text{(a)}$$

The pressure drop for the series connection must satisfy

$$\Delta p = \Delta p_1 + \Delta p_2 \qquad \text{(b)}$$

Substituting (a) to (b) and assuming throughput is continuous, i.e.,

$$\Phi = \Phi_1 = \Phi_2 \qquad (b)$$

the series law is then proved.

The parallel law is proved by the relation

$$\Delta p_1 = \Delta p_2 = \Delta p \qquad (d)$$

and

$$\Phi = \Phi_1 + \Phi_2 \qquad (e)$$

Substituting (a), (d) to (e) yields $(C_1 + C_2)\Delta p = C\Delta p$ which proves the parallel law.

C.7 DERIVATION OF EQUATIONS (3.29) AND (3.30) USED IN CHAPTER 3

To find the effective pumping speed for the situation shown in Fig.3.1, we use the requirement of throughput continuity

$$\Phi = p\, S_e = p_{in}\, S_p = C_{or}\,(p - p_{in})$$

then

$$p - p_{in} = \frac{\Phi}{C_{or}} = \frac{\Phi}{S_e} - \frac{\Phi}{S_p}$$

which yields the result

$$S_e = \frac{S_p\, C_{or}}{S_p + C_{or}}$$

By the definition of the effective pumping speed, the mass flow rate can be calculated by

$$\dot{m}_2 = \rho\, S_e$$

where ρ is the gas density within the chamber.

APPENDIX D

CALCULATION OF EFFECTIVE PUMPING SPEED

The equations to be solved are found from the requirement of throughput continuity:

$$C_{or}\,(p - p_{in}) = p_{in}\,S_p \tag{D-1}$$

$$p_{in}\,Sp = p\,S_e \tag{D-2}$$

The conductance of the orifice C_{or} is a piecewise function of the pressure ratio, r

$$C_{or} = \begin{cases} c_d'' \left(\dfrac{2\gamma}{\gamma - 1}\right)^{1/2} r^{1/\gamma} \left\{1 - r^{(\gamma-1)/\gamma}\right\}^{1/2} \dfrac{Aor}{1 - r}\sqrt{RT} & r > r^* \\ c_d' \left(\dfrac{2\gamma}{\gamma - 1}\right)^{1/2} r^{*1/\gamma} \left\{1 - r^{*(\gamma-1)/\gamma}\right\}^{1/2} \dfrac{Aor}{1 - r}\sqrt{RT} & r \le r^* \end{cases} \tag{D-3}$$

$$r = \frac{p_{in}}{p} \tag{D-4}$$

$$r^* = \left(\frac{2}{\gamma - 1}\right)^{\gamma/(\gamma-1)} \tag{D-5}$$

In the above equations, p is the chamber gas pressure; T, the gas temperature; p_{in}, the pump inlet pressure; S_p, the pumping speed of the vacuum pump; S_e, the effective pumping speed; A_{or}, the area of the orifice; r^*, the critical pressure ratio below which choked (sonic) flow occurs; c_d', the orifice discharge coefficient for unchoked flow; c_d'', the discharge coefficient for choked flow. For air, $\gamma = 1.4$, then $r^* = 0.5283$.

The objective is to find S_e for a given A_{or}, γ, p, T and S_p. To do this, dividing equations (D.1) and (D.2) by p yields

$$C_{or}(1 - r) = r S_p \tag{D.6}$$

$$S_e = r S_p \tag{D.7}$$

There are two unknowns, r and S_e, in the above two equations which are solvable. In the following, S_p is assumed to be constant (independent of p_{in}).

For choked flow, substituting Eq. (D.3) for the case $r \le r^*$ into (D.7), one can find

$$S_e = S^*_e = C_d' \left\{\gamma\left(\frac{2}{\gamma+1}\right)^{(\gamma+1)/(\gamma-1)}\right\}^{1/2} A_{or}\sqrt{RT} \tag{D.8}$$

It is noted that S^*_e is the volumetric flow rate across the orifice which depends only on the A_{or}, independent of S_p. We may refer to this situation as orifice controlled flow.

For unchoked flow, substituting Eq. (D.3) for the case $r > r^*$ into Eq.(D.6), one can find a quadratic function

$$x^2 + Bx - B = 0 \tag{D.9}$$

where

$$x = r^{(\gamma-1)/\gamma} \tag{D.10}$$

$$B = \left\{\left(\frac{2\gamma}{\gamma-1}\right)^{1/2} \frac{C_d'' A_{or}\sqrt{RT}}{S_p}\right\}^2 \tag{D.11}$$

the solution of Eq. (D.9) yields

$$r = \left\{0.5B\left(\sqrt{1 + 4/B} - 1\right)\right\}^{\gamma/(\gamma-1)} \qquad (D.12)$$

and

$$S_e = r\, S_p \qquad (D.13)$$

In this case, S_e depends on both orifice size and S_p. If there is no orifice restriction -- assume $A_{or} = \infty$ in Eq. (D.11), $r = 1$ and $S_e = S_p$. The flow is controlled by the pump only.

The original criterion for choked flow is $p_{in}/p < r^*$. To use it, one must solve for p_{in} for a given pumping condition. Since $r = S_e/S_p$, the criterion for choked flow can be also expressed as

$$\frac{S^*_e}{S_e} \leq r^* \qquad (D.14)$$

This criterion provides more convenience than the original one because it can be directly checked for the given values of A_{or}, γ, p, T and S_p without solving for p_{in}.